

**CHARACTERISTICS OF HYBRID NANOFUID
FLOW OVER A RIGA PLATE IN THE
PRESENCE OF MIXED CONVECTION**

BY

SIDRA SEHR ABBASI



NATIONAL UNIVERSITY OF MODERN LANGUAGES

ISLAMABAD

June, 2024

Characteristics of Hybrid Nanofluid Flow over a Riga Plate in the Presence of Mixed Convection

By

SIDRA SEHR ABBASI

MS Mathematics, National University of Modern Languages, Islamabad, 2024

A THESIS SUBMITTED IN PARTIAL FULLFILMENT OF THE REQUIREMENT FOR
THE DEGREE OF

MASTER OF SCIENCE

In Mathematics

To

FACULTY OF ENGINEERING & COMPUTING



NATIONAL UNIVERSITY OF MODERN LANGUAGES ISLAMABAD

© Sidra Sehr Abbasi, 2024



THESIS AND DEFENSE APPROVAL FORM

The undersigned certify that they have read the following thesis, examined the defense, are satisfied with overall exam performance, and recommend the thesis to the Faculty of Engineering and Computing for acceptance.

Thesis Title: Characteristics of Hybrid Nanofluid Flow over a Riga Plate in the Presence of Mixed Convection

Submitted By: Sidra Sehr Abbasi

Registration #: 47/MS/Math/S22

Master of Science in Mathematics (MS Math)
Title of the Degree

Mathematics
Name of Discipline

Dr. Anum Naseem
Name of Research Supervisor

Signature of Research Supervisor

Dr. Sadia Riaz
Name of HOD (MATH)

Signature of HOD (MATH)

Dr. Noman Malik
Name of Dean (FEC)

Signature of Dean (FEC)

Date: 7th June, 2024

AUTHOR'S DECLARATION

I, Sidra Sehr Abbasi

Daughter of Muhammad Khatab

Registration # 47/MS/MATH/S22

Discipline Mathematics

Candidate of Master of Science in Mathematics at National University of Modern Languages do here by declare that the thesis Characteristics of Hybrid Nanofluid Flow over a Riga Plate in the Presence of Mixed Convection submitted by me in fractional fulfillment of MS Mathematics degree, is my original work, and has not been submitted or published earlier. I also solemnly declare that it shall not, in future, be submitted by me for obtaining any other degree from this or any other university or institution. I also understand that if evidence of plagiarism is found in my thesis/dissertation at any stage, even after the award of a degree, the work may be cancelled and degree revoked.

Signature of Candidate

Sidra Sehr Abbasi

Name of Candidate

7th June, 2024

Date

ABSTRACT

Title: Characteristics of Hybrid Nanofluid Flow over a Riga Plate in the Presence of Mixed Convection

The hybrid nanofluid flow can be helpful in improving the efficiency and effectiveness of heat transfer systems like in heat exchangers, electronic devices for thermal management automotive engine and cooling system. The aim of the study is to focus on the hybrid nanofluid flow ($\text{Cu} - \text{Al}_2\text{O}_3/\text{H}_2\text{O}$) over a Riga surface placed in a permeable medium. The flow experiences electromagnetohydrodynamics (EMHD) and is observed near a stagnation point. The effects of mixed convection, viscous dissipation, thermal radiation, Joule heating as well as heat generation/absorption are examined for the considered flow. The problem is modelled as a system of complex and coupled partial differential equations. The system is further reduced into system of ordinary differential equations by employing the suitable similarity transformation. The reduced system is solved through bvp4c function in MATLAB software and the numerical results of the nonlinear ordinary differential equations are generated. For several important parameters, the velocity and temperature distributions are analyzed. The mixed convection parameter results in an enhancement of velocity profile. The nanoparticle volume fractions for both the nanoparticles raises temperature of the hybrid nanofluid. Further, the graphical influence of various parameters is also examined for friction drag and Nusselt number. The authenticity of the obtained results is validated through a comparison study which is in correspondence with the previous published research.

TABLE OF CONTENTS

CHAPTER	TITLE	PAGE
	AUTHOR'S DECLARATION	iii
	ABSTRACT	iv
	TABLE OF CONTENTS	v
	LIST OF TABLES	ix
	LIST OF FIGURES	x
	NOMENCLATURE	xiii
	ACKNOWLEDGEMENT	xvi
	DEDICATION	xvii
1.	Introduction	1
	1.1 Hybrid Nanofluid	1
	1.2 Riga Surface	3
	1.3 Mixed Convection	4
	1.4 Stagnation Flow	5
	1.5 Heat Generation/Absorption	6
	1.6 Thesis Organization	6
2.	Literature Review	8
	2.1 Hybrid Nanofluid	8
	2.2 Riga Surface	9
	2.3 Mixed Convection	10
	2.4 Stagnation Flow	11
	2.5 Heat Generation/Absorption	12

3.	Preliminaries	14
3.1	Fluid	14
3.2	Fluid Mechanics	14
3.2.1	Fluid Statics	15
3.2.2	Fluid Dynamics	15
3.3	Stress	15
3.3.1	Shear Stress	15
3.3.2	Normal Stress	16
3.4	Viscosity	16
3.4.1	Dynamic Viscosity	16
3.4.2	Kinematics Viscosity	16
3.5	Newton's Law of Viscosity	17
3.6	Newtonian Fluids	17
3.7	Non-Newtonian Fluids	17
3.8	Nanofluid	18
3.9	Hybrid Nanofluid	18
3.10	Flow	18
3.10.1	Compressible Flow	19
3.10.2	Incompressible Flow	19
3.10.3	Laminar Flow	19
3.10.4	Turbulent Flow	19
3.10.5	Steady Flow	20
3.10.6	Unsteady Flow	20
3.11	Density	20
3.12	Pressure	21

3.13	Thermal Conductivity	21
3.14	Thermal Diffusivity	21
3.15	Method of Heat Transfer	22
3.15.1	Conduction	22
3.15.2	Convection	22
3.15.2.1	Force Convection	22
3.15.2.2	Natural Convection	23
3.15.2.3	Mixed Convection	23
3.15.3	Radiation	23
3.16	Dimensionless Numbers	23
3.16.1	Reynolds Number	23
3.16.2	Prandtl Number	24
3.16.3	Eckert Number	24
3.16.4	Nusselt Number	25
3.16.5	Skin Friction	25
3.16.6	Grashof Number	25
4.	The Stagnation Point Flow of Hybrid Nanofluid Flow past a Shrinking Surface	27
4.1	Introduction	27
4.2	Mathematical Construction for Model	28
4.3	Numerical Stratagem	32
4.4	Graphical Analysis and Discussion	33
5.	The Mixed Convection Flow of Hybrid Nanofluid over a Riga Plate in a Porous Medium	39
5.1	Introduction	39
5.2	Mathematical Construction for Model	40

5.3	Numerical Stratagem	47
5.4	Graphical Analysis and Discussion	48
6.	Conclusion And Future Work	66
6.1	Concluding Remarks	66
6.2	Future Work	67
7.	References	68

LIST OF TABLES

TABLE NO.	TITLE	PAGE
4.1	Thermophysical characteristics of nanofluid (Al_2O_3/H_2O).	30
4.2	Thermophysical characteristics of hybrid nanofluid ($Al_2O_3 - Cu/H_2O$).	30
4.3	Thermophysical properties of hybrid nanofluid ($Al_2O_3 - Cu /H_2O$).	31
4.4	Comparative values of stretching parameter λ_1 on $f''(0)$ and $-\theta'(0)$ if $\phi_1 = \phi_2 = 0$.	38
4.5	Comparative values of $f''(0)$ and $-\theta'(0)$ for various values of ϕ_2 , λ_1 and ϕ_1 if $Pr = 6.2$.	38
5.1	Thermophysical features of nanofluid (Al_2O_3/H_2O).	43
5.2	Thermophysical features of hybrid nanofluid ($Al_2O_3 - Cu/H_2O$).	44
5.3	Thermophysical properties of hybrid nanofluid ($Al_2O_3 - Cu /H_2O$).	44
5.4	Dimensionless parameters involved in the hybrid nanofluid flow.	46
5.5	Comparative values of stretching parameter λ_1 on $f''(0)$ and $-\theta'(0)$ if $\phi_1 = \phi_2 = Z = \lambda = R = Q = \gamma = M = Ec = \omega = E_1 = 0$.	64
5.6	Comparative values of skin friction coefficient $f''(0)$ and Nusselt number $-\theta'(0)$ for several values of ϕ_2 , ϕ_1 and λ_1 if $Z = \lambda = R = Q = \gamma = M = Ec = \omega = E_1 = 0$.	65

LIST OF FIGURES

FIGURE NO.	TITLE	PAGE
3.1	Nanofluid.	18
3.2	Hybrid nanofluid.	18
4.1	Physical model.	28
4.2	Effects of nanoparticle volume fraction ϕ_2 of Cu upon $f'(\eta)$.	34
4.3	Effect of stretching parameter λ_1 upon $f'(\eta)$.	35
4.4	Effect of nanoparticle volume fraction ϕ_2 of Cu upon $\theta(\eta)$.	35
4.5	Effect of stretching parameter λ_1 upon $\theta(\eta)$.	36
4.6	Effect of Prandtl number Pr upon $\theta(\eta)$.	36
4.7	Skin friction towards λ_1 with various values of ϕ_2 .	37
4.8	Nusselt number towards λ_1 with various values of ϕ_2	37
5.1	An illustration of Riga plate.	40
5.2	An illustration of flow toward Riga plate in Cartesian system.	40
5.3	Effect of stretching parameter λ_1 upon $f'(\eta)$.	51
5.4	Effect of nanoparticle volume fraction ϕ_1 of Al_2O_3 upon $f'(\eta)$.	51
5.5	Effect of nanoparticle volume fraction ϕ_2 of Cu upon $f'(\eta)$.	52
5.6	Effect of modified Hartmann number Z upon $f'(\eta)$.	52

5.7	Effect of dimensionless quantity γ upon $f'(\eta)$.	53
5.8	Effect of porosity parameter ω upon $f'(\eta)$.	53
5.9	Effect of mixed convection parameter λ upon $f'(\eta)$.	54
5.10	Effect of stretching parameter λ_1 upon $\theta(\eta)$.	54
5.11	Effect of nanoparticle volume fraction ϕ_1 of Al_2O_3 upon $\theta(\eta)$.	55
5.12	Effect of nanoparticle volume fraction ϕ_2 of Cu upon $\theta(\eta)$.	55
5.13	Effect of radiation parameter R upon $\theta(\eta)$.	56
5.14	Effect of Eckert number Ec upon $\theta(\eta)$.	56
5.15	Effect of Prandtl number Pr upon $\theta(\eta)$.	57
5.16	Effect of modified Hartmann number Z upon $\theta(\eta)$.	57
5.17	Effect of dimensionless quantity γ upon $\theta(\eta)$.	58
5.18	Effect of magnetic parameter M upon $\theta(\eta)$.	58
5.19	Effect of electric field parameter E_1 upon $\theta(\eta)$.	59
5.20	Effect of heat absorption/generation parameter Q upon $\theta(\eta)$.	59
5.21	Effect of mixed convection parameter λ upon $\theta(\eta)$.	60
5.22	Skin friction towards Z with various values of γ .	60
5.23	Nusselt number towards Z with various values of γ .	61
5.24	Skin friction towards λ_1 with various values of ϕ_1 .	61
5.25	Nusselt number towards λ_1 with various values of ϕ_1 .	62
5.26	Skin friction towards λ_1 with various values of ϕ_2 .	62
5.27	Nusselt number towards λ_1 with various values of ϕ_2 .	63
5.28	Skin friction towards λ with various values of Z .	63

5.29	Nusselt number towards λ with various values of Z .	64
------	---	----

NOMENCLATURE

Acronyms

MHD	Magnetohydrodynamics
EMHD	Electromagnetohydrodynamics
PDEs	Partial differential equations
ODEs	Ordinary differential equations
Cu	Copper
Al_2O_3	Alumina/Aluminum oxide
MATLAB	Matrix Laboratory
Bvp4c	Boundary Value Problem for 4th Order Collocation
Nu_x	Local Nusselt Number
C_f	Skin Friction Coefficient
H_2O	Water

Symbols

x, y	Cartesian coordinates
u, v	Velocity components
T	Temperature
T_w	Temperature of the wall
T_∞	Ambient temperature of the hybrid nanofluid
θ_w	Ratio of temperature
ϕ_1	Concentration 1st nano-particle
ϕ_2	Concentration 2nd nano-particle

$s1$	1 st nanoparticle
$s2$	2 nd nanoparticle
α	Thermal diffusivity
σ	Electrical conductivity
σ_{nf}	Electrical conductivity of nanofluid
σ_{hnf}	Electrical conductivity of hybrid nanofluid
ν	Kinematic viscosity
k	Thermal Conductivity
k_{nf}	Thermal Conductivity nanofluid
k_{hnf}	Thermal Conductivity hybrid nanofluid
C_p	Fluid heat capacity
$(C_p)_{nf}$	Specific heat capacity of nanofluid
$(C_p)_{hnf}$	Specific heat capacity of hybrid nanofluid
ρ	Density
ρ_{nf}	Density of nanofluid
ρ_{hnf}	Density of hybrid nanofluid
μ	Dynamic Viscosity
μ_{nf}	Dynamic viscosity nanofluid
μ_{hnf}	Dynamic viscosity hybrid nanofluid
β_T	Thermal expansion
$(\beta_T)_{nf}$	Thermal expansion of nanofluid
$(\beta_T)_{hnf}$	Thermal expansion hybrid nanofluid
Pr	Prandtl number
Re_x	Reynolds number
Ec	Eckert number
Nu_x	Nusselt number
Gr	Grashof number
q_r	Radiative heat flux
ω	Porosity parameter

γ	Width of electric and magnetic parameter
R	Thermal radiation
M	Magnetic field parameter
Q	Heat generation/absorption parameter
Z	Modified Hartman number
λ	Mixed convection parameter
λ_1	Stretching parameter
E_1	Electric field parameter

ACKNOWLEDGEMENT

In the name of Allah, the most gracious and merciful, I begin with a heart full of gratitude. I am deeply thankful to Almighty Allah for granting me the strength, knowledge, and opportunity to complete this study successfully.

I wish to extend my sincere appreciation to my research supervisor, Dr. Anum Naseem, whose guidance has been invaluable throughout this journey. Her vision and unwavering support have been a constant source of inspiration. Under her tutelage, I have learned the intricacies of research methodology and the art of presenting the findings effectively. Working under her guidance has been a privilege and an honor, and I am profoundly grateful for her expertise, encouragement, and constructive feedback, which have enriched this work significantly.

I also wish to express my deepest gratitude to my parents and friends for their unwavering support and encouragement. Their belief in me has been a constant source of strength, sustaining me through the challenges of academic life and the rigors of research. This achievement would not have been possible without their love, encouragement, and sacrifices. Thank you from the depth of my heart.

In conclusion, I am grateful to Allah, my supervisor, and my loved ones for their profound impact on this journey. Their support has been the cornerstone of my success, and for that, I am eternally grateful.

DEDICATION

I dedicate my thesis to my parents and teachers for their endless support and encouragement throughout my pursuit for education. I hope this achievement will fulfill the dream they envisioned for me.

Chapter 1

Introduction

1.1 Hybrid Nanofluid

In modern world, the enhanced thermal performance of the fluids has become the top priorities of the researcher. The development of hybrid nanofluids has undoubtedly gain the researchers' interest in enhancing the efficiency of numerous industrial equipment's, technological devices, and the mechanisms that involve heat transfer because traditional fluids do not allow for the necessary intensification for transfer of heat and fluid flow. Choi *et al.* [1] initially put forward the idea to use the nanofluids as a potential alternate for traditional fluids in industrial processes. Nanofluids are an especially engineered fluid made by merging nanoparticles into a base fluid (engine oil, ethylene glycol, oil and water) of size varying from 1 to 100 nanometers. These nanoparticles can be formed from variety of materials, such as metals (*Au, Ag, Cu etc.*), oxides (*ZnO, CuO, Al₂O₃*) and carbon nanotubes. The concept of nanofluid was later refined by Turcu *et al.* [2] and Jana *et al.* [3]. Their research led to the finding that merging two nanoparticles of multiple types into base fluid can significantly elevate the physical and thermal characteristics of nanofluids, fabricating what they termed as "hybrid nanofluids". By integration of nanoparticles, the heat transfer efficiency improves substantially due to the enhancement in the thermal conductivity of working fluids. Hybrid nanofluids have illustrated better heat transfer performance and rheological characteristics when contrasted to both base fluids and mono

nanofluids. Hybrid nanofluids have wide engineering potential applications in thermal insulation, aerodynamics, building construction, geothermal systems, heat exchangers, crude oil extractions, groundwater pollution, storage of nuclear waste and agriculture etc. Suresh *et al.* [4] experimentally investigated ($Al_2O_3 - Cu/H_2O$) hybrid fluid that was developed using the hydrogen reduction technique from a powder combination of CuO and Al_2O_3 and the nanoparticles was incorporated using chemical process. Suresh *et al.* [5] performed an experiment using hybrid nanofluid ($Cu - Al_2O_3/H_2O$) creating it via a thermochemical process that involved hydrogen reduction technique in circular tube to analyze the characteristic of heat transfer in laminar force convection. Labib *et al.* [6] studied the laminar flow of two phase mixture model using the circular tube that was evenly heated. Hydrodynamics and heat transfer phenomenon of both nanofluid ($Al_2O_3/(CH_2OH)_2$) and (Al_2O_3/H_2O) and hybrid nanofluid ($Al_2O_3/CNTs-H_2O$) based were examined. Madhesh *et al.* [7] carried out experimental study using the titanium-copper hybrid nanofluid to investigate the rheological attributes and heat transfer potential using the tube-in-tube counter flow heat exchanger. Takabi *et al.* [8] investigated the turbulent flow of pure nanofluid (Al_2O_3/H_2O) and hybrid nanofluid ($Al_2O_3 - Cu/H_2O$) using the uniformly heated circular tube. The study of Farooq *et al.* [9] is on the boundary layer flow of a ($Al_2O_3 - Cu/H_2O$) hybrid nanofluid flow across a disk which was permeable. Entropy generation was also studied for the flow with the impact of nonlinear thermal radiations in relation to the impacts of viscous dissipation and suction or injection. Parsian *et al.* [10] performed an experiment to examine the enhancement of thermal conductivity of ($Cu - Al_2O_3/(CH_2OH)_2$) hybrid nanofluid using the transient heated wire technique. Chamkha *et al.* [11] analyzed the flow under the impacts of Joule heating and thermal radiation of magnetohydrodynamic flow as well as heat transfer between two rotating surfaces in case of ($C_8O_2(OH)_2 - Cu/H_2O$) hybrid nanofluid. The system's top and bottom plates were considered to be stretchable and penetrable correspondingly. The goal of the study done by Khashi *et al.* [12] was to find out the dual solutions of the hybrid nanofluid ($Cu - Al_2O_3/H_2O$) flow and heat transfer in the presence of Joule heating for a porous cylinder which was a shrinking. Megahed *et al.* [13] study examined the problem of heat transfer and MHD boundary layer flow caused due to unstable sheet that was stretched with the effects of thermal radiation.

1.2 Riga Surface

Gailitis [14] put forward the idea of Riga surface, which are electromagnetic surfaces composed of an alternation of electrode arrangements. As a result of this configuration the fluid flow exhibits electromagnetic behavior. It develops electric and magnetic fields and by applying an external electric field, one can use the resulting Lorentz force acting parallel to the wall in order to regulate the fluid flow. Riga plates have several applications in enhancing a fluid's thermophysical attributes. Heat transfer can be enhanced by incorporating turbulence and vortices to fluid flow due to Riga plates. Potential application is in cooling systems, electronic devices, thermal management and heat exchangers. Ahmed *et al.* [15] aim was to examine the flow of $(Fe_3O_4 - Ag/H_2O)$ hybrid nanofluid which was squeezed among parallel Riga plates. The plates used were stretchable and electromagnetohydrodynamic (EMHD) phenomenon was studied. The analysis was carried out by incorporating chemical reaction effects and nonlinear thermal radiation. Nayak *et al.* [16] analyzed how electromagnetic forces impact the velocity slip flow as well as transfer of heat across a heated Riga plate for a hyperbolic tangent nanofluid. The investigation considered the effects of viscous dissipation, suction, thermal radiation, and chemical reactions and activation energy. Shah *et al.* [17] studied the improved Cattaneo-Christov heat flux model for the fluid flow over a Riga plate surface that was linearly stretched and the plate was placed in a porous medium and the effects of mixed convective and stagnation point were employed. The homotopy analysis method was utilized to develop series solutions. Abbas *et al.* [18] analyzed the heat transfer rate and microplar hybrid nanofluid flow for a magnetized curved Riga surface stretching exponentially. This investigation also took into consideration the effects of velocity slip and the bvp4c scheme in MATLAB was utilized to solve the reduced model. This work of Wakif *et al.* [19] observes the flow of EMHD convective problem of an electrically conducting, incompressible fluid across a Riga plate inserted horizontally and is heated by taking into account the important effects of Joule heating and viscous dissipations in addition to the presence of a Wall-penetrating downward channel. The aim of Khashi' *et al.* [20] work was to analyze the hybrid nanofluid flow $(Al_2O_3 - Cu/H_2O)$ towards a shrinking/stretching Riga surface by considering the impact of different nanoparticle shape factors, radiation parameters and MHD. Nadeem *et al.* [21] discussed the stagnation point

flow of nanoliquid under the impact of induced magnetic field generated by Riga plate with Troian slip and Thomson conditions.

1.3 Mixed Convection

Merkin [22] looked into the concept of mixed convection that takes place when a flow is simultaneously affected by internal volumetric forces and external forcing systems. Mixed convection, that combines free and forced convection, is frequently utilized as a technique for an efficient heat transfer. The phenomenon of heat transfer occurs when a fluid, including the air or water, is moving and convection begins when the temperature differences occur within that fluid flow. Ahmad *et al.* [23] referred to a few possible potential applications for mixed convection including cooling a nuclear reactor on an emergency shutdown, heat exchangers positioned in low-velocity environments, using a fan for cooling electronic equipment, currents of wind exposed to the solar receiver, and flows in the atmosphere and ocean. The efficiency of such systems might be optimized and safety may be ensured via the study of mixed convection flows. Momin *et al.* [24] conducted two experiments for investigation of a mixed convection, one on the nanofluid ($Al_2O_3 - H_2O$) with a copper tube surface that was inclined and second on the hybrid nanofluid ($Cu - Al_2O_3/H_2O$) using the constantly heated circular tube to determine laminar convective flow. Under conditions of laminar flow, the impact of the power sources and nanoparticles volume concentration on the growth of a thermal field were investigated and addressed. Mehryan *et al.* [25] examined how mixed convection effects the flow of ($Cu - Al_2O_3/H_2O$) hybrid nanofluid and (Al_2O_3/H_2O) nanofluid past a hot oscillating cylinder placed inside a square cavity. It was discovered that a nanofluid (Al_2O_3/H_2O) has a greater convection rate than a hybrid nanofluid ($Cu - Al_2O_3/H_2O$). The aim of Khan *et al.* [26] study was to look into the impact of a magnetic field that was applied on mixed convective and stagnation point flow of a hybrid nanofluid ($Cu - TiO_2/H_2O$) moving in the direction of stretchable sheet. Heat source/sink and nonlinear thermal radiation were taken into consideration as well. Elsaid *et al.* [27] explored the analytical solution for the mixed convection flow of hybrid nanofluid ($Al_2O_3 - Cu/H_2O$) in vertical channel with variable temperature and thermal radiation impact.

1.4 Stagnation Flow

Stagnation points in a fluid flow is a point where the velocity of fluid is zero and an object's surface triggers the fluid to stop flowing. This phenomenon is useful in many procedures such as electronic devices chilling, polymers extrusion, wire drawing, fans utilization, hydrodynamic procedures and nuclear reactors chilling. Lok *et al.* [28] performed an experiment on the micropolar fluid flow over a flat infinite double plate that was inserted vertically to study the steady boundary layer flow near the stagnation point in the presence of mixed convection. Rostami *et al.* [29] addressed the laminar and steady boundary layer flow problem of $(Al_2O_3 - SiO_2/H_2O)$ hybrid nanofluid flowing over a vertically placed permeable plate with magneto hydrodynamics, mixed convection near the stagnation point. The purpose of Ghalambaz *et al.* [30] work was to investigate the flow of hybrid nanofluid composed of $Al_2O_3 - Cu$ nanoparticles and water was the base fluid. The study of heat transfer was done for mixed convection fluid flow over the plate that was placed vertically. The study of Khashi *et al.* [31] investigated how boundary layer flow and heat transfer of a hybrid nanofluid $(Cu - Al_2O_3/H_2O)$ are impacted by combining the both effects of mixed convection and thermal stratification. The fluid wall suction was made possible by the stretching/shrinking surface's permeability. Anantha *et al.* [32] explored the stagnation point and MHD flow of a micro polar fluid across a narrow stretching surface under the effects of frictional heat, temperature dependent thermal conductivity, variable heat sink or source and thermal radiation. Jamaludin *et al.* [33] addressed the problem under the impact of heat sink/source and magnetic field and considered the flow over a porous shrinking/stretching sheet near a stagnation point. The study also included mixed convection flow using $(Cu - Al_2O_3/H_2O)$ hybrid nanofluid. Khashi *et al.* [34] inspected the heat transfer of hybrid nanofluid $(Al_2O_3 - Cu/H_2O)$ above a flat plate that was shrinking/stretching and also investigated the non-axisymmetric Homann flow near a stagnation point.

1.5 Heat Generation/Absorption

Many researchers are taking keen interest in the phenomenon of heat generation or absorption. The scientists and researchers have studied the significance of heat generation or absorption effects that have the potential to alter distribution of temperature and, consequently, rate of heat transfer. In particular contexts, its applications can be found in nuclear reactors, semiconductors and electronic devices etc. Hayat *et al.* [35] studied the magnetohydrodynamic and stagnation point flow of Jeffrey fluid on a stretching surface that was a nonlinear and the surface thickness was considered variable. The heat generation, melting heat transfer and viscous dissipation effects, are utilized to study the heat transfer properties. Hayat *et al.* [36] investigated the heat transfer and flow characteristics under the impact of the magnetohydrodynamics and heat generation/absorption for the flow of a hybrid nanofluid through a stretched surface. Tayebi *et al.* [37] explored the three dimensional flow on stretching sheet under the impact of Lorentz force. The impact of heat generation/absorption and natural convection was examined for the hybrid nanofluid flow in an annular cavity enclosed by two elliptical cylinders. Shoaib *et al.* [38] looked into the flow dynamics and heat transfer features of a MHD hybrid nanofluid flow among two parallel placed plates under the influence of heat absorption or generation and Joule heating. The work of Masood *et al.* [39] studied the stagnation point flow of hybrid nanofluid ($TiO_2 - C_8H_8/H_2O$) under the impact of heat generation/absorption and the flow was caused by a stretchy surface. The results inferred that the temperature field grows with the heat generation/absorption coefficient whereas the velocity field enhanced for the velocity ratio parameter increment.

1.6 Thesis Organization

This thesis involves six chapters.

Chapter 1 is about comprehensive introduction related to the important effects incorporated in the study, supported by previously existing literature.

Chapter 2 gives comprehensive review of the relevant literature. It contains the literature that is the base of this present work's.

Chapter 3 represents fundamental concepts and definitions utilized in the study. This chapter also includes the fundamental laws that will be utilized during the evaluation of the next chapters.

Chapter 4 involves the investigation of a two dimensional time independent stagnation point flow induced by a shrinking sheet using a hybrid nanofluid. The fluid flow and heat transfer properties are impacted in the presence of stagnation point. The model equations are transformed through similarity transformations into system of ODEs, and then solved by applying the bvp4c technique in MATLAB.

Chapter 5 focuses on the analysis for hybrid nanofluid flow across Riga plate that is linearly stretched. The study involves the presence of mixed convective, stagnation point Joule heating, thermal radiation, heat generation/absorption and viscous dissipation. The model equations are transformed into nonlinear ODEs, and the resulting system is solved through the application of bvp4c method. A comprehensive review of the obtained outcomes has been conducted.

Chapter 6 embraces the conclusions of hybrid nanofluid flow problem obtained after conducting the study. It comprises a few possible future research projects as well.

Chapter 2

Literature Review

2.1 Hybrid Nanofluid

By incorporating two distinct kinds of nanoparticles into a base fluid, hybrid nanofluids are made, that boost the thermophysical features of nanofluids. These days, a lot of researchers are indulged in the investigation of hybrid nanofluids for boundary layer flow. Recently, Jalili *et al.* [40] addressed mass and heat transfer problem by employing a novel semi-analytical approach. This problem included a laminar, axisymmetric, viscous, incompressible fluid in the presence of a magnetic field while the micropolar fluid flowed over stretchable disks. Tabassum *et al.* [41] examined the impact of thermal jump conditions and temperature dependent viscosity on a hybrid nanofluid composed from both multi-walled carbon nanotubes (MWCNTs) and single-walled carbon nanotubes (SWCNTs), across a Riga plate. The modified Brinkman's viscosity model was utilized in the study to examine the variation in viscosity within a flow regime. The study of Khan *et al.* [42] investigated the steady, two dimensional, hydromagnetic flow under the impact of convective conditions, heat generation, velocity slip, and thermal radiations. The problem involved ($Cu - Al_2O_3/H_2O$) hybrid nanofluid flowing across a permeable sheet with both stretching and shrinking characteristics. The study of Xia *et al.* [43] investigated the three dimensional mixed convection flow of micropolar hybrid nanofluid flowing over a surface in the presence of convective boundary conditions, slip conditions and

microorganisms. The fluid model was further modified with the existence of Joule heating and activation energy. Dero *et al.* [44] examined a two dimensional, steady flow of a hybrid nanofluid ($Cu - Al_2O_3/H_2O$) driven by the stretching/shrinking of the porous surface. The occurrence of viscous dissipation also contributes towards fluid flow features. Aminuddin *et al.* [45] examined the impacts of magnetic effect and radiation on ($C_8O_2(OH)_2 - Fe_2O_4/C_2H_6O_2$) non-Newtonian hybrid nanofluid flow across the surface stretching horizontally while the flow was considered axisymmetric. The work of Yahaya *et al.* [46] investigated the three dimensional $Cu - Al_2O_3/H_2O$ hybrid nanofluid flow induced due to stretching or shrinking of a biaxial sheet under suction and thermal radiation impact. The goal of the inquiry done by Mahesh *et al.* [47] was to demonstrate the MHD ($Ag - TiO_2/H_2O$) hybrid nanofluid flowing on a permeable shrinking sheet with the significant effects of viscous dissipation and thermal radiation and dual solutions were attained using the hypergeometric functions. Rasool *et al.* [48] explored the influence of magnetohydrodynamics, Joule heating and viscous dissipation on hybrid nanofluid ($Cu - Al_2O_3/H_2O$) moving across a permeable, shrinking sheet while the flow was considered to be steady.

2.2 Riga Surface

Riga plate is widely used in numerous technical as well as industrial fields such as it can be utilized to decrease the submarine's friction and pressure drag by preventing the boundary layer from separating and decreasing the turbulence generation. The study done by Zainal *et al.* [49] analyzed the time dependent flow of hybrid nanofluid ($Cu - Al_2O_3/H_2O$) across a porous Riga surface that was stretching or shrinking. Additionally, the impact of thermal radiation on the flow of the boundary layer was considered and the flow was examined near a stagnation point. Khan *et al.* [50] examined the hybrid nanofluid flow across a vertical Riga wedge under the combined impact of velocity slip and mixed convection when the flow is studied near a stagnation point. Nidhi *et al.* [51] attempted to study the properties of fluid flow under the impact of convective boundary conditions, thermal radiation and viscous dissipation, and the fluid was flowing via Riga plate. The shooting strategy was used to find two solutions (a stable as well as unstable solution) for the nonlinear coupled equations. Ghazwani *et al.* [52] studied the flow of

unsteady stagnation point flow of nanofluid over the rotating Riga plate under the impact of radiative heat flux, mixed convection, porous medium, thermal radiation and viscous dissipation. By combining the shooting idea with the bvp4c approach in MATLAB, computational results were calculated. Khan *et al.* [53] examined the influence of binary chemical reaction with known activation energy and thermal radiation, and determined the free convective, time dependent, stagnation point flow of nanofluid over a vertically placed Riga surface. Khashi *et al.* [54] investigated the numerical results of the unsteady stagnation point flow caused by a Riga surface employing hybrid nanofluids made of alumina, graphene and copper with H_2O as base fluid. Yahaya *et al.* [55] presented a mathematical model to study the time dependent, two dimensional flow of $Cu - Al_2O_3/H_2O$ hybrid nanofluid moving across a fixed Riga surface near a stagnation point. The study was conducted under the impact of mixed convection, convective boundary conditions and thermal radiation. The research performed by Shoukat *et al.* [56] investigated how Joule heating and thermal radiation influenced the Powell-Eyring fluid flow in the presence of magnetic field. The rapidly heated Riga plate and the double diffusion Cattaneo-Christov model was utilized to examine the mass and heat transfer.

2.3 Mixed Convection

The concept of mixed convection is utilized extensively in numerous industries and engineering fields. Elsaid *et al.* [57] presented the flow of a Ferrohybrid nanofluid ($Cu - Fe_3O_4/H_2O$) flow across a vertical channel in the presence of mixed convection and magnetic field. A system of partial differential equations was developed under the assumptions of variable temperature and thermal radiation. Abdelaziz *et al.* [58] determined the impact of mixed convection on the magnetohydrodynamic flow of nanofluid and a comparison was done through numerical investigation for three kinds of nanofluids, simple, ionic and hybrid. Khan *et al.* [59] investigated the MHD flow of Jeffery hybrid nanofluid by developing the fractional model under effects of magnetic field and thermal radiation and the fluid flowed across the permeable plate with rotating frame. Asghar *et al.* [60] utilized the bvp4c function in MATLAB software to evaluate the two dimensional flow of $Cu - Al_2O_3/H_2O$ hybrid nanofluid and investigated the MHD and mixed convection flow on a vertically placed sheet that was exponentially shrinking.

The study was performed under the effects of slip velocity and heat generation or absorption. Wahid *et al.* [61] obtained numerical outcomes for the mixed convection flow of hybrid nanofluid through a vertical flat plate with porosity. The fluid model was further influenced by MHD and thermal radiation. When specified values of other parameters are combined with the opposing flow of the mixed convection parameter, the dual solutions are possible. A study was organized by Khan *et al.* [62] in order to compare the thermal effectiveness of nanofluid and hybrid nanofluid model that included the novel impacts of viscous dissipation, magnetic field and mixed convection. Jiang *et al.* [63] studied three dimensional mixed convection flow of nanofluid across a porous cavity with two cylinders that were rotating under the impact of magnetic field. The governing equations were solved via the Galerkin finite element method (GFEM). Hussain *et al.* [64] examined the stagnation point flow of Walters-B hybrid nanofluid across the circular cylinder placed horizontally under the impact of mixed convection, thermal radiation and uniform heat flux.

2.4 Stagnation Flow

The stagnation point flow can be helpful in a variety of tasks, such as wire drawing, cooling nuclear reactors, hydrodynamic processes, chilling electronic equipment, and polymer extrusion etc. The study of Wahid *et al.* [65] explored numerically the stagnation point flow of hybrid nanofluid across a Riga surface that was shrinking with the impact of magnetohydrodynamics and velocity slip. The relevant profiles are assessed with specified values of dimensionless parameters. Zainal *et al.* [66] examined the time dependent and stagnation point flow of hybrid nanofluid. The flow characteristics was examined under the combined impact of both the thermal and velocity slips. Khashi *et al.* [67] explained the impact of convective boundary conditions, suction, Joule heating and viscous dissipation on the stagnation point flow of hybrid nanofluid across the rapidly heated and shrinking disk. Yahaya *et al.* [68] studied the stagnation point flow while evaluating the impact of suction on the flow of a hybrid over a surface. Bvp4c package in MATLAB was used for computation of numerical results. Khashi *et al.* [69] investigated the unsteady flow of hybrid nanofluid under the impact of heat generation and electro-magnetohydrodynamic (EMHD) toward the Riga surface near a stagnation point. The

purpose of Yahaya *et al.* [70] work was to investigate the stagnation point flow of ($Cu - Al_2O_3/H_2O$) hybrid nanofluid over a disk that was radially shrinking under the influence of Ohmic dissipation, magnetic field and convective boundary conditions. The numerical study was conducted by Zainodin *et al.* [71] in order to analyze the performance of the magnetic effect on the combined free and force convection stagnation-point flow of the hybrid ferro nanofluid. This study looked at the impacts of convective boundary condition, Joule heating and viscous dissipation throughout a surface that was nonlinearly moving.

2.5 Heat Generation/Absorption

The mechanism of heat generation or absorption attracts the attention of many researchers. Nuwairan *et al.* [72] examined magnetic flow of hybrid nanofluid (SWCNTs – $CuO/(CH_2OH)_2$) across the porous sheet which was placed vertically and was shrinking under the impact of thermal radiation, heat generation/absorption, melting heat parameter and MHD. The results showed that as the heat generation parameter and thermal radiation parameter was raised, the liquid's temperature also showed an increment. Yaseen *et al.* [73] examined the heat transfer characteristics under the impact of heat source/sink, thermal radiation, porous medium, magnetic field and suction/injection for a hybrid nanofluid, MHD and squeezing flow of nanofluid between plates that were parallel and the flow was considered unsteady. Asghar *et al.* [74] looked at the numerical solutions of a two dimensional flow of ($Cu - Al_2O_3/H_2O$) hybrid nanofluid flow. The study examined the effects of MHD and mixed convection for the flow over the vertically placed sheet shrinking exponentially. The main objective of the investigation was to observe the impact of various factors on velocity and temperature distributions, involving heat generation/absorption, velocity slip and MHD and utilizing the Tiwari-Das model. Kumar *et al.* [75] investigated the unsteady mixed convective flow over a revolving sphere with heat generation/absorption effects. Additionally, the impact of a variety of nanoparticle shapes such as bricks, cylinders, spheres, platelets, and blades in a $Cu - Al_2O_3/H_2O$ hybrid nanofluid was also studied. The work of Mahmood *et al.* [76] focused on the impact of mass suction and production or absorption of heat on MHD stagnation point flow across the sheet which was nonlinearly shrinking or stretching using the tri-hybrid nanofluid.

From the studies mentioned above it has been found that no research has been conducted regarding the hybrid nanofluid flow across linearly stretchable Riga plate under the influence of thermal radiation, viscous dissipation, heat generation or absorption and Joule heating. This work also aims to investigate the impact of mixed convection and stagnation point on the flow. The fundamental principles of heat transfer and fluid flow have been taken into account when modeling the flow problem. By using appropriate similarity transformations, the fluid's model equations are converted into a set of ODEs. The `bvp4c` function in MATLAB is employed to solve the resulting system. The impacts of several flow parameters are graphically studied in relation to the fluid flow outcomes. It is anticipated that the current work's findings will support future research with the goal of advancing the growth of the scientific as well as technical fields.

Chapter 3

Preliminaries

This chapter introduces key terminologies and laws necessary for comprehending the analysis presented in the subsequent chapters and to establish a firm basis for understanding the concepts that follows.

3.1 Fluid

When a material or substance is exposed to an external force, a fluid whether it is a gas or liquid exhibits minor resistance to the applied shearing force but ultimately continues its motion and deformation. In other word fluids are unable to resist shear forces. Liquids, gases, blood, and plasmas are examples of fluids [77].

3.2 Fluid mechanics

A subfield of applied mechanics known as fluid mechanics focuses on the characteristics and actions of fluids as well as the forces that affect them. Two primary branches may be found in this particular field [77].

3.2.1 Fluid statics

The discipline of fluid mechanics designated to fluid statics explores the properties of fluids while they are at rest [77].

3.2.2 Fluid dynamics

The discipline of fluid mechanics nominated as fluid dynamics analyses how forces impact the physical features and actions of fluids in motion [77].

3.3 Stress

It is the average force imposed on the surface of an object by numerous factors. Usually, stress is characterized in term of direction and magnitude.

$$\text{Stress}(\sigma) = \frac{\text{Force}(F)}{\text{Area}(A)}. \quad (3.1)$$

In the SI system, stress is quantified in units as Nm^{-2} or kg/ms^{-2} , with dimensions $\left[\frac{M}{LT^2}\right]$.

It is composed up of two parts [77].

3.3.1 Shear Stress

Shear stress [77] is a type of stress that takes place when the applied force operates parallel to the material's cross-sectional area.

3.3.2 Normal Stress

Normal stress [77] is the kind of stress that takes place when an applied force operates perpendicular to a material's cross-sectional area.

3.4 Viscosity

Viscosity [77] is a physical characteristic of fluids that refers to the shear deformation of fluid. There are two ways to define the viscosity.

3.4.1 Dynamic Viscosity

Dynamic viscosity [77] also known as absolute viscosity (μ), is a measure that demonstrates how shear stress relates to the rate at which velocity varies inside a fluid. Mathematically

$$\text{Viscosity } (\mu) = \frac{\text{Shear Stress}}{\text{Velocity Gradient}}. \quad (3.2)$$

In the SI system, dynamic viscosity is quantified in units as Ns/m^2 or $kg/m.s$ with dimensions $\left[\frac{M}{LT}\right]$.

3.4.2 Kinematic Viscosity

Kinematic viscosity [77] can be expressed as the ratio of dynamic viscosity to the density of the fluid. Mathematically,

$$\nu = \frac{\mu}{\rho}, \quad (3.3)$$

where μ and ρ signifies the viscosity and density. In the SI system, kinematic viscosity is quantified in units as $\frac{m^2}{s}$ with dimension $\left[\frac{L^2}{T}\right]$.

3.5 Newton's Law of Viscosity

This statement indicates that the shear stress of a fluid and the velocity gradient it experiences are directly proportional. It has an associated mathematical expression as

$$\tau_{yx} \propto \frac{du}{dy}, \quad (3.4)$$

$$\tau_{yx} = k \frac{du}{dy}, \quad (3.5)$$

where $\left(\frac{du}{dy}\right)$ signifies the rate of strain and shear stress imposed on the fluid component is indicated by the symbol τ_{yx} [77].

3.6 Newtonian Fluids

Newtonian fluids [78] are characterized by their adherence to Newton's viscosity law, which states that there is a linear relationship between velocity gradients and shear stress. Examples of Newtonian fluids include commonly encountered substances such as water, glycerin, air, milk, honey and alcohol.

3.7 Non-Newtonian Fluids

Non-Newtonian fluids [78] are those that fail to adhere to Newton's law of viscosity and have a nonlinear relationship between shear stress and strain rate. This link may be mathematically represented as follows

$$\tau_{yx} \propto \left(\frac{du}{dy}\right)^n \quad n \neq 1, \quad (3.6)$$

$$\tau_{yx} = \eta \left(\frac{du}{dy}\right)^n, \quad \eta = k \left(\frac{du}{dy}\right)^{n-1}, \quad (3.7)$$

whereas flow behavior index is indicated by n , consistency index is denoted by k , and the apparent viscosity is denoted by η . Non-Newtonian fluids include well-known fluids such as blood, toothpaste, and ketchup.

3.8 Nanofluids

Nanofluids [78] are fluids containing nanoparticle that are made through the mixture of suspensions of colloidal nanoparticles in a base fluid.

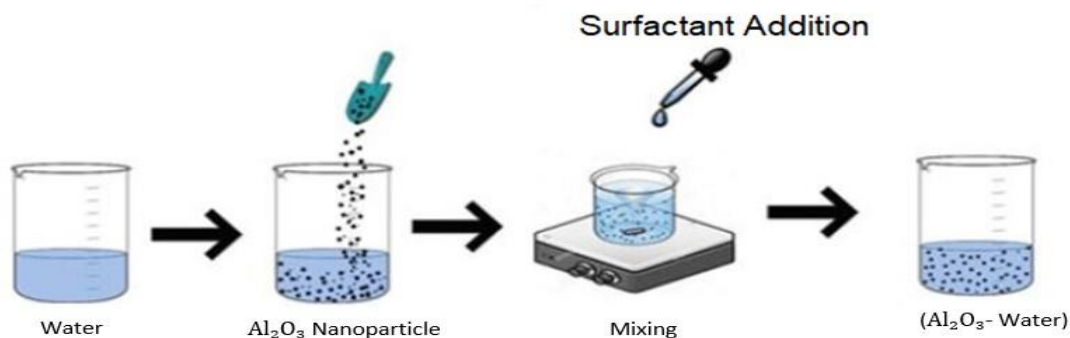


Figure 3.1: Nanofluid.

3.9 Hybrid Nanofluids

The advanced type of nanofluids are hybrid nanofluids that are created by combining two distinct kind of nanoparticles within a base fluid [78].

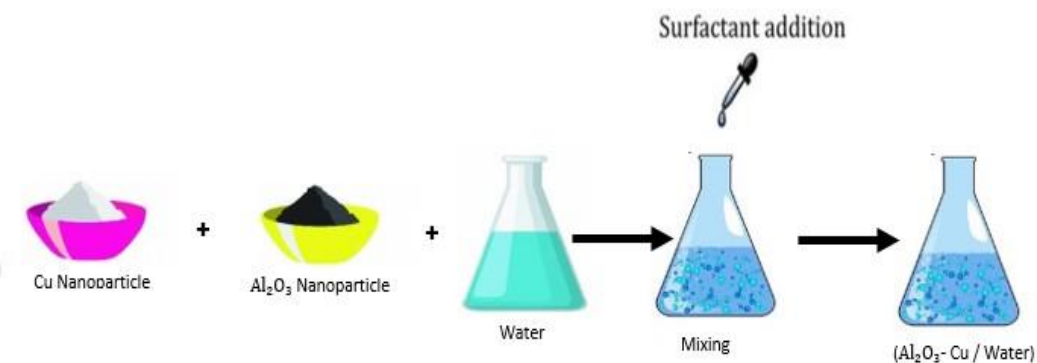


Figure 3.2: Hybrid nanofluid.

3.5 Flow

The term flow [78] refers to the movement of either liquids or gases through a medium. When uneven forces are exerted on the flow of fluid, then fluid motion remain

for as long as the imbalanced forces are exerted. There are different kinds of flow that are discussed below.

3.5.1 Compressible Flow

A flow in which the fluid's density keeps on varying with the flow, is specified as compressible flow [78]. It is essential in a variety of fluid systems, especially those that comprise high velocity and deviations in pressure or temperature such as the creation of supersonic aircraft or rocket engines.

3.5.2 Incompressible Flow

A flow in which the density of fluid remains constant during the entire flow is designated as incompressible flow [78]. In the construction of a turbine or pump, for instance, where the fluid is moving at a slow rate and with little variations in density, incompressible flow may be assumed.

3.5.3 Laminar Flow

The movement of fluid particles in parallel layers or along specified paths without intermixing or overlapping into each other can be termed as laminar flow [78]. Typically, flow is laminar when the fluid velocity is lower and viscosity is high.

3.5.4 Turbulent Flow

Movement of fluid is referred as turbulent flow [78] when the motion of fluid particles is characterized irregular and lacks a regular pattern or direction. Typically, flow is turbulent when the fluid velocity is higher and viscosity is lower.

3.5.5 Steady Flow

The flow is designated as steady flow [78] when attributes of fluid (like pressure, viscosity, velocity and density etc.) does not depend on time or it can be said that they are unaffected by time. Mathematically,

$$\frac{D\eta}{Dt} = 0, \quad (3.8)$$

where η represent the fluid attributes.

3.5.6 Unsteady Flow

Unsteady flow [78] happens if the fluid features (like density, viscosity, pressure and velocity etc.) alter at a specific point as time passes. Mathematically,

$$\frac{D\eta}{Dt} \neq 0. \quad (3.9)$$

For instance, while constructing power canals, unsteady flow is usually assumed.

3.11 Density

The ratio of a substance's mass with its volume or the amount per unit volume is designated as density [79]. It is represented by ρ . Mathematically,

$$\rho = \frac{m}{u}, \quad (3.10)$$

where m symbolizes the mass and u denotes the velocity. The SI system, density is quantified in units as kg/m^3 with dimensions $\left[\frac{M}{L^3}\right]$.

3.12 Pressure

The ratio of the force imposed on an object to the surface area it is exerted on, is designated as the pressure [79]. It refers to the exertion of physical forces on an object. Mathematically,

$$P = \frac{F}{A}, \quad (3.11)$$

where F indicates the force and A indicates the area. In SI system, pressure is quantified in units as N/m^2 with dimensions $ML^{-1}T^{-2}$.

3.13 Thermal Conductivity

The property of a substance to transmit heat is termed as thermal conductivity [79]. Mathematically,

$$\begin{aligned} \text{Thermal conductivity} &= \frac{\text{Heat} \times \text{Distance}}{\text{Area} \times \text{Temperature gradient}} \\ k &= \frac{Q \times L}{A \times \Delta T}, \end{aligned} \quad (3.12)$$

where k is designated for thermal conductivity, A indicates the area of cross section, Q represents flow of heat per unit time and ΔT denotes temperature difference. In SI system thermal conductivity is quantified in unit as $kg \cdot m/s^3K$ with dimensions $\left[\frac{ML}{T^3\theta}\right]$.

3.14 Thermal Diffusivity

The relationship that exists among heat conduction and the total material's density and specific heat capacity can be measured as thermal diffusivity [79]. Mathematically,

$$\alpha = \frac{k}{\rho c_p}, \quad (3.13)$$

where ρ is the density, k is the thermal conductivity and c_p is the specific heat capacity.

The provided units of thermal diffusivity in SI system are m^2/s and dimensions are $\left[\frac{L^2}{T}\right]$.

3.15 Methods of Heat Transfer

Heat is transmitted from one location to another in three forms which are radiation, convection and conduction [79].

3.15.1 Conduction

Conduction [79] is the transmission of heat from a higher temperature zone to a lower temperature zone by the collisions and interaction of particles of a substance

3.15.2 Convection

The process of heat transfer in which heat travels from a hot to a cool position due to the mobility of the fluid's particles is defined as convection. Mathematically,

$$Q = h \times A \times \nabla T, \quad (3.14)$$

where the coefficient of convective transfer of heat is h , the surface area is A , and the temperature difference is ∇T [79].

3.15.1 Forced Convection

The procedure of transferring heat for fluid flow when it is intentionally placed in motion by external forces such as pumps, mechanical devices and fans is termed as forced convection [79].

3.15.2.2 Natural Convection

Natural convection [79] or free convection is triggered by the buoyancy forces caused by density variations. The examples of free convection are the sea breeze, land breeze and rise of warm air etc.

3.15.2.3 Mixed Convection

Mixed convection [79] is a kind of convection that takes place when natural and forced convection exist together typically as an outcome of the interaction of external forces and buoyancy forces.

3.15.3 Radiation

Radiation [79] is a mechanism through which thermal energy gets transmitted as particles or waves throughout a medium. Radiation is particularly use in energy production like nuclear power plant, radiation therapy, medical diagnosis, imaging and in food preservation.

3.16 Dimensionless Numbers

3.16.1 Reynolds Number

The association between inertial forces and viscous forces in a fluid that flows is illustrated by the Reynolds number [80]. In mathematical form,

$$Re = \frac{\text{inertial forces}}{\text{viscous forces}}, \quad (3.15)$$

$$Re = \frac{\rho v^2 / L}{\mu u / L^2} = \frac{\nu L}{u}, \quad (3.16)$$

where ρ be the density, velocity is denoted by u , L be the characteristic, μ is the dynamic viscosity and ν be the kinematic viscosity. It helps to figure out whether the fluid flow is turbulent or laminar.

3.16.2 Prandtl Number

The non-dimensional number that shows the association between kinematic viscosity and thermal diffusivity is illustrated as Prandtl number [80]. Mathematically,

$$Pr = \frac{\text{viscous diffusion rate}}{\text{thermal diffusion rate}}, \quad (3.17)$$

$$Pr = \frac{\nu}{\alpha^*} = \frac{\mu/\rho}{k/\rho c_p} = c_p \mu / k, \quad (3.18)$$

where α^* is the thermal diffusivity, k is thermal conductivity, c_p is specific heat capacity and ν is the kinematic viscosity.

3.16.3 Eckert Number

The non-dimensional quantity that characterize the connection between the kinetic and thermal energy in fluid flow.

$$Ec = \frac{\text{kinetic energy}}{\text{thermal energy}} = \frac{u^2}{c_p \nabla T}, \quad (3.19)$$

where u , c_p , ∇T are the velocity, specific heat capacity and temperature difference of fluid [80].

3.16.4 Nusselt Number

The quantity that characterize the relationship between conductive and convective heat flow throughout the boundary is referred as the Nusselt number [80]. Mathematically,

$$Nu_x = \frac{\text{Convective heat transfer}}{\text{Conductive heat transfer}} = \frac{hL}{k}, \quad (3.20)$$

where k be the thermal conductivity, L be the characteristic length and h be the coefficient of convective heat transfer.

3.16.5 Skin Friction

The particular type of friction that is skin friction [80] occur when a fluid, such water or air, flows over a surface that is solid. It arises because of the difference in velocities within the fluid layers that come in contact with the surface of the solid. Mathematically,

$$\text{Skin friciton} = C_f = \frac{\tau_w}{\frac{1}{2}\rho u^2}, \quad (3.21)$$

where ρ , u be the density and velocity of fluid and τ_w be the shear stresses at the wall. The drag formed by the viscous stresses at the boundary layer produces skin friction. Skin friction has lesser impact in laminar flow because the boundary layer is less than it is in turbulent flow.

3.16.6 Grashof Number

It illustrates how buoyancy forces respond against the viscous forces in a moving fluid. It is used in laminar systems for establishing the fluid boundary layer. Mathematically,

$$Gr = \frac{L^3}{\nu^2} g\beta(T - T_\infty), \quad (3.22)$$

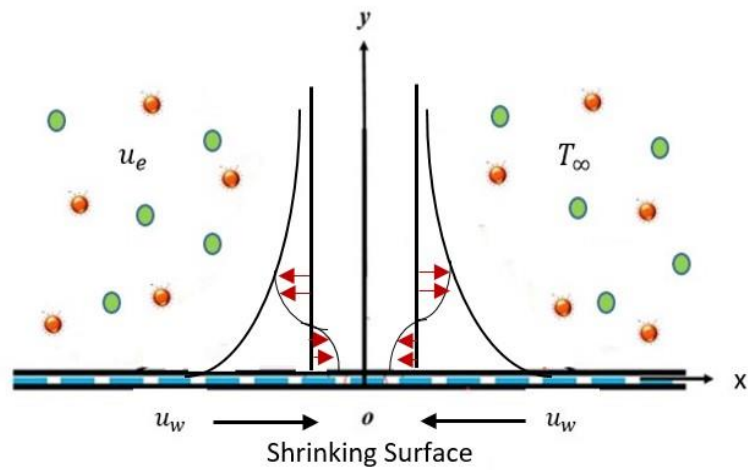
where β be the coefficient of volumetric thermal expansion, g be the acceleration due to gravity, ν be the kinematic viscosity, L be the characteristic length, T be the fluid and surrounding temperature and T_∞ be the ambient temperature respectively [80].

Chapter 4

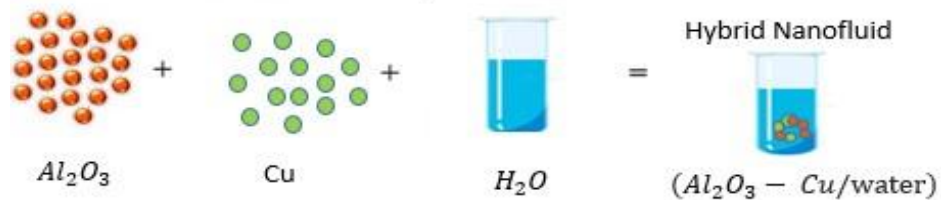
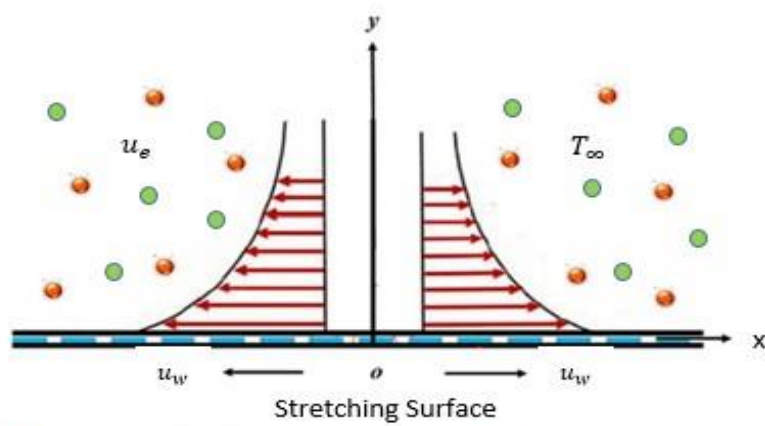
The Stagnation Point Flow of Hybrid Nanofluid Flow past a Shrinking Surface

4.1 Introduction

Many scientists are engaged in exploring how hybrid nanofluids behave due to their unique thermodynamic properties. The stagnation point flow of hybrid nanofluid over a linearly stretching/shrinking surface is analyzed in this chapter. Heat transfer analysis also is performed in the study. The governing PDEs of the fluid model can be rendered in a system of ODEs by employing a suitable similarity technique. By employing the Bvp4c method in MATLAB, graphical demonstration of velocity as well as temperature and the corresponding skin friction coefficient and Nusselt number are presented. The authenticity of the results is validated by conducting a comparative analysis of the already present literature.



(a) Shrinkage Surface



(b) Stretching Surface

Figure 4.1: Physical model.

4.2 Mathematical Formulation of Fluid Model

The current model relies on the stagnation point flow of an incompressible, viscous and steady flow of hybrid nanofluid. Cu and Al_2O_3 are the considered as nanoparticles while the basefluid will be water. The fluid is flowing across a horizontally stretching/shrinking surface

along x -axis with $u_w(x) = U_w x$ given as its surface velocity and T_w is the wall temperature. The free stream velocity will be $u_e(x) = U_e x$ and the ambient temperature is T_∞ .

The velocity field considered for this model is expressed as

$$\mathbf{V} = [u(x, y), v(x, y), 0]. \quad (4.1)$$

The governing equations for fluid problem of current model is represented by continuity, momentum and as well as energy equation which are given in the form as

$$\frac{\partial \rho}{\partial t} + \nabla \cdot (\rho \mathbf{V}) = 0, \quad (4.2)$$

$$\rho_{hnf} \left[\frac{\partial \mathbf{V}}{\partial t} + (\mathbf{V} \cdot \nabla) \mathbf{V} \right] = \nabla \cdot \boldsymbol{\tau} + \rho_{hnf} \mathbf{b}, \quad (4.3)$$

$$(\rho c_p)_{hnf} \left[\frac{\partial T}{\partial t} + (\mathbf{V} \cdot \nabla) T \right] = -\nabla \cdot \mathbf{q} + \text{Tr}(\boldsymbol{\tau} \cdot \mathbf{L}) + q_r, \quad (4.4)$$

$$\mathbf{q} = -k \text{grad } T,$$

where \mathbf{V} indicates the fluid velocity, ρ_{hnf} indicates the fluid density, \mathbf{b} denotes the body force, $(c_p)_{hnf}$ designated specific heat capacity, T indicates the temperature, $\boldsymbol{\tau} = -p\mathbf{I} + \mu\mathbf{A}_1$ indicates the Cauchy stress tensor, $\mathbf{A}_1 = \nabla \mathbf{V} + (\nabla \mathbf{V})^t$ represents the first Erikson tensor, $\mathbf{L} = \nabla \mathbf{V}$ symbolizes velocity gradient, \mathbf{q} indicates the heat flux, k denotes the thermal conductivity and q_r is designated as radiative heat flux .

After the implementation of boundary layer assumptions, the following subsequent equations are obtained.

$$\frac{\partial u}{\partial x} + \frac{\partial v}{\partial y} = 0, \quad (4.5)$$

$$u \frac{\partial u}{\partial x} + v \frac{\partial v}{\partial y} = u_e \frac{\partial u_e}{\partial x} + \frac{\mu_{hnf}}{\rho_{hnf}} \frac{\partial^2 u}{\partial y^2}, \quad (4.6)$$

$$u \frac{\partial T}{\partial x} + v \frac{\partial T}{\partial y} = \frac{k_{hnf}}{(\rho c_p)_{hnf}} \frac{\partial^2 T}{\partial y^2}. \quad (4.7)$$

The following boundary conditions are provided by the current model.

$$u = u_w(x) = U_w x \text{ and } v = 0, \quad T = T_w \quad \text{at } y = 0, \quad (4.8)$$

$$u \rightarrow u_e(x) = U_e x \quad \text{and } T \rightarrow T_\infty \quad \text{as } y \rightarrow \infty, \quad (4.9)$$

where u and v are designated as the velocity components, U_e and U_w symbolizes arbitrary constants, $u_w(x)$ indicate stretching velocity, T_w specifies the wall temperature, $u_e(x)$ indicates the free stream velocity and T_∞ represents the ambient temperature.

The local Nusselt number (Nu_x) and the skin-friction coefficient (C_f) are the quantities that have immense significance and are given as

$$C_f = \frac{\mu_{hnf}}{\rho_f u_e^2} \left(\frac{\partial u}{\partial y} \right)_{y=0}, \quad Nu_x = - \frac{x k_{hnf}}{k_f (T_w - T_\infty)} \left(\frac{\partial T}{\partial y} \right)_{y=0}, \quad (4.10)$$

where $\tau_w = \mu_{hnf} \left(\frac{\partial u}{\partial y} \right)_{y=0}$ signifies surface shear stress and $q_w = -k_{hnf} \left(\frac{\partial T}{\partial y} \right)_{y=0}$ is the heat flux.

Tables 4.1 & 4.2 provide a brief description of the thermophysical characteristics of conventional and hybrid nanofluids.

Table 4.1: Thermophysical characteristics of nanofluid (Al_2O_3/H_2O) [81], [82].

Properties	Nanofluid
Density (ρ)	$\rho_{nf} = (1 - \phi_{s1})\rho_f + \phi_{s1}\rho_{s1}$
Specific Heat capacity (C_p)	$(\rho C_p)_{nf} = (1 - \phi_{s1})(\rho C_p)_f + \phi_{s1}(\rho C_p)_{s1}$
Dynamic Viscosity (μ)	$\mu_{nf} = \frac{\mu_f}{(1 - \phi_{s1})^{2.5}}$
Thermal Conductivity (k)	$\frac{k_{nf}}{k_f} = \frac{k_{s1} + 2k_f - 2\phi_{s1}(k_f - k_{s1})}{k_{s1} + 2k_f + \phi_{s1}(k_f - k_{s1})}$

Table 4.2: Thermophysical characteristics of hybrid nanofluid ($Al_2O_3 - Cu/H_2O$) [81], [82].

Properties	Hybrid Nanofluid
Density (ρ)	$\frac{\rho_{hnf}}{\rho_f} = (1 - \phi_{s2}) \left[(1 - \phi_{s1}) + \phi_{s1} \frac{\rho_{s1}}{\rho_f} \right] + \phi_{s2} \frac{\rho_{s2}}{\rho_f}$
Specific Heat capacity (C_p)	$\frac{(\rho C_p)_{hnf}}{(\rho C_p)_f} = (1 - \phi_{s2}) \left[(1 - \phi_{s1}) + \phi_{s1} \frac{(\rho C_p)_{s1}}{(\rho C_p)_f} \right] + \phi_{s2} \frac{(\rho C_p)_{s2}}{(\rho C_p)_f}$
Dynamic Viscosity (μ)	$\frac{\mu_{hnf}}{\mu_f} = \frac{1}{(1 - \phi_1)^{2.5} (1 - \phi_2)^{2.5}}$
Thermal conductivity (k)	$\frac{k_{nf}}{k_f} = \left[\frac{k_{s2} + 2k_{nf} - 2\phi_{s2}(k_{nf} - k_{s2})}{k_{s2} + 2k_{nf} + \phi_{s2}(k_{nf} - k_{s2})} \right] \times \left[\frac{k_{s1} + 2k_{nf} - 2\phi_{s1}(k_{nf} - k_{s1})}{k_{s1} + 2k_{nf} + \phi_{s1}(k_{nf} - k_{s1})} \right]$

Table 4.3: Thermophysical properties of hybrid nanofluid ($Al_2O_3 - Cu/H_2O$) [81], [82].

Properties	Water	Al_2O_3	Cu
$\rho(kg/m^3)$	997.0	3970	8933
$C_p(J/kgK)$	4180	765	385
$k(W/mK)$	0.613	40	400
Prandtl number (Pr)	6.2	-	-

The similarity dimensionless variables are considered for the flow problem [83].

$$\eta = \left(\frac{U_e}{v_f}\right)^{\frac{1}{2}} y, \quad \psi = (U_e v_f)^{\frac{1}{2}} x f(\eta), \quad \theta(\eta) = \frac{T - T_\infty}{T_w - T_\infty}, \quad (4.11)$$

$$u = U_e x f'(\eta), \quad v = -(U_e v_f)^{\frac{1}{2}} f(\eta). \quad (4.12)$$

In which ψ is the stream function and v_f is the kinematic viscosity of base fluid. In highlight of Eqs. (4.11) and (4.12), the continuity equation (4.5) is clearly satisfied and the rest of the Eqs. (4.6) - (4.9), reduce as

$$\frac{\frac{\mu_{hnf}}{\rho_{hnf}}}{\rho_f} f''''(\eta) - f'(\eta)^2 + f''(\eta) f(\eta) + 1 = 0, \quad (4.13)$$

$$\frac{1}{Pr} \frac{(k)_{hnf}}{(k)_f} \theta''(\eta) + \frac{(\rho C_p)_{hnf}}{(\rho C_p)_f} f(\eta) \theta'(\eta) = 0, \quad (4.14)$$

$$f(0) = 0, \quad f'(0) = \lambda_1, \quad \theta(0) = 1 \quad \text{at} \quad \eta = 0, \quad (4.15)$$

$$f'(\infty) \rightarrow 1, \quad \theta(\infty) \rightarrow 0 \quad \text{as} \quad \eta \rightarrow \infty. \quad (4.16)$$

The dimensionless terms used in the above equations are $\lambda_1 = \frac{U_w}{U_e}$ representing the stretching parameter and $Pr = \frac{(\mu C_p)_f}{k_f}$ is the Prandtl number. Additionally, the dimensionless forms of Nu_x and C_f are attainable as

$$(Re_x)^{\frac{1}{2}} C_f = \frac{\mu_{hnf}}{\mu_f} f''(0), \quad (Re_x)^{-\frac{1}{2}} Nu_x = -\frac{k_{hnf}}{k_f} \theta'(0), \quad (4.17)$$

where the local Reynolds number is $Re_x = \frac{x u_e(x)}{v_f}$.

Also to avoid complexity, the simple symbols are used

$$a = \frac{\mu_{hnf}}{\mu_f}, \quad b = \frac{\rho_f}{\rho_{hnf}}, \quad c = \frac{(\rho C_P)_{hnf}}{(\rho C_P)_f} \text{ and } K = \frac{k_{hnf}}{k_f}, \quad (4.18)$$

$$\frac{a}{b} f'''(\eta) - f'(\eta)^2 + f''(\eta) f(\eta) + 1 = 0, \quad (4.19)$$

$$\frac{1}{Pr} K \theta''(\eta) + c f(\eta) \theta'(\eta) = 0. \quad (4.20)$$

4.3 Numerical Stratagem

The governing flow ODEs are solved in MATLAB by employing the bvp4c package. The higher order differential equations are transformed into first order form, and then further executed by MATLAB bvp4c technique. [84] & [85].

$$f = y(1), \quad (4.21)$$

$$f' = y(2) = y'(1), \quad (4.22)$$

$$f'' = y(3) = y'(2), \quad (4.23)$$

$$\theta = y(4), \quad (4.24)$$

$$\theta' = y(5) = y'(4), \quad (4.25)$$

$$y'(3) = -\frac{b}{a} [-\{y(2)\}^2 + y(1) y(3) + 1], \quad (4.26)$$

$$y'(5) = -Pr \left[\frac{c}{K} y(1) y(5) \right]. \quad (4.27)$$

With boundary conditions

$$y_0(1) = 0, \quad y_0(2) = \lambda_1, \quad y_0(4) = 1 \quad \text{at} \quad \eta = 0, \quad (4.28)$$

$$y_\infty(2) \rightarrow 1, \quad y_\infty(4) \rightarrow 0 \quad \text{as} \quad \eta \rightarrow \infty. \quad (4.29)$$

4.4 Graphical Analysis and Discussion

The stagnation point flow of hybrid nanofluid flow is analyzed. This section meticulously highlights the significant influence caused by numerous dimensionless parameters upon velocity as well as temperature profile and coefficient of skin friction and Nusselt number. Thus induce the essential outturns of dimensionless parameters on the considerable entities through implementing numerical technique (bvp4c code) in MATLAB. The reliable dimensionless parameters that impact the velocity profile $f'(\eta)$ and temperature field $\theta(\eta)$ are λ_1 the stretching parameter and the nanoparticle volume fraction ϕ_2 . Firstly, an increase in solid nanoparticle volume fraction ϕ_2 brings about continual positive influence on velocity profile and is represented in Figure 4.2. The increase in the velocity profile is obvious through the raised values of ϕ_2 . Figure 4.3 illustrates the alterations in velocity against raising λ_1 , for which a decline in results for velocity is recorded. Figure 4.4 demonstrates the effect of nanoparticle volume fraction ϕ_2 on the temperature profile. It is evident from the figure that an increases in ϕ_2 corresponds to the decline in the temperature profile. Figure 4.5 reveals the increase of stretching parameter λ_1 on the temperature profile and the figure shows that the profile boosts up. Figure 4.6 is sketched to show the influence of Prandtl number Pr on the temperature profile and the raising values of Pr produce reduction in the temperature profile. Figure 4.7 signifies the variations of skin friction coefficient about λ_1 with altered values of ϕ_2 . The consequences specify that mounting ϕ_2 , the skin friction above the surface goes higher and change its behavior later on. The reversing behavior is also observed for λ_1 . Furthermore, Figure 4.8 the Nusselt number behavior is illustrated with the increasing range of λ_1 stretching parameter and volume concentration of copper ϕ_2 . An effective rate of heat transfer is attained with the rising λ_1 and ϕ_2 . The numerical values of skin friction coefficient $f''(0)$, by altering λ_1 while maintaining a small range of other physical constants are compared. These numerical values of friction drag are shown in Table 4.4 and have been compared with the findings made by Wang [86], Bachok *et al.* [87] and Waini *et al.* [89]. Moreover, the numerical values of Nusselt number have been calculated and the values of Nusselt number increase with the rising values of λ_1 . Additionally, Table 4.5 presents the values of $f''(0)$ and $-\theta'(0)$ under different values of λ_1 , ϕ_1 and ϕ_2 when $Pr = 6.2$. It illustrates that the values of $f''(0)$ and $-\theta'(0)$ accelerate with the rise of ϕ_2 for the case of rigid surface ($\lambda_1 = 0$). In contrast to (Cu /water, $\phi_1 = 0$), these physical quantities are greater for ($Cu - Al_2O_3$ /water, $\phi_1 = 0.05$). Further the

reduction in $f''(0)$ and a rise in $-\theta'(0)$ is seen for larger λ_1 with range -0.5 to 0.5. The values of $f''(0)$ and $-\theta'(0)$ are comparable to those found by Waini *et al.* [88].

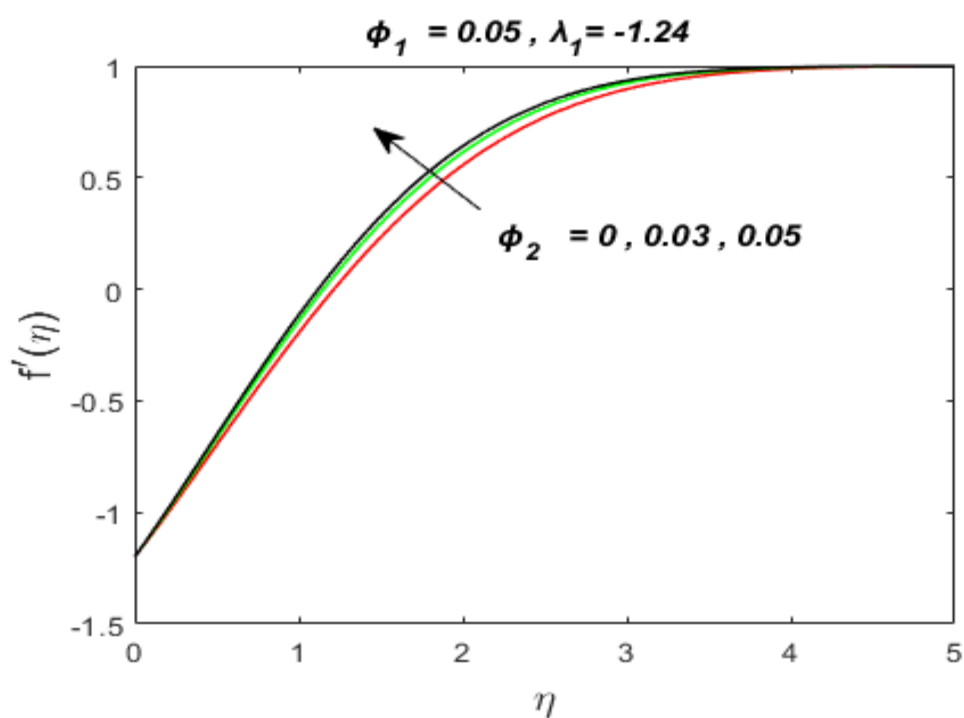


Figure 4.2: Effect of nanoparticle volume fraction ϕ_2 of *Cu* upon $f'(\eta)$.

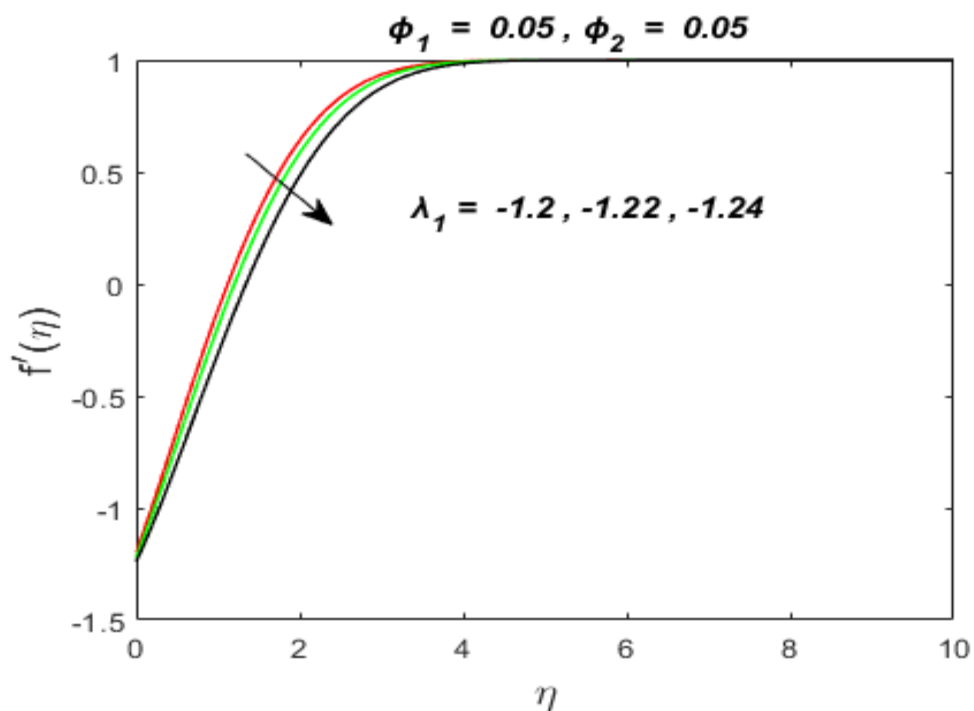


Figure 4.3: Effect of stretching parameter λ_1 upon $f'(\eta)$.

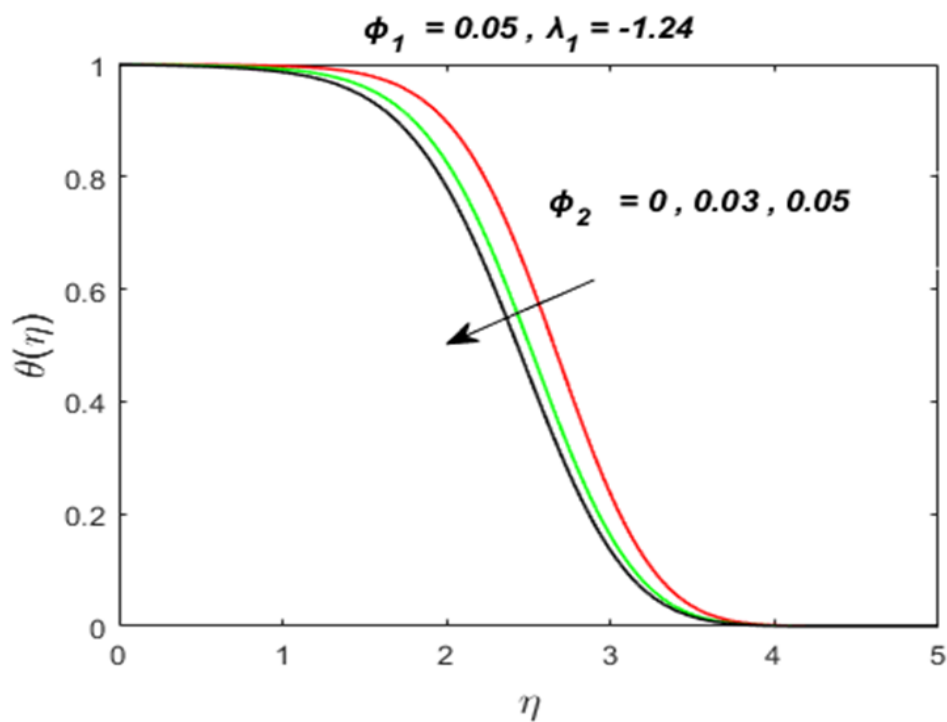


Figure 4.4: Effect of nanoparticle volume fraction ϕ_2 of Cu upon $\theta(\eta)$.

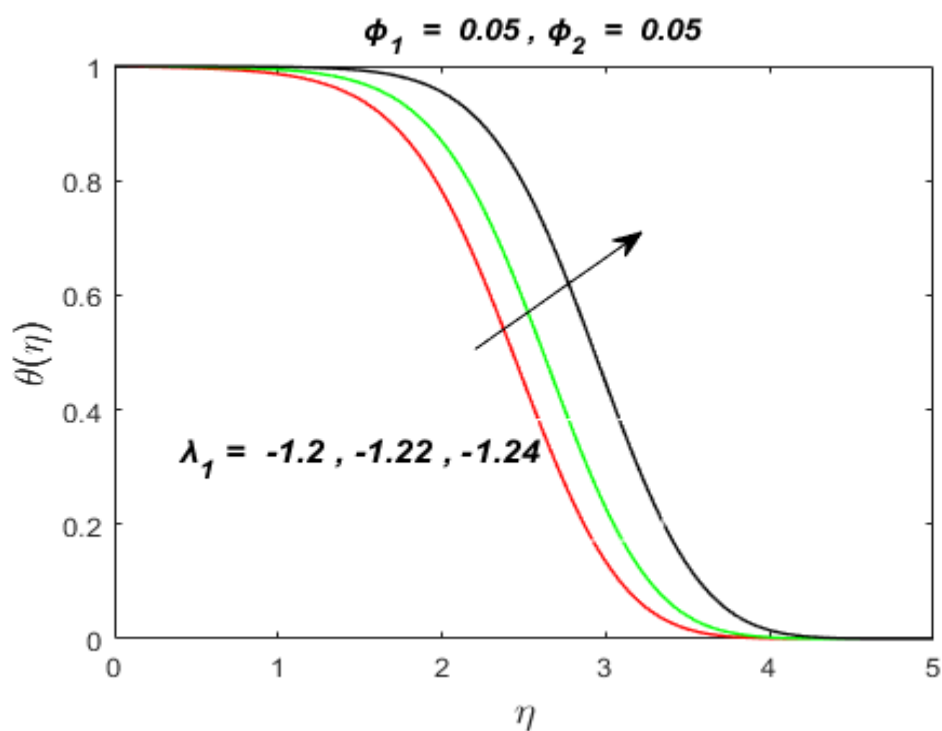


Figure 4.5: Effect of stretching parameter λ_1 upon $\theta(\eta)$.

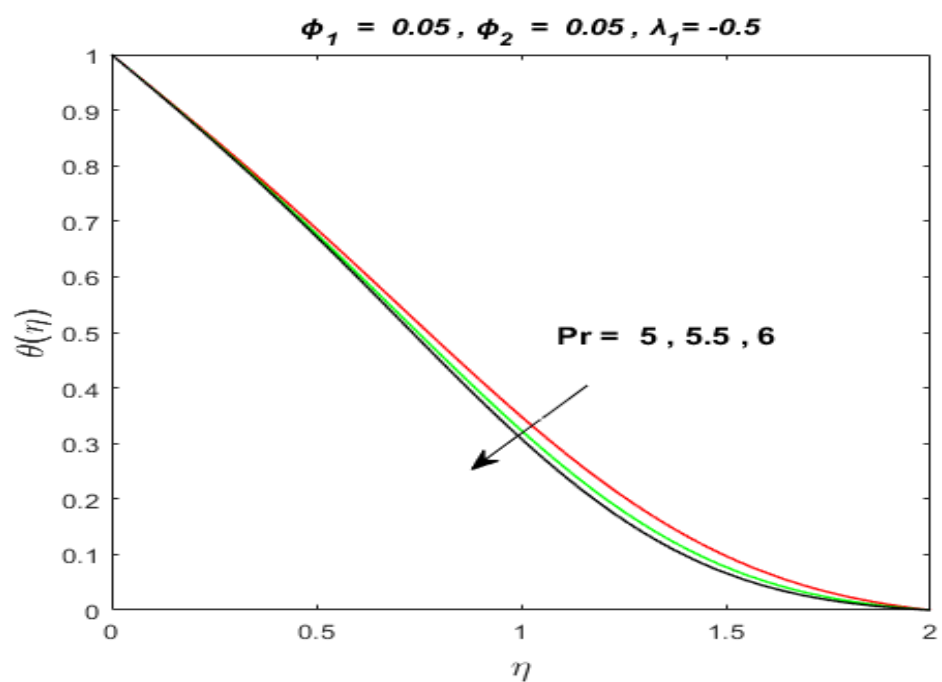


Figure 4.6: Effect of Prandtl number Pr upon $\theta(\eta)$.

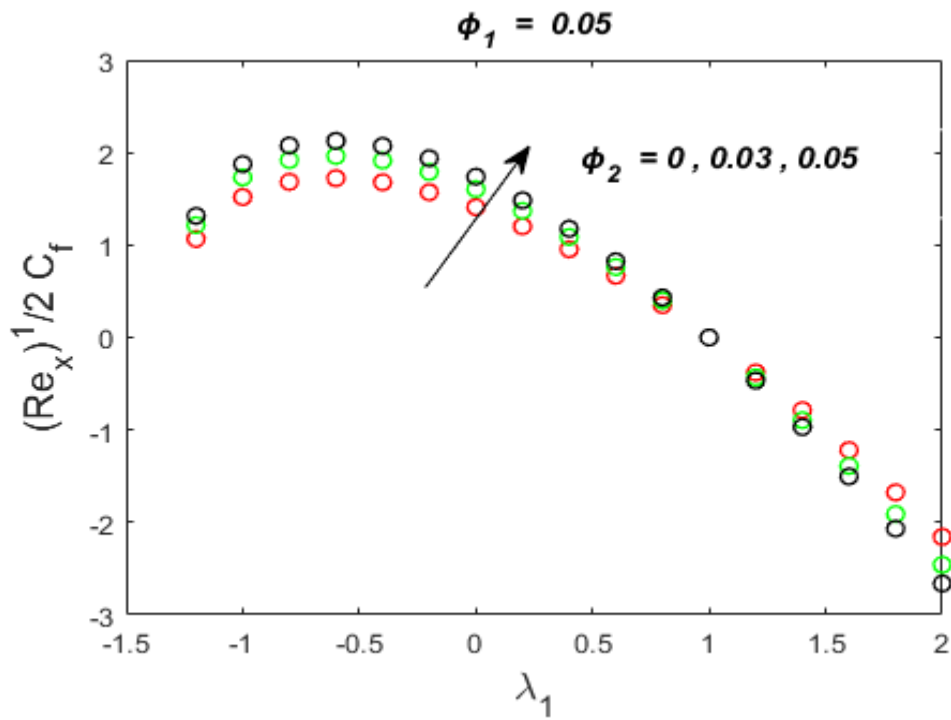


Figure 4.7: Skin Friction towards λ_1 with various values of ϕ_2 .

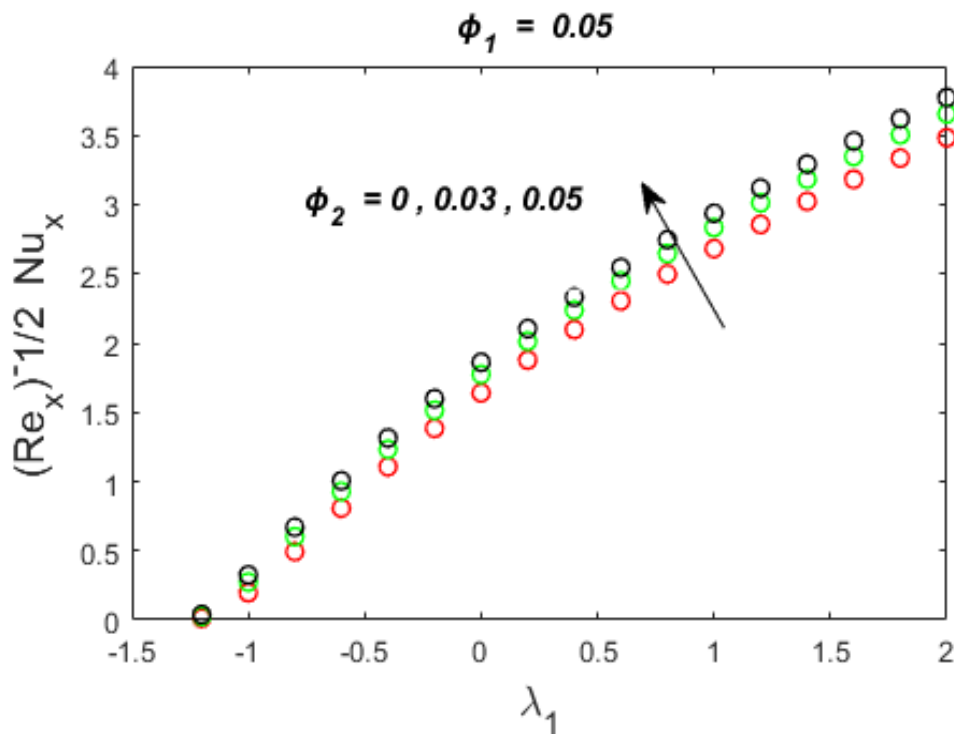


Figure 4.8: Nusselt Number towards λ_1 with various values of ϕ_2 .

Table 4.4: Comparative values of stretching parameter λ_1 on $f''(0)$ and $-\theta'(0)$ if ($\phi_1 = \phi_2 = 0$).

λ_1	Wang [86]	Bachok <i>et al.</i> [87]	Waini <i>et al.</i> [89]	Present Results	
	$f''(0)$	$f''(0)$	$f''(0)$	$f''(0)$	$-\theta'(0)$
2.0	-1.88731	-1.887307	-1.887307	-1.887306490	2.627736190
1.0	0	0	0	0	1.986760057
0.5	0.71330	0.713295	0.713295	0.713293939	1.595480754
0.0	1.232588	1.232588	1.232588	1.232586110	1.127977904
-0.5	1.49567	1.495670	1.495670	1.495667433	0.558409442
-1	1.32882	1.328817	1.328817	1.328814048	0.043554855
-1.15	1.08223	1.082231	1.082231	1.082230540	0.002617194

Table 4.5: Comparative values of $f''(0)$ and $-\theta'(0)$ for various values of ϕ_2 , λ_1 and ϕ_1 if $Pr = 6.2$.

ϕ_2	λ_1	Waini <i>et al.</i> [88] $\phi_1 = 0$ (Cu/water)		Waini <i>et al.</i> [89]				Present Results			
				$\phi_1 = 0$ (Cu/water)		$\phi_1 = 0.05$ (Cu-Al ₂ O ₃ /water)		$\phi_1 = 0$ (Cu/water)		$\phi_1 = 0.05$ (Cu-Al ₂ O ₃ /water)	
		$f''(0)$	$-\theta'(0)$	$f''(0)$	$-\theta'(0)$	$f''(0)$	$-\theta'(0)$	$f''(0)$	$-\theta'(0)$	$f''(0)$	$-\theta'(0)$
0	0	-	-	1.232588	1.127964	1.408763	1.229275	1.232587676	1.127964367	1.408763013	1.229274844
0.03	0	-	-	1.425110	1.213918	1.605715	1.317395	1.425109996	1.213918328	1.605715180	1.317394637
0.05	0	-	-	1.553850	1.269379	1.738637	1.374810	1.553849595	1.269379146	1.738636826	1.374809951
0.05	-0.5	1.885501	0.706314	1.885501	0.706314	2.109729	0.791231	1.885501498	0.706314063	2.109729515	0.791230825
0.05	0	1.553850	1.269379	1.553850	1.269379	1.738637	1.374810	1.553849595	1.269379146	1.738636826	1.374809951
0.05	0.5	0.899208	1.733859	0.899208	1.733859	1.006144	1.856885	0.899208322	1.733859221	1.006144165	1.856884600

Chapter 5

The Mixed Convection Flow of Hybrid Nanofluid Flow over a Riga Plate in a Porous Medium

5.1 Introduction

The prime focuses of this chapter is to study the flow behavior of a hybrid nanofluid ($Cu - Al_2O_3/H_2O$) with mixed convection near a stagnation point and the fluid is induced by a Riga plate. The mass and heat transfer is analyzed under the impact of viscous dissipation, thermal radiation, mixed convection, Joule heating and as well as heat generation/absorption. The governing complex coupled PDEs of the model are reduced into ODEs via employing the technique of similarity transformation, then further the `bvp4c` function in MATLAB software is used for generating the numerical results of nonlinear ODEs. For several important parameters, the temperature and velocity distributions are also analyzed. The graphical influence of various parameters is examined for skin friction and Nusselt number. For the authenticity of the obtained results, comparison study is carried out in correspondence with the previous research.

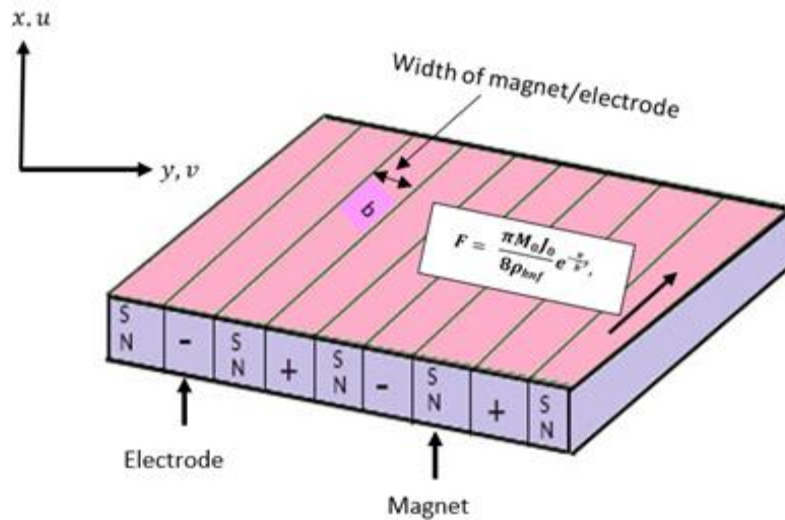


Figure 5.1: An illustration of Riga plate.

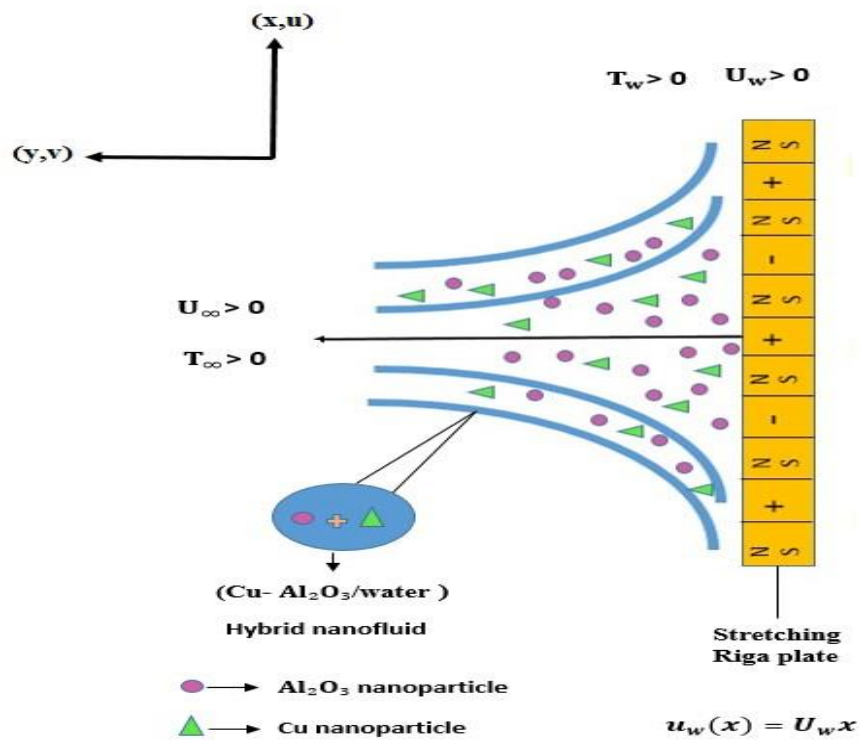


Figure 5.2: An illustration of flow toward Riga plate in Cartesian coordinate system.

5.2 Mathematical Construction of Model

The present model consider water as the regular fluid with ($Al_2O_3 - Cu$) hybrid nanoparticles in spherical shape and in thermal equilibrium state. The steady, laminar and incompressible mixed convection and stagnation point flow over a vertically placed Riga plate

is examined. The Riga plate is composed of electrodes and magnets arranged alternatively having the identical width b . The magnet's polarity is indicated by the letters north (N) and south (S) and electromagnetic field of riga plate generates the Lorentz force that is parallel to wall. When the flow is in uniform direction the uniform magnetic field is applied along y - axis, i.e., $\mathbf{B} = (0, B_0, 0)$, meanwhile, the fluid is electrically conducting because of an electric field figured to be $\mathbf{E} = (0, 0, -E_0)$ along negative z -axis with both fields adhering to Ohm's law [90]. The flow of fluid is along x -axis over a vertical riga plate that is radiated with uniform temperature $T_w > 0$ having condition $T_w > T_\infty$ and stretching with $u_w(x) = U_w x$ as its linearly stretching velocity where $U_w > 0$. The free stream velocity is assumed to be $u_e(x) = U_e x$ and T_∞ is the ambient temperature. Figure 5.2. projects the physical layout with $Al_2O_3 - Cu/H_2O$ hybrid nanofluid flow restricted to $y \geq 0$.

The velocity profile which this model takes into account is demonstrated as

$$\mathbf{V} = [u(x, y), v(x, y), 0]. \quad (5.1)$$

For the current model, the governing equations are expressed in the form as

$$\frac{\partial \rho}{\partial t} + \nabla \cdot (\rho \mathbf{V}) = 0, \quad (5.2)$$

$$\rho_{hnf} \left[\frac{\partial \mathbf{V}}{\partial t} + (\mathbf{V} \cdot \nabla) \mathbf{V} \right] = \nabla \cdot \boldsymbol{\tau} + \rho_{hnf} \mathbf{b}, \quad (5.3)$$

$$\text{where } \boldsymbol{\tau} = -p\mathbf{I} + \mu \mathbf{A}_1 \text{ and } \mathbf{A}_1 = \nabla \mathbf{V} + (\nabla \mathbf{V})^t$$

$$(\rho c_p)_{hnf} \left[\frac{\partial T}{\partial t} + (\mathbf{V} \cdot \nabla) T \right] = -\nabla \cdot \mathbf{q} + \text{Tr}(\boldsymbol{\tau} \cdot \mathbf{L}) + q_r, \quad (5.4)$$

$$\text{where } \mathbf{q} = -k \text{grad } T.$$

In Eqs. (5.2 to 5.4), the velocity field is introduced as \mathbf{V} , fluid density is indicated as ρ_{hnf} , the body force is denoted by \mathbf{b} , specific heat capacity is designated as $(c_p)_{hnf}$, the temperature is indicated as T , the Cauchy stress tensor is demonstrated as $\boldsymbol{\tau}$, heat flux is indicated as \mathbf{q} , the thermal conductivity is denoted by k and radiative heat flux is designated as q_r .

Moving forward, the PDEs are formed after the execution of boundary layer theory and the subsequent equations are obtained.

$$\frac{\partial u}{\partial x} + \frac{\partial v}{\partial y} = 0, \quad (5.5)$$

$$u \frac{\partial u}{\partial x} + v \frac{\partial v}{\partial y} = u_e \frac{\partial u_e}{\partial x} + \frac{\mu_{hnf}}{\rho_{hnf}} \frac{\partial^2 u}{\partial y^2} + \frac{\pi M_0 J_0}{8 \rho_{hnf}} e^{-\frac{\pi}{b}y} + \frac{g(\rho\beta)_{hnf}}{\rho_{hnf}} (T - T_\infty) - \frac{\mu_{hnf}}{\rho_{hnf}} \frac{(u-u_e)}{k'}, \quad (5.6)$$

$$u \frac{\partial T}{\partial x} + v \frac{\partial T}{\partial y} = \alpha_{hnf} \frac{\partial^2 T}{\partial y^2} - \frac{1}{(\rho C_P)_{hnf}} \left(\frac{\partial q_r}{\partial y} \right) + \frac{\mu_{hnf}}{(\rho C_P)_{hnf}} \left(\frac{\partial u}{\partial y} \right)^2 + \frac{\sigma_{hnf}}{(\rho C_P)_{hnf}} (B_0 u - E_0)^2 \quad (5.7)$$

$$+ \frac{Q_0}{(\rho C_P)_{hnf}} (T - T_\infty).$$

The following boundary conditions are delivered by the present model

$$u = u_w(x) = U_w x \text{ and } v = 0, \quad T = T_w \quad \text{at } y = 0, \quad (5.8)$$

$$u \rightarrow u_e(x) = U_e x \quad \text{and } T \rightarrow T_\infty \quad \text{as } y \rightarrow \infty, \quad (5.9)$$

where u and v nominate velocity components along x and y directions, U_w and U_e signifies arbitrary constants, $u_w(x)$ and $u_e(x)$ specify stretching and free stream velocities, T_w and T_∞ designates the wall and ambient temperatures. Moreover, in Eq. (5.6), $\frac{\pi M_0 J_0}{8 \rho_{hnf}} e^{-\frac{\pi}{b}y}$ term demonstrates the magnetic forces produced span-wise through Riga plate by the magnetization of the magnets (M_0) and the current density present in the electrodes (J_0). However, in Equation (5.7), $\frac{\partial q_r}{\partial y}$ designates rate of thermal radiation q_r all over the surface and $\mu_{hnf} \left(\frac{\partial u}{\partial y} \right)^2$ defines the rate of the viscous dissipation produced by the viscous aspects of hybrid nanofluid. Also $\frac{\sigma_{hnf}}{(\rho C_P)_{hnf}} (B_0 u - E_0)^2$ specifies Joule heating due to electric and magnetic fields of Riga plate. An estimated value of the radiative heat flux is [81] & [91]

$$q_r = -\frac{4 \sigma^*}{3 k^*} \frac{\partial T^4}{\partial y}, \quad (5.10)$$

where σ^* and k^* are mean absorption coefficient and Stefan-Boltzman constant respectively. The Taylor expansion of T^4 in form of T_∞ is indicated as $T^4 \approx 4T_\infty^3 T - 3T_\infty^4$ and thus,

$$q_r = -k_f \frac{4}{3} R \frac{\partial T}{\partial y}, \quad (5.11)$$

where radiation parameter nominated as $R = 4T_\infty^3 \left(\frac{\sigma^*}{k_f k^*} \right)$ and Eq. (5.7) take the form as

$$u \frac{\partial T}{\partial x} + v \frac{\partial T}{\partial y} = \frac{k_{hnf}}{(\rho C_P)_{hnf}} \left(1 + \frac{4}{3} \frac{k_f}{k_{hnf}} R \right) \frac{\partial^2 T}{\partial y^2} + \frac{\mu_{hnf}}{(\rho C_P)_{hnf}} \left(\frac{\partial u}{\partial y} \right)^2 \quad (5.12)$$

$$+ \frac{\sigma_{hnf}}{(\rho C_P)_{hnf}} (B_0 u - E_0)^2 + \frac{Q_0}{(\rho C_P)_{hnf}} (T - T_\infty).$$

The local Nusselt number (Nu_x) and the skin-friction coefficient (C_f) are given as

$$C_f = \frac{\mu_{hnf}}{\rho_f u_e^2} \left(\frac{\partial u}{\partial y} \right)_{y=0}, \quad Nu_x = \frac{x}{k_f (T_w - T_\infty)} \left[-k_{hnf} \left(\frac{\partial T}{\partial y} \right)_{y=0} + (q_r)_{y=0} \right], \quad (5.13)$$

where $\tau_w = \mu_{hnf} \left(\frac{\partial u}{\partial y} \right)_{y=0}$ and $q_w = -k_{hnf} \left(\frac{\partial T}{\partial y} \right)_{y=0}$ indicates surface shear stress and thermal flux.

The Table 5.1 and Table 5.2 summarize the thermo-physical characteristics of traditional and hybrid nanofluid and their correlations. Table 5.3 shows the physical properties of water and nanoparticles and Table 5.4 illustrates the dimensionless parameters involved in the problem.

Table 5.1: Thermophysical features of nanofluid (Al_2O_3/H_2O) [81, 92, 93].

Properties	Nanofluid
Density (ρ)	$\rho_{nf} = (1 - \phi_{s1})\rho_f + \phi_{s1}\rho_{s1}$
Specific Heat capacity (C_p)	$(\rho C_p)_{nf} = (1 - \phi_{s1})(\rho C_p)_f + \phi_{s1}(\rho C_p)_{s1}$
Dynamic Viscosity (μ)	$\mu_{nf} = \frac{\mu_f}{(1 - \phi_{s1})^{2.5}}$
Thermal Conductivity (k)	$\frac{k_{nf}}{k_f} = \frac{k_{s1} + 2k_f - 2\phi_{s1}(k_f - k_{s1})}{k_{s1} + 2k_f + \phi_{s1}(k_f - k_{s1})}$
Electrical conductivity (σ)	$\frac{\sigma_{nf}}{\sigma_f} = \frac{\sigma_{s1} + 2\sigma_f - 2\phi_{s1}(\sigma_f - \sigma_{s1})}{\sigma_{s1} + 2\sigma_f + \phi_{s1}(\sigma_f - \sigma_{s1})}$
Thermal Expansion (β_T)	$(\rho\beta_T)_{nf} = (1 - \phi_{s1})(\rho\beta_T)_f + \phi_{s1}(\rho\beta_T)_{s1}$

Table 5.2: Thermophysical features of hybrid nanofluid ($Al_2O_3 - Cu/H_2O$) [81, 92, 93].

Properties	Hybrid Nanofluid
Density (ρ)	$\frac{\rho_{hnf}}{\rho_f} = (1 - \phi_{s2}) \left[(1 - \phi_{s1}) + \phi_{s1} \frac{\rho_{s1}}{\rho_f} \right] + \phi_{s2} \frac{\rho_{s2}}{\rho_f}$
Specific Heat capacity (C_p)	$\frac{(\rho C_p)_{hnf}}{(\rho C_p)_f} = (1 - \phi_{s2}) \left[(1 - \phi_{s1}) + \phi_{s1} \frac{(\rho C_p)_{s1}}{(\rho C_p)_f} \right] + \phi_{s2} \frac{(\rho C_p)_{s2}}{(\rho C_p)_f}$
Dynamic Viscosity (μ)	$\frac{\mu_{hnf}}{\mu_f} = \frac{1}{(1 - \phi_1)^{2.5} (1 - \phi_2)^{2.5}}$
Thermal conductivity (k)	$\frac{k_{nf}}{k_f} = \left[\frac{k_{s2} + 2k_{nf} - 2\phi_{s2}(k_{nf} - k_{s2})}{k_{s2} + 2k_{nf} + \phi_{s2}(k_{nf} - k_{s2})} \right] \times \left[\frac{k_{s1} + 2k_{nf} - 2\phi_{s1}(k_{nf} - k_{s1})}{k_{s1} + 2k_{nf} + \phi_{s1}(k_{nf} - k_{s1})} \right]$
Electrical conductivity (σ)	$\frac{\sigma_{hnf}}{\sigma_f} = \frac{\sigma_{s2} + 2\sigma_{nf} - 2\phi_{s2}(\sigma_{nf} - \sigma_{s2})}{\sigma_{s2} + 2\sigma_{nf} + \phi_{s2}(\sigma_{nf} - \sigma_{s2})} \times \frac{\sigma_{s1} + 2\sigma_f - 2\phi_{s1}(\sigma_f - \sigma_{s1})}{\sigma_{s1} + 2\sigma_f + \phi_{s1}(\sigma_f - \sigma_{s1})}$
Thermal Expansion (β_T)	$\frac{(\rho\beta_T)_{hnf}}{(\rho\beta_T)_f} = (1 - \phi_{s2}) \left[(1 - \phi_{s1}) + \phi_{s1} \frac{(\rho\beta_T)_{s1}}{(\rho\beta_T)_f} \right] + (\phi_{s2} \frac{(\rho\beta_T)_{s2}}{(\rho\beta_T)_f})$

Table 5.3: Thermophysical properties of hybrid nanofluid ($Al_2O_3 - Cu/ H_2O$) [81, 92, 93].

Properties	Water	Al_2O_3	Cu
$\rho(kg/m^3)$	997.0	3970	8933
$C_p(J/kgK)$	4180	765	385
$k(W/mK)$	0.613	40	400
$\sigma(\Omega m)^{-1}$	5.5×10^{-6}	35×10^6	59.6×10^6
$\beta_T(K)^{-1}$	21×10^{-5}	0.85×10^{-5}	1.67×10^{-5}
Prandtl number (Pr)	6.2	-	-

For considered flow problem the similarity transformation is given in equation in (5.14) defined by Waini *et al.* [89]. The velocity components through the transformation are given in equation (5.15).

$$\eta = \left(\frac{U_e}{v_f}\right)^{\frac{1}{2}} y, \quad \psi = (U_e v_f)^{\frac{1}{2}} x f(\eta), \quad \theta(\eta) = \frac{T - T_\infty}{T_w - T_\infty}, \quad (5.14)$$

$$u = U_e x f'(\eta), \quad v = -(U_e v_f)^{\frac{1}{2}} f(\eta), \quad (5.15)$$

where ψ and v_f be the stream function and kinematic viscosity respectively.

The continuity equation (5.5) is easily satisfied and the remaining equations (5.6)–(5.11) reduces through the utility of equation (5.14) and (5.15) as

$$f'(\eta)^2 - f''(\eta) f(\eta) = 1 + \frac{\frac{\mu_{hnf}}{\rho_f}}{\frac{\mu_f}{\rho_{hnf}}} f'''(\eta) + \frac{1}{\frac{\rho_{hnf}}{\rho_f}} Z e^{-\gamma \eta} + \frac{\frac{(\rho \beta_T)_{hnf}}{\rho_f}}{\frac{(\rho \beta_T)_f}{\rho_f}} \lambda \theta(\eta) \quad (5.16)$$

$$\begin{aligned} & - \frac{\frac{\mu_{hnf}}{\rho_f}}{\frac{\mu_f}{\rho_{hnf}}} [f'(\eta) - 1] \omega, \\ & \frac{(\rho C_P)_{hnf}}{(\rho C_P)_f} f(\eta) \theta'(\eta) + \frac{1}{Pr} \frac{k_{hnf}}{k_f} \left(1 + \frac{4}{3} \frac{1}{\frac{k_{hnf}}{k_f}} R \right) \theta''(\eta) + Ec \left[\frac{\mu_{hnf}}{\mu_f} f''(\eta)^2 \right. \\ & \left. + M \frac{\sigma_{hnf}}{\sigma_f} [f'(\eta) - E_1]^2 \right] + Q \theta(\eta) = 0. \end{aligned} \quad (5.17)$$

With boundary conditions

$$f(0) = 0, \quad f'(0) = \lambda_l, \quad \theta(0) = 1 \quad \text{at} \quad \eta = 0, \quad (5.18)$$

$$f'(\infty) \rightarrow 1, \quad \theta(\infty) \rightarrow 0 \quad \text{as} \quad \eta \rightarrow \infty. \quad (5.19)$$

Table 5.4: Dimensionless parameters involved in the hybrid nanofluid flow.

Non-dimensional parameters	Mathematical formulation
Modified Hartman number	$Z = \frac{\pi M_0 J_0}{8 \rho_f} \frac{1}{U_e^2 x}$
Mixed convection parameter	$\lambda = \frac{Gr}{Re_x^2} = \frac{g(\rho\beta T)_f (T_w - T_\infty)x^3}{\frac{x^4 U_e^2}{v_f^2}}$
Radiation parameter	$R = 4T_\infty^3 \left(\frac{\sigma^*}{k^* k_f} \right)$
Eckert number	$EC = \frac{(u_e(x))^2}{(C_p)_f T_\infty (\theta_w - 1)}$
Heat generation/absorption parameter	$Q = \frac{Q_0}{U_e (\rho C_p)_f}$
Magnetic field parameter	$M = \frac{\sigma_f B_0^2}{\rho_f U_e}$
Prandtl number	$Pr = \frac{(\mu C_p)_f}{k_f}$
Widths magnets and electrodes	$\gamma = \frac{\pi}{b} \left(\frac{U_e}{v_f} \right)^{\frac{1}{2}}$
Electric field parameter	$E_1 = \frac{E_0}{B_0 U_e x}$
Stretching parameter	$\lambda_1 = \frac{U_w}{U_e}$
Porosity parameter	$\omega = \frac{v_f}{k' U_e}$

Moreover, Nu_x and C_f dimensionless notions are achievable as

$$(Re_x)^{\frac{1}{2}} C_f = \frac{\mu_{hnf}}{\mu_f} f''(0), \quad (Re_x)^{-\frac{1}{2}} Nu_x = - \left(\frac{k_{hnf}}{k_f} + \frac{4}{3} R \right) \theta'(0), \quad (5.20)$$

whereas the local Reynolds number is specified as $Re_x = \frac{x u_e(x)}{v_f}$.

Also we have used symbol to reduce the complexity as

$$a = \frac{\mu_{hnf}}{\mu_f}, \quad b = \frac{\rho_{hnf}}{\rho_f}, \quad c = \frac{(\rho C_p)_{hnf}}{(\rho C_p)_f}, \quad d = \frac{(\rho\beta T)_{hnf}}{(\rho\beta T)_f} \quad (5.21)$$

$$K = \frac{k_{hnf}}{k_f} \text{ and } S = \frac{\sigma_{hnf}}{\sigma_f},$$

$$-f'(\eta)^2 + f''(\eta)f(\eta) + 1 + \frac{a}{b}f'''(\eta) + \frac{1}{b}Ze^{-\gamma\eta} + \frac{d}{b}\lambda\theta \quad (5.22)$$

$$- \frac{a}{b} [f'(\eta) - 1]\omega = 0,$$

$$c f(\eta) \theta'(\eta) + \frac{1}{Pr}K \left(1 + \frac{4}{3} \frac{1}{K}R\right) \theta''(\eta) + Ec [a f''(\eta)^2 + MS [f'(\eta) - E_1]^2] \quad (5.23)$$

$$+ Q \theta(\eta) = 0.$$

5.3 Numerical Stratagem

To obtain a numerical solution of the problem, Eqs. (5.22) and (5.23) are solved. These are particularly coupled nonlinear equations combined with Equation (5.18) and (5.19) creating a complex nonlinear boundary value problem. Hale *et al.* [94] developed the `bvp4c` solver in MATLAB that is broadly used to produce the numerical solution. The finite modification algorithm known as the `bvp4c` solver that implement three-stage Lobatto IIIA generate numerical solutions having fourth order precision. This strategy achieves the necessary accuracy when step-size alterations are made and an initial guess is provided at the initial mesh positions. The following set of equations is required to initiate the methodology.

$$f = y(1), \quad (5.24)$$

$$f' = y(2) = y'(1), \quad (5.25)$$

$$f'' = y(3) = y'(2), \quad (5.26)$$

$$\theta = y(4), \quad (5.27)$$

$$\theta' = y(5) = y'(4), \quad (5.28)$$

$$y'(3) = \frac{b}{a} \{y(2)^2 - y(1)y(3) - \left(1 + \frac{1}{b}Ze^{-\gamma\eta}\right) - \frac{d}{b}\lambda y(4) \quad (5.29)$$

$$+ \frac{a}{b} [y(2) - 1]\omega\},$$

$$y'(5) = -\frac{Pr}{K\left(1 + \frac{4}{3} \frac{1}{K}R\right)} \{c y(1)y(5) + Ec [a(y(3))^2 + MS [y(2) - E_1]^2] \quad (5.30)$$

$$+ Qy(4)\}.$$

With boundary condition

$$y_0(1) = 0, \quad y_0(2) = \lambda_1, \quad y_0(4) = 1, \quad \text{at} \quad \eta = 0, \quad (5.31)$$

$$y_\infty(2) \rightarrow 1, \quad y_\infty(4) \rightarrow 0, \quad \text{as} \quad \eta \rightarrow \infty. \quad (5.32)$$

5.4 Graphical Analysis and Discussion

The inquiry of diverse emerging effect arising from various dimensional parameters on velocity as well as on temperature profiles is of chief importance. With the conduct of a detailed analysis of the fluid problem, this section set aside to the prominent flow features and exposes the remarkable outcomes of non-dimensional parameters on the significant entities of concern. The dimensionless parameters that influence the velocity profile $f'(\eta)$ are the stretching parameter λ_1 , corresponding the nanoparticle volume fraction of alumina ϕ_1 and nanoparticle volume fraction of copper ϕ_2 , modified Hartmann number Z , width of magnets and electrode γ , the porosity parameter ω and mixed convection parameter λ . The consequences of these parameters are effectively illustrated in Figures 5.3 – 5.9. First, the variability in velocity against rising λ_1 can be seen in Figure 5.3 and positive outcomes are observed with an increase in the velocity profile. The next two figures Figure 5.4 and Figure 5.5 are sketched with regard to the nanoparticles volume fraction of Al_2O_3 (ϕ_1) and Cu (ϕ_2) as they are crucial factors because of their amplifying impacts on kinematic viscosity, shear stresses, and dynamic viscosity. The increasing results for velocity profile are obtained for higher ϕ_1 while decreasing impact on velocity profile is evident for ϕ_2 are evident. The Riga plate which is an electromagnetic actuator is the cause of the body force entangled in the flow. The electric and magnetic fields are developed when an electrically conductive fluid flows across the plate. This give rise to the Lorentz force, resulting in a speed up flow outcomes. Therefore, in Figure 5.6, the modified Hartmann number Z is boosted while maintain the constant values of other flow parameters and this has a beneficial impact on the fluid flow which is shown by the rising behavior of the velocity. Further, there is an intriguing effect from the strength of the magnetic and electric fields. Figure 5.7 is displayed to reveal the effect of the parameter γ on the velocity and the figure illustrates that as the parameter γ rises, the fluid velocity rises with it. Figure 5.8 portrays the relation between porosity parameter ω and the velocity. It shows a reduction in velocity as porosity parameter ω grows. Figure 5.9 reflects the velocity profile for mixed

convection parameter λ depicts a rise of velocity in response to an increment in λ . Likewise, the, outcomes of important parameters on temperature profile that include the stretching parameter λ_1 , nanoparticle volume fraction of alumina ϕ_1 and as well as nanoparticle volume fraction of copper ϕ_2 , radiation parameter R , the Eckert number Ec , Prandtl number Pr , modified Hartmann number Z , width of magnets and electrode γ , the magnetic parameter M , electric parameter E_1 , heat generation and absorption parameter Q and mixed convection parameter λ are shown in Figures 5.10 – 5.21. As the stretching ratio parameter λ_1 is increased, the temperature $\theta(\eta)$ rapidly reduces and this can be observed in Figure 5.10. It has been found that the energy measurement, which generates positive outcomes within the thermal boundary layer, are greatly impacted by λ_1 . The graphical demonstration in Figure 5.11 & 5.12 illustrates the impact of nanoparticle volume fractions ϕ_1 and ϕ_2 on the temperature distributions. The increasing developments are resulted from raising both ϕ_1 and ϕ_2 , in relation to most effective rates of heat flow. The effect of modifications in R is another essential component for heat transfer. Figure 5.13 indicates that if the parameter R rises, the temperature profile $\theta(\eta)$ increases correspondingly. Therefore, heat transfers quicker with a boost in R , leading the surface to cool down faster. Figure 5.14 illustrates the impact of Eckert number Ec on temperature and the results show that boosting the parameter Ec leads to significant rise in temperature. Figure 5.15 depicts a rise in Prandtl number Pr enables the temperature profile $\theta(\eta)$ to go down with a decrease in thermal boundary layer. The result of raising the modified Hartmann number Z is shown in Figure 5.16. $\theta(\eta)$ reduces as an increase in Z is done. The reduction in temperature is observed by raising the parameter γ and this is clearly shown in Figure 5.17. Figure 5.18 demonstrate how an increase in the magnetic parameter M boosts the temperature. Figure 5.19 is sketched to relate the increasing electric parameter E_1 with temperature profile. The figure illustrates that the drop in temperature is followed by a rise in the E_1 . Figure 5.20 reveals that due to the increase in heat generation/absorption parameter Q , the temperature profile upsurges. The effect of mixed convection parameter λ on the temperature profile is presented in Figure 5.21 which depicts a reduced temperature for λ variation.

The impact of distinct values of parameters like Z , λ_1 , γ , λ , ϕ_1 and ϕ_2 on skin friction coefficient and Nusselt number is illustrated in Figures 5.22 - 5.29. Figure 5.22 and Figure 5.23 portray the alterations of Z with different values of γ for both skin friction and Nusselt number respectively. It is evident that a smaller value of γ can generate a higher friction drag and

reverse response is observed in case of Nusselt number. Thus the rate of heat transfer can be regulated by declining the width of the electrodes and magnets γ . The effect of enhanced Z on friction drag and Nusselt number is observed to be in opposite trends. Figure 5.24 and Figure 5.25 depict the modifications of skin friction and Nusselt number concerning λ_1 with altered values of ϕ_1 . The outcomes specify that increasing ϕ_1 , the friction drag as well as Nusselt number go up. Moreover, the rate of heat transmission ascends for increased ϕ_1 . The impact of rising λ_1 on Nusselt number points towards a decline but this is not the case with friction drag. The behaviors of increased ϕ_2 along with λ_1 for friction drag and Nusselt number are witnessed through Figure 5.26 and 5.27 respectively. The increase in ϕ_2 corresponds to more friction drag and a better rate of heat transfer. The skin friction coefficient and Nusselt number behave differently for enlarged λ_1 . Figure 5.28 and Figure 5.29 portray the impact of concerning λ with distinct values of Z on skin friction and Nusselt number. The results state that rising Z , the friction drag above the surface ascends while the Nusselt number declines. The effect of λ on both friction drag and rate of heat transfer is significantly noticed through these figures.

The validity of numerical result by comparing the current MATLAB numerical code with the published literature is performed. Furthermore, $f''(0)$, $\theta'(0)$ are estimated by varying the parameter λ_1 while keeping exactly the same values for the other physical parameters. The numerical values gained are presented in Table 5.5 which shows the calculated values along their comparison with the values from earlier research conducted by Wang [86], Bachok *et al.* [87] and Waini *et al.* [89]. These calculations additionally demonstrate that λ_1 has an advantageous impact on $\theta'(0)$, $f''(0)$ leading to the skin friction coefficient to go down and the Nusselt number to rise. The findings match well with the already existing literature. Table 5.6 represent the comparison for the numerical values of Nusselt number and friction drag. This comparison is carried out by Waini *et al.* [88] for the conventional fluid (Cu/H_2O) and hybrid nanofluid ($Al_2O_3 - Cu/H_2O$).

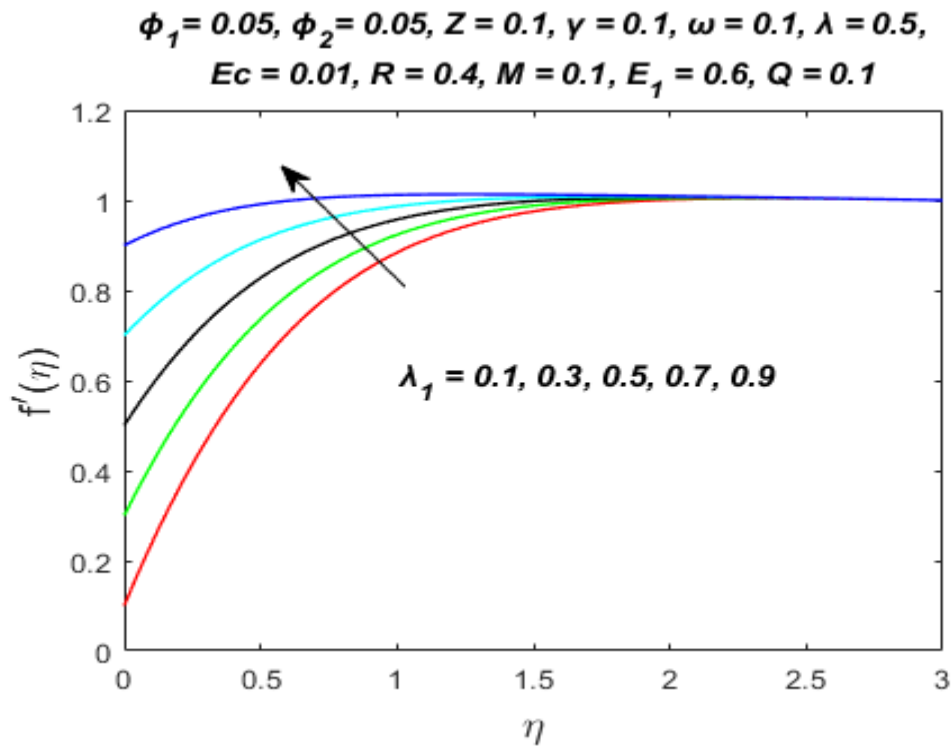


Figure 5.3: Effect of stretching parameter λ_1 upon $f'(\eta)$.

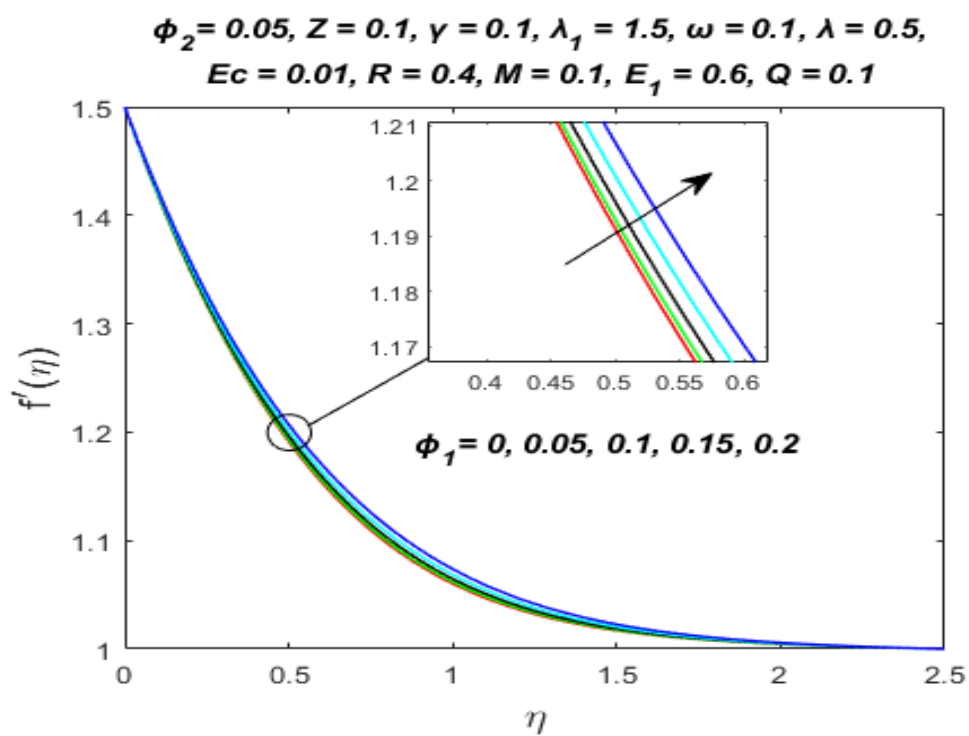


Figure 5.4: Effect of nanoparticle volume friction ϕ_1 of Al_2O_3 upon $f'(\eta)$.

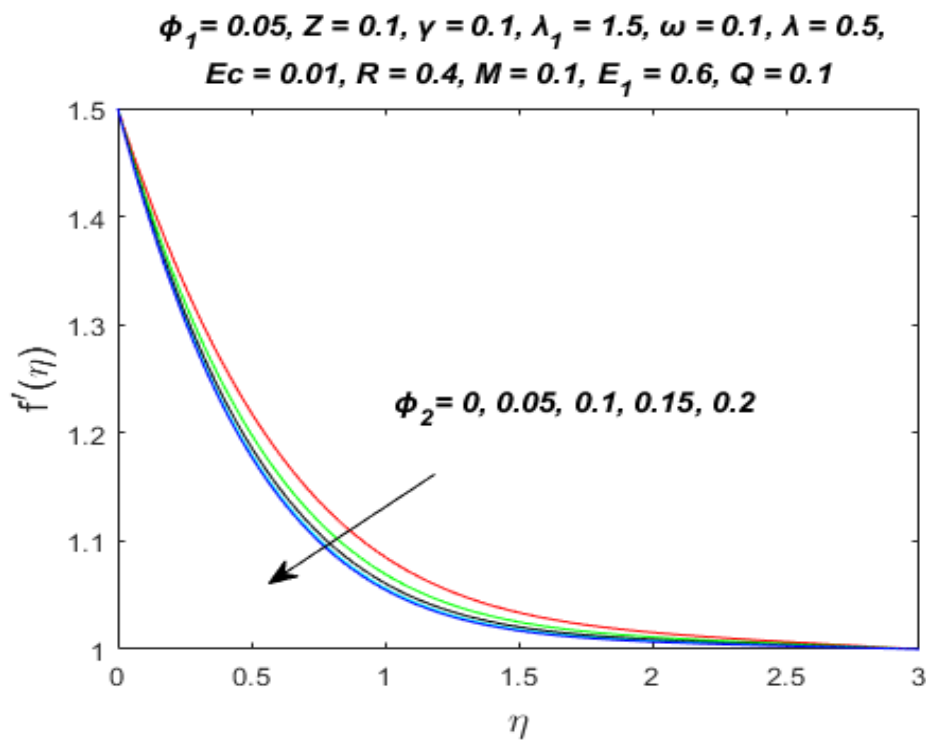


Figure 5.5: Effect of nanoparticle volume fraction ϕ_2 of Cu upon $f'(\eta)$.

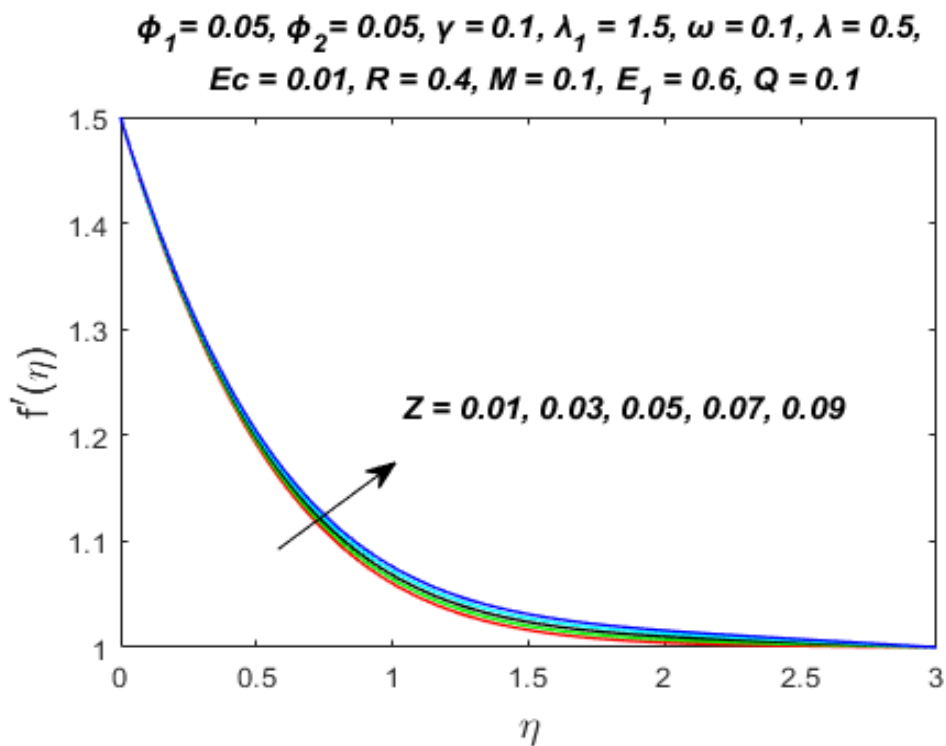


Figure 5.6: Effect of modified Hartmann number Z upon $f'(\eta)$.

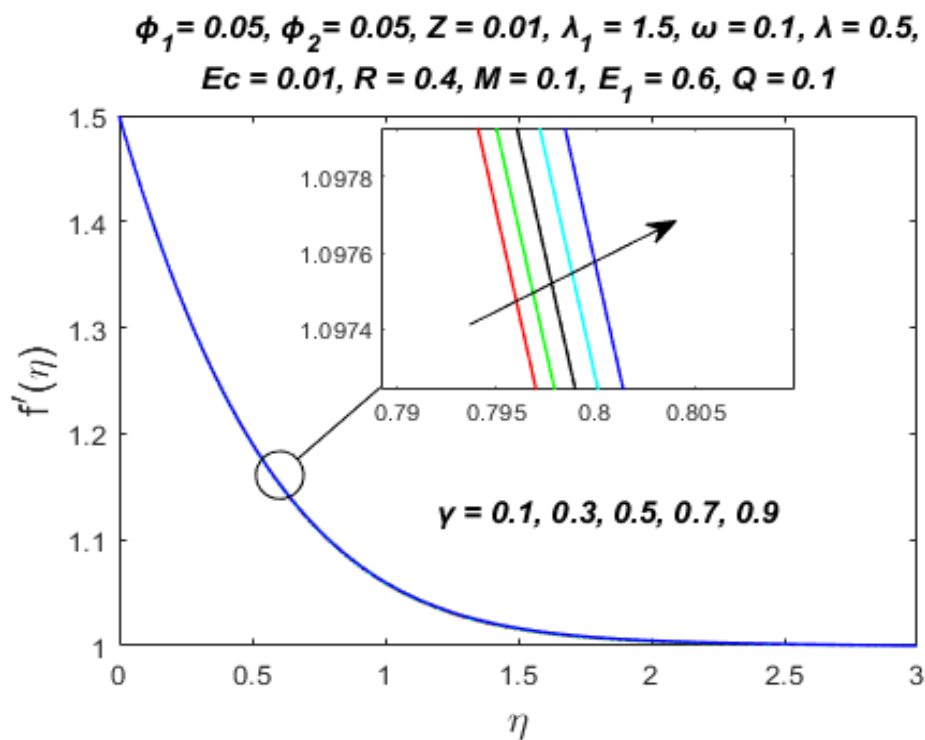


Figure 5.7: Effect of dimensionless quantity γ upon $f'(\eta)$.

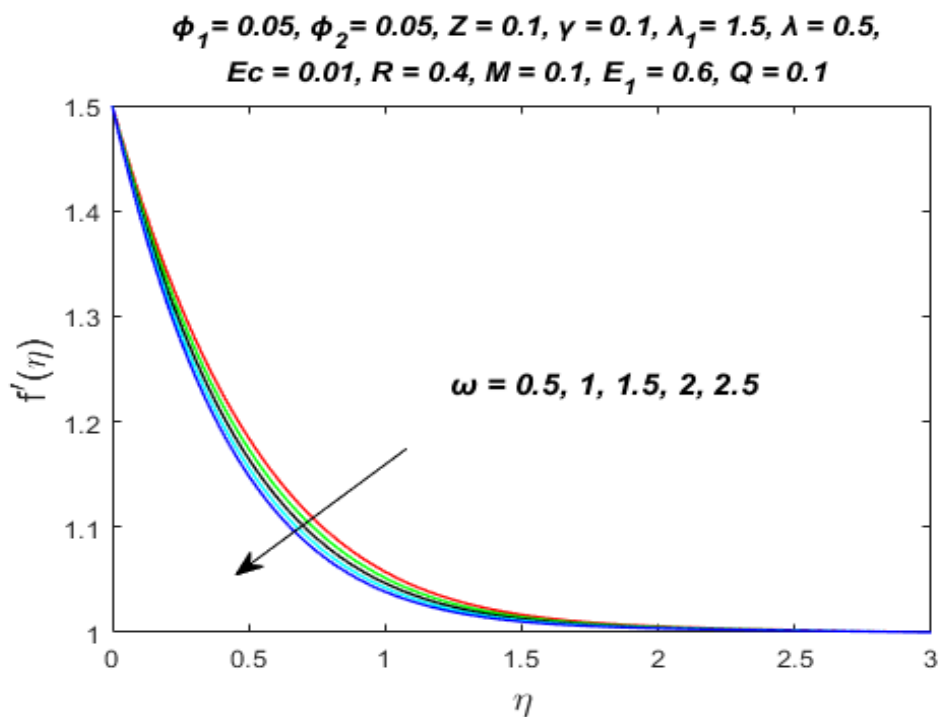


Figure 5.8: Effect of porosity parameter ω upon $f'(\eta)$.

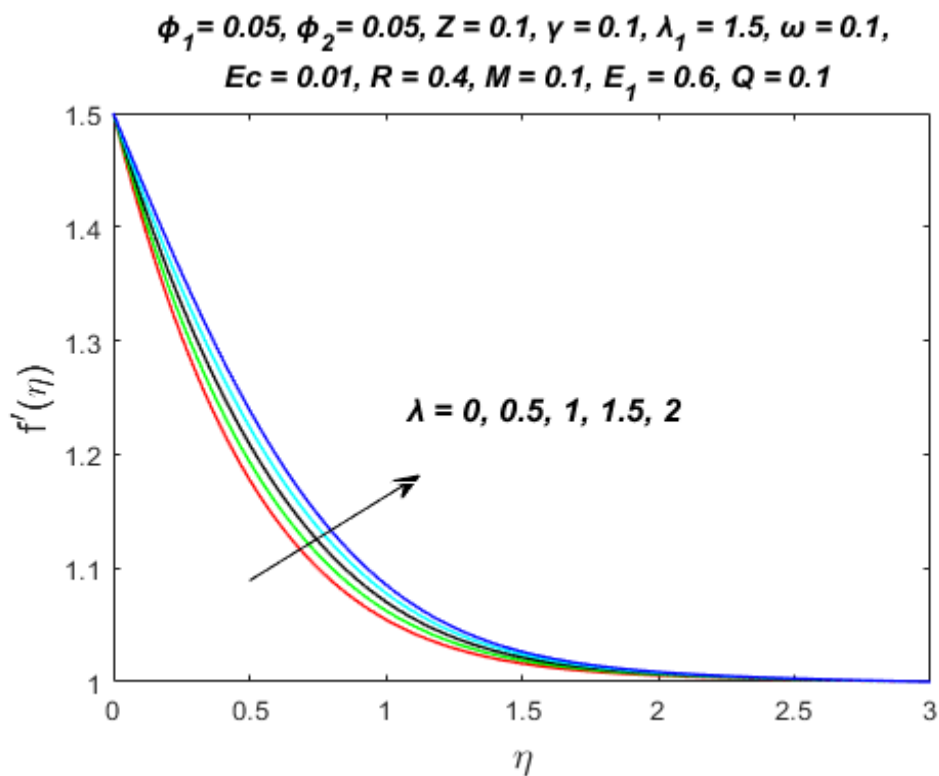


Figure 5.9: Effect of mixed convection parameter λ upon $f'(\eta)$.

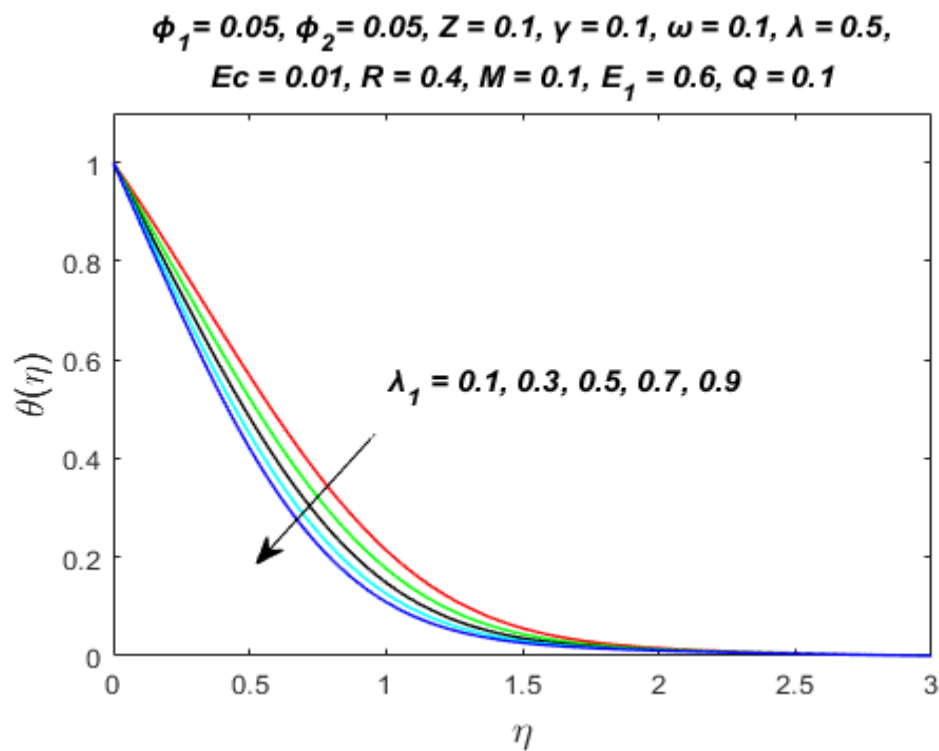


Figure 5.10: Effect of stretching parameter λ_1 upon $\theta(\eta)$.

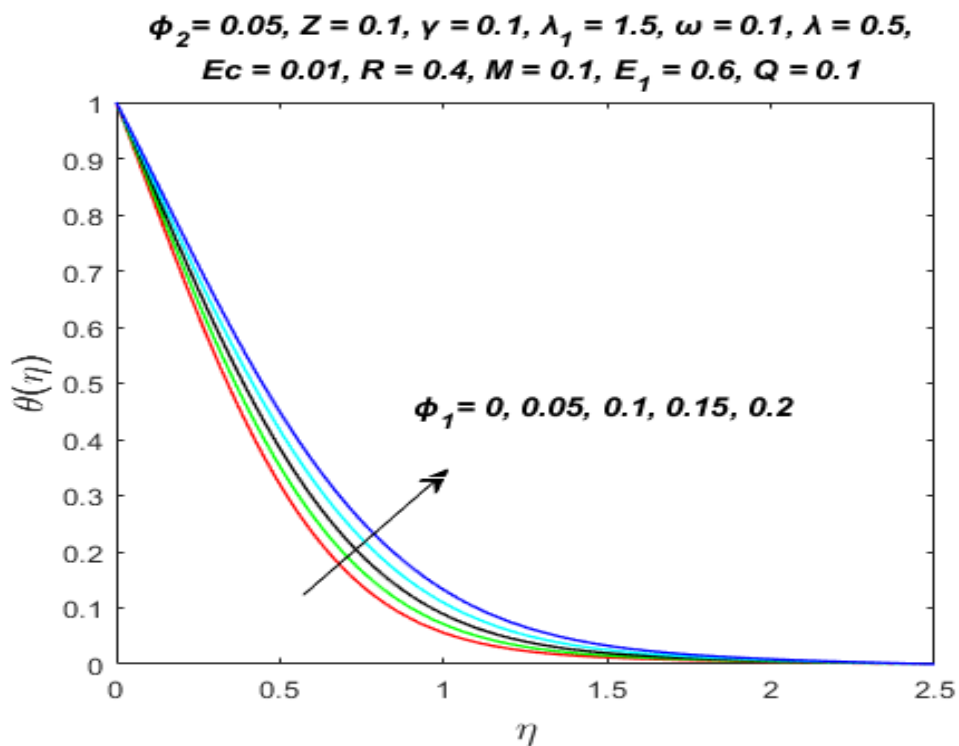


Figure 5.11: Effect of nanoparticle volume fraction ϕ_1 of Al_2O_3 upon $\theta(\eta)$.

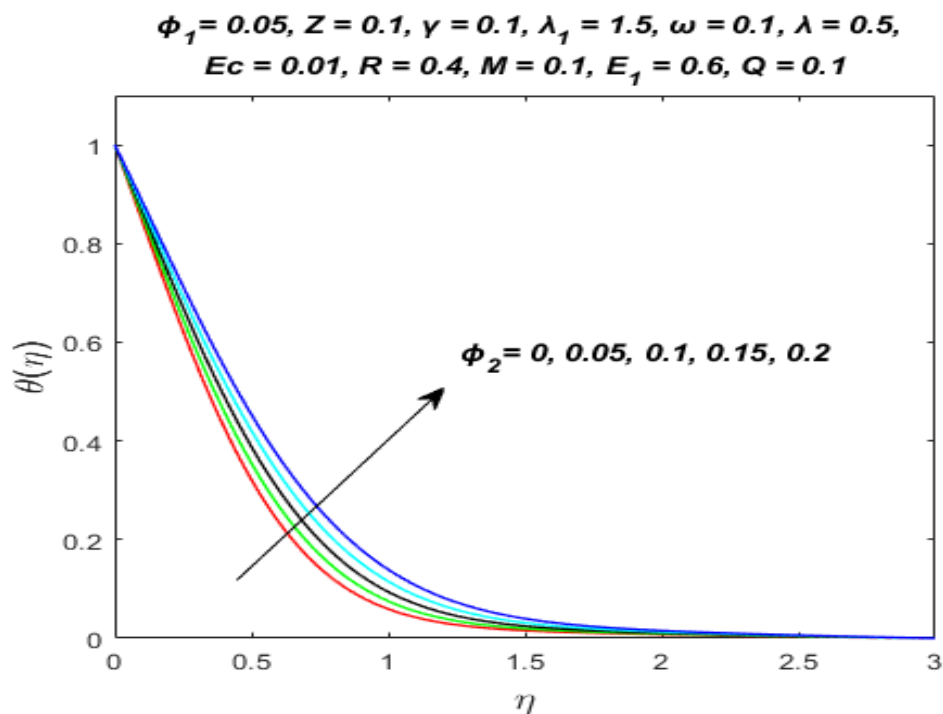


Figure 5.12: Effect of nanoparticle volume fraction ϕ_2 of Cu upon $\theta(\eta)$.

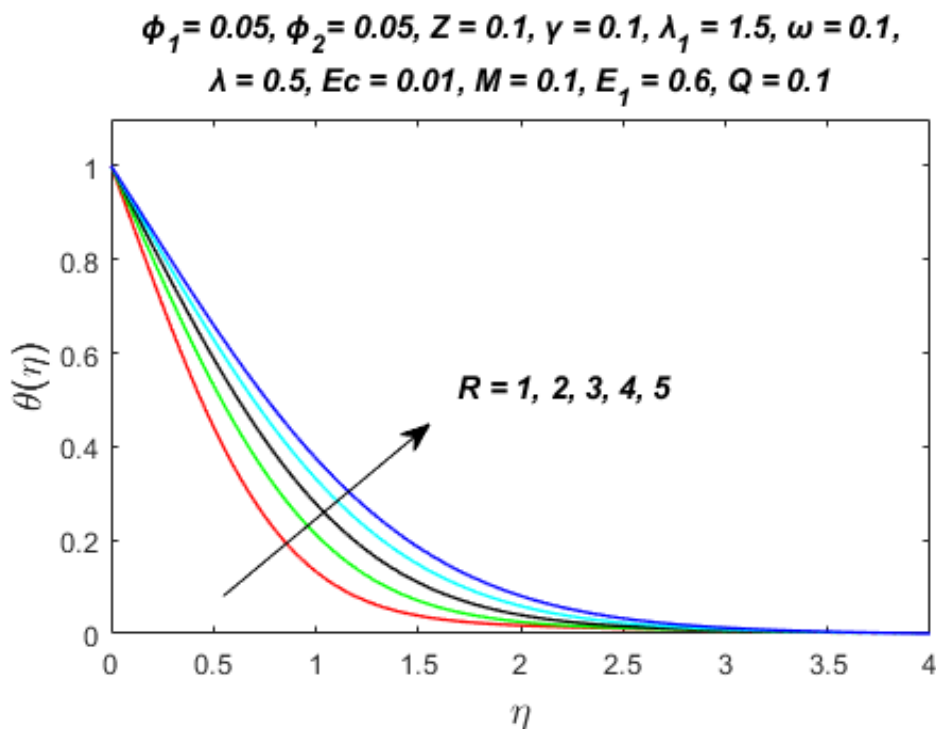


Figure 5.13: Effect of radiation parameter R upon $\theta(\eta)$.

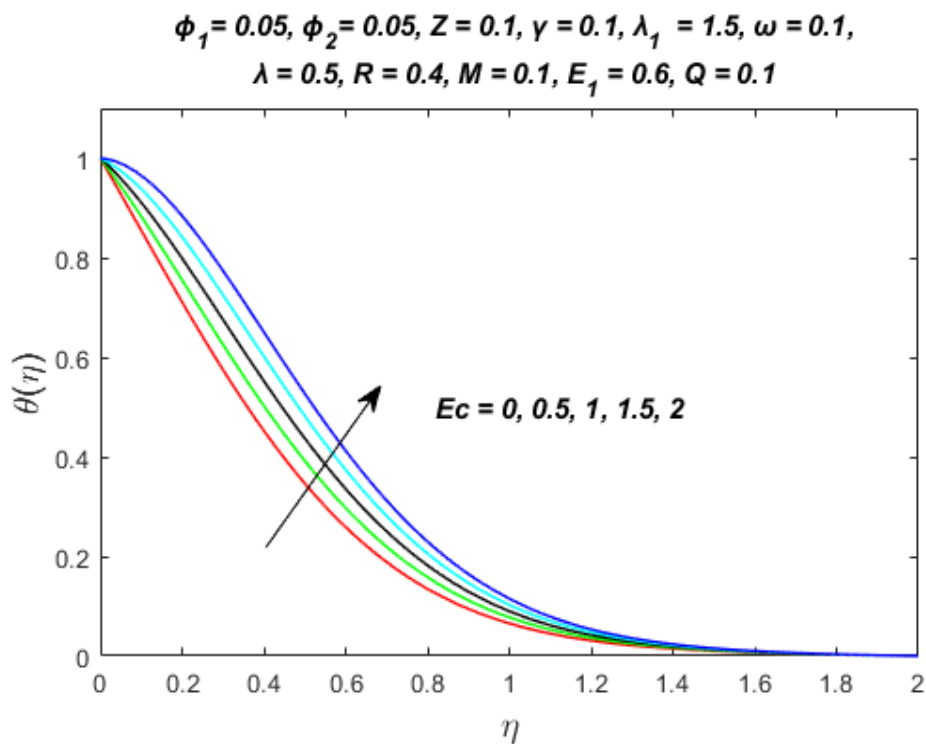


Figure 5.14: Effect of Eckert number Ec upon $\theta(\eta)$.

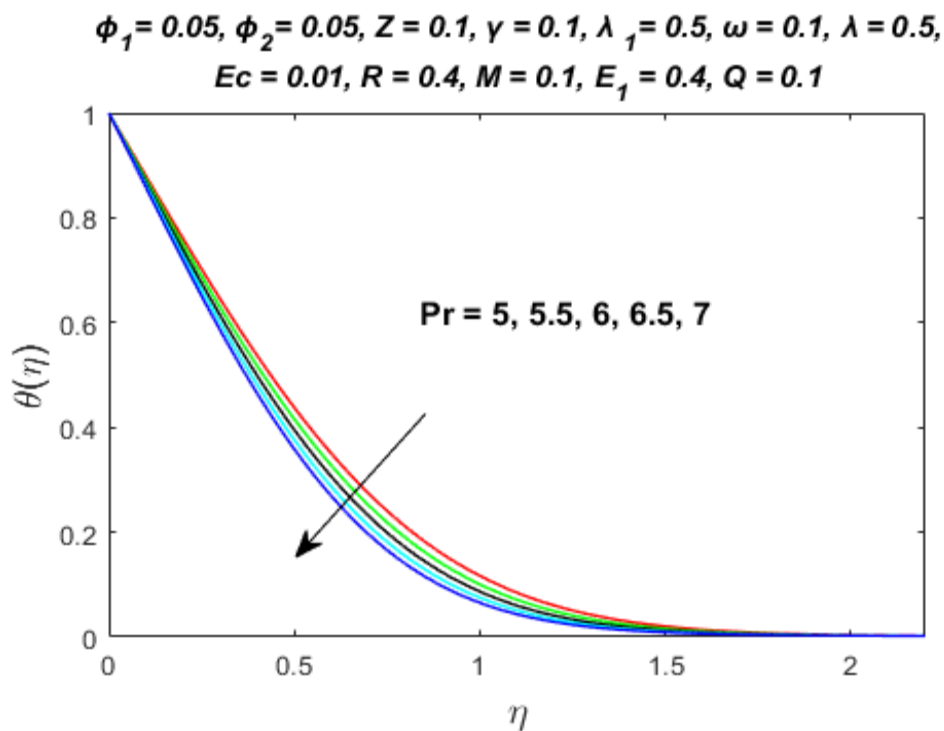


Figure 5.15: Effect of Prandtl number Pr upon $\theta(\eta)$.

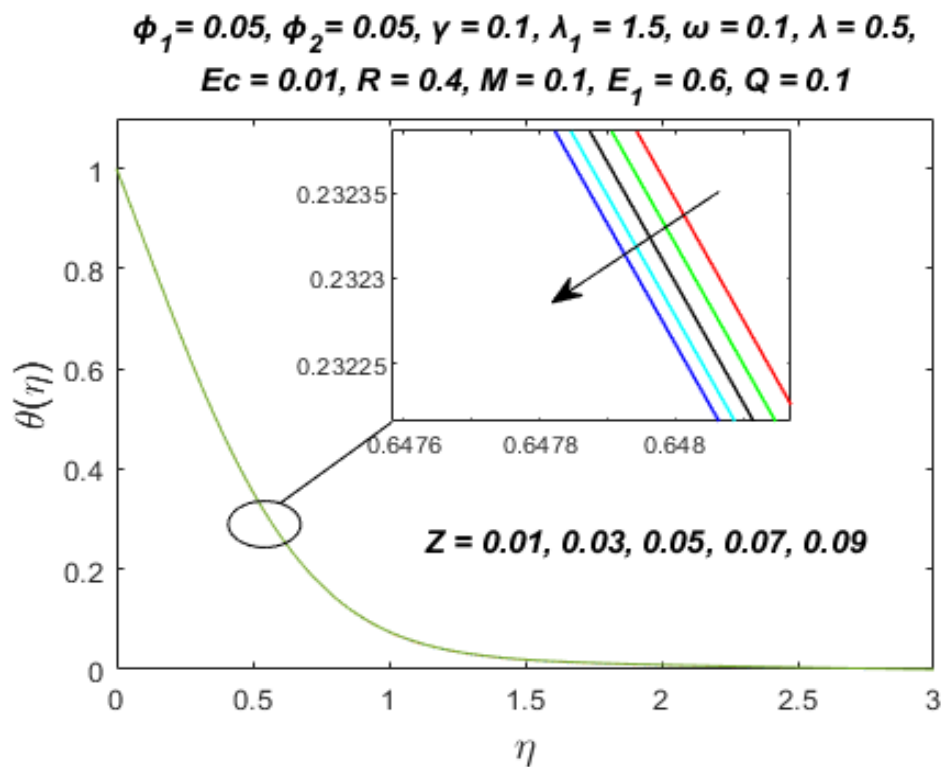


Figure 5.16: Effect of modified Hartmann number Z upon $\theta(\eta)$.

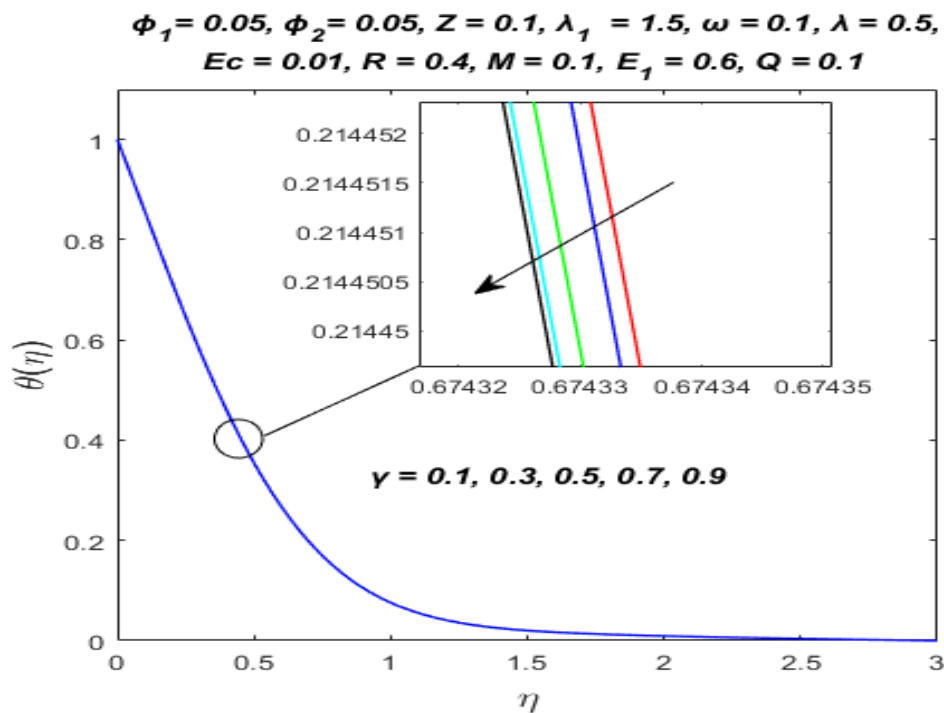


Figure 5.17: Effect of dimensionless quantity γ upon $\theta(\eta)$.

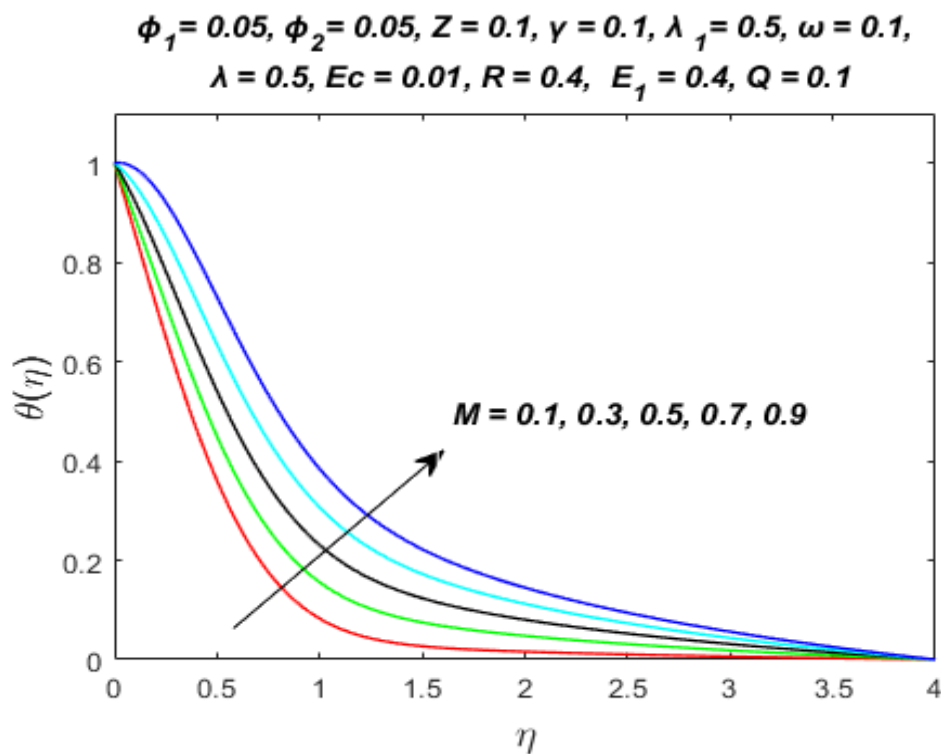


Figure 5.18: Effect of magnetic parameter M upon $\theta(\eta)$.

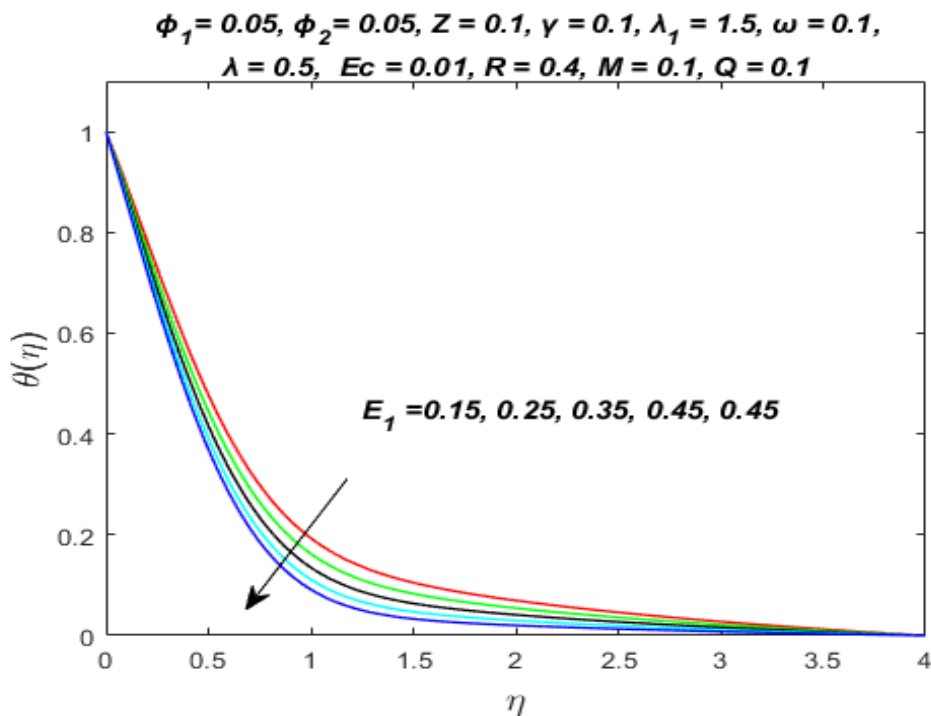


Figure 5.19: Effect of electric field parameter E_1 upon $\theta(\eta)$.

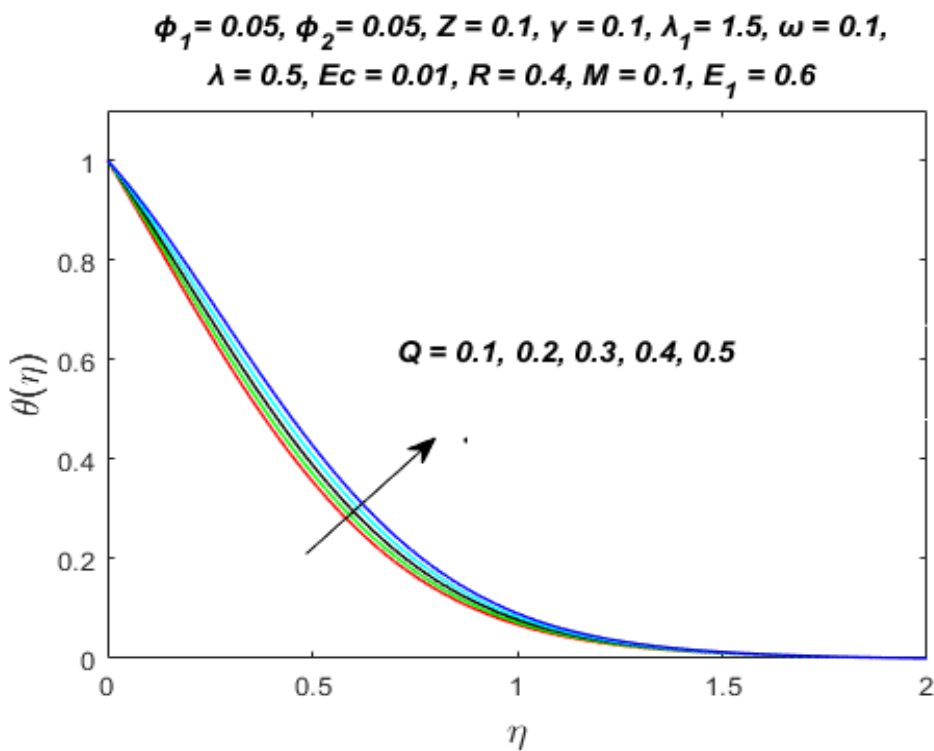


Figure 5.20: Effect of heat absorption/generation parameter Q upon $\theta(\eta)$.

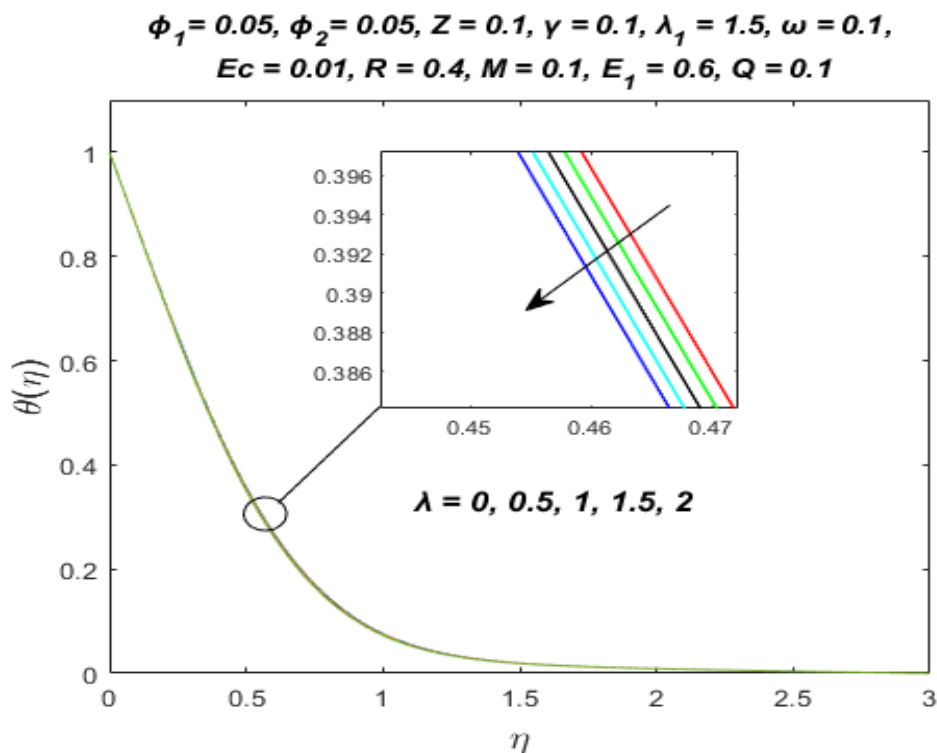


Figure 5.21: Effect of mixed convection parameter λ upon $\theta(\eta)$.

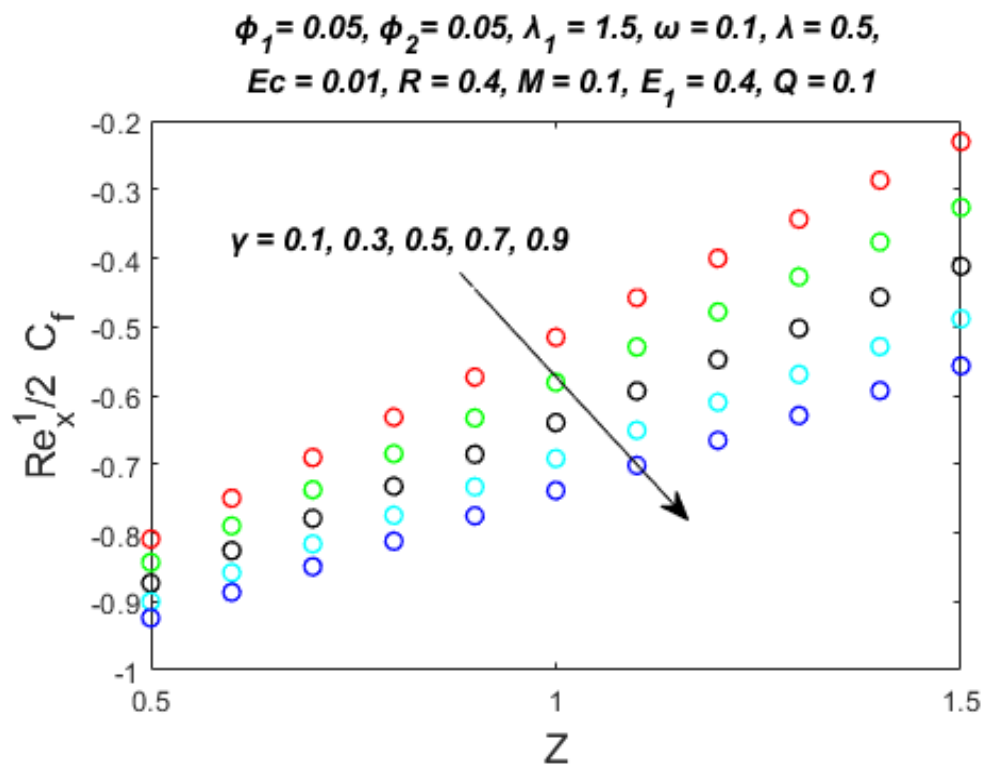


Figure 5.22: Skin friction towards Z with various values of γ .

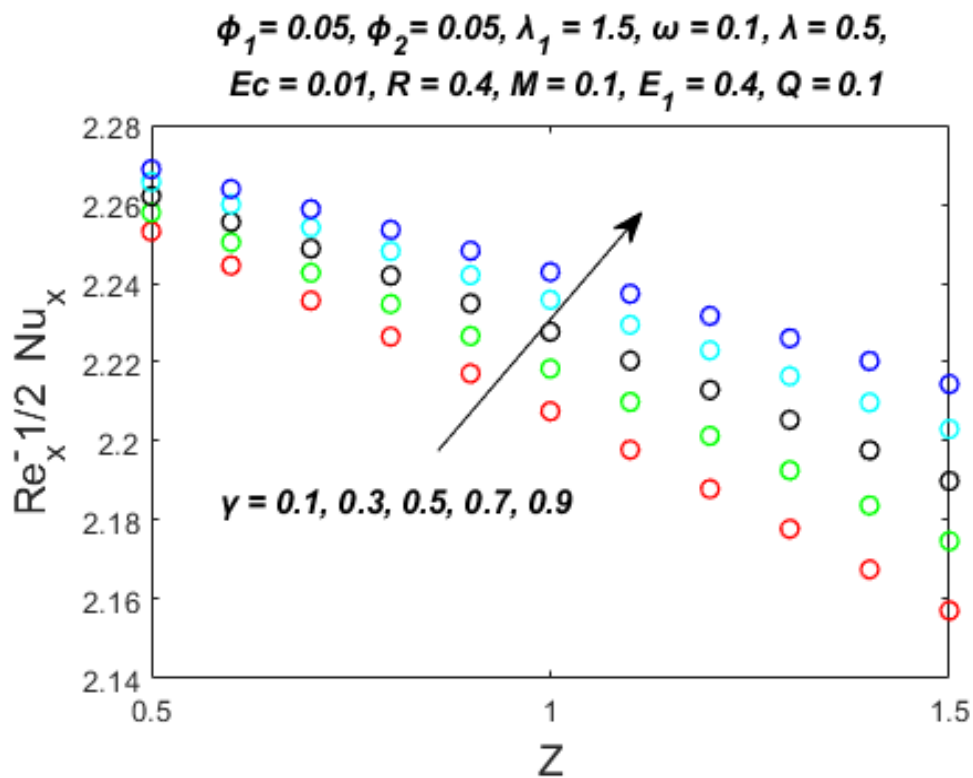


Figure 5.23: Nusselt number towards Z with various values of γ .

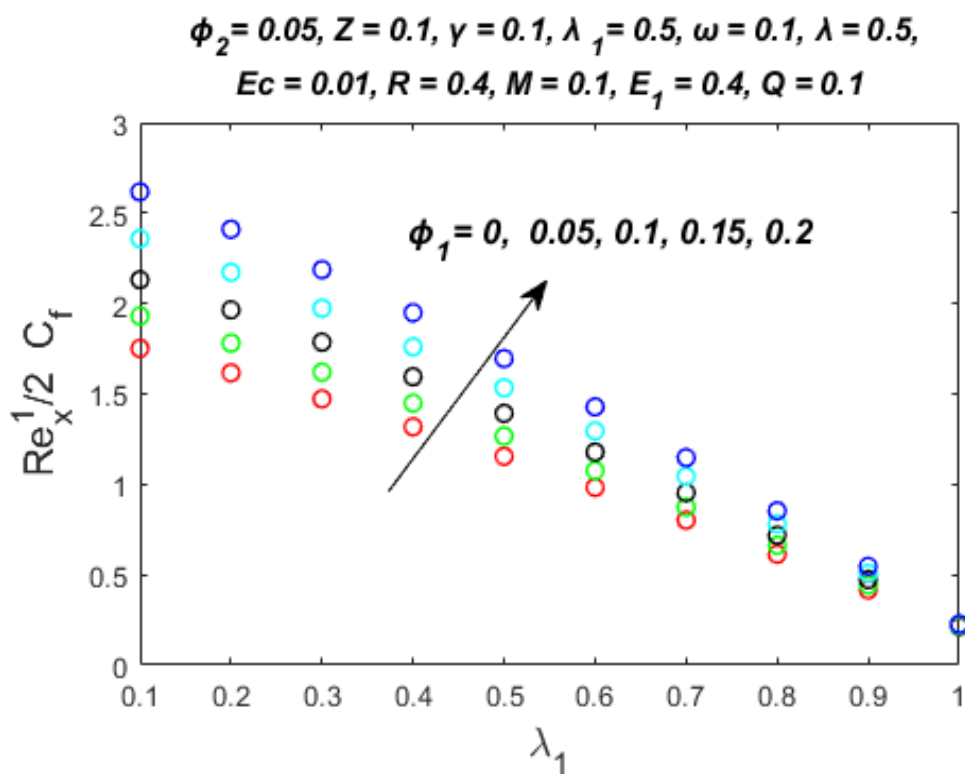


Figure 5.24: Skin friction towards λ_1 with various values of ϕ_1 .

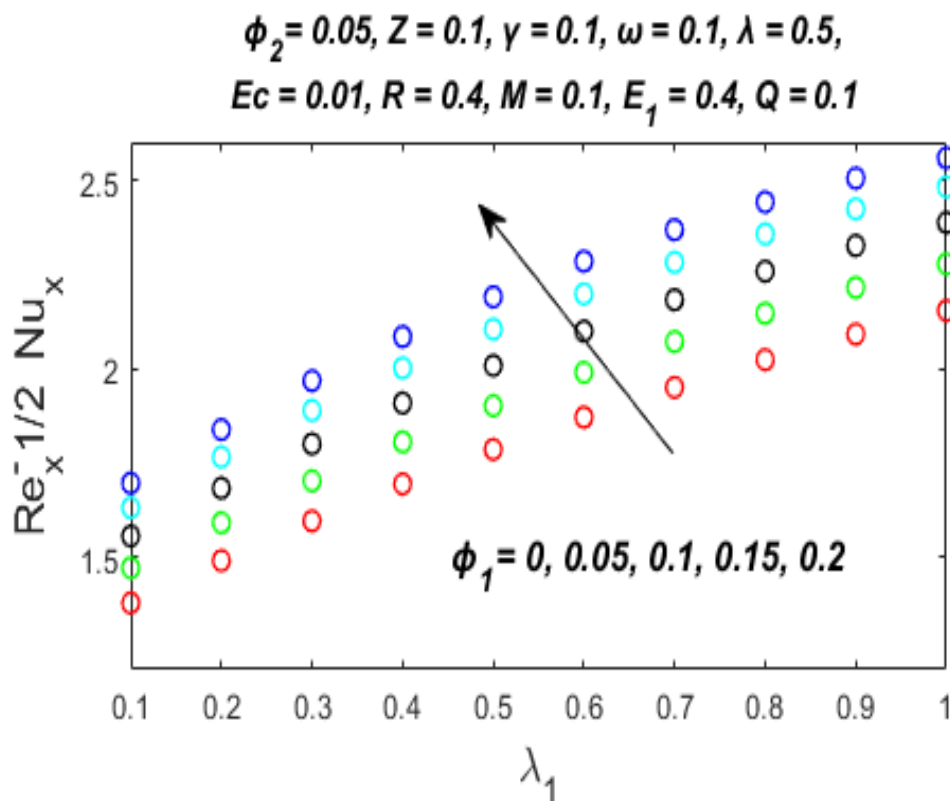


Figure 5.25: Nusselt number towards λ_1 with various values of ϕ_1 .

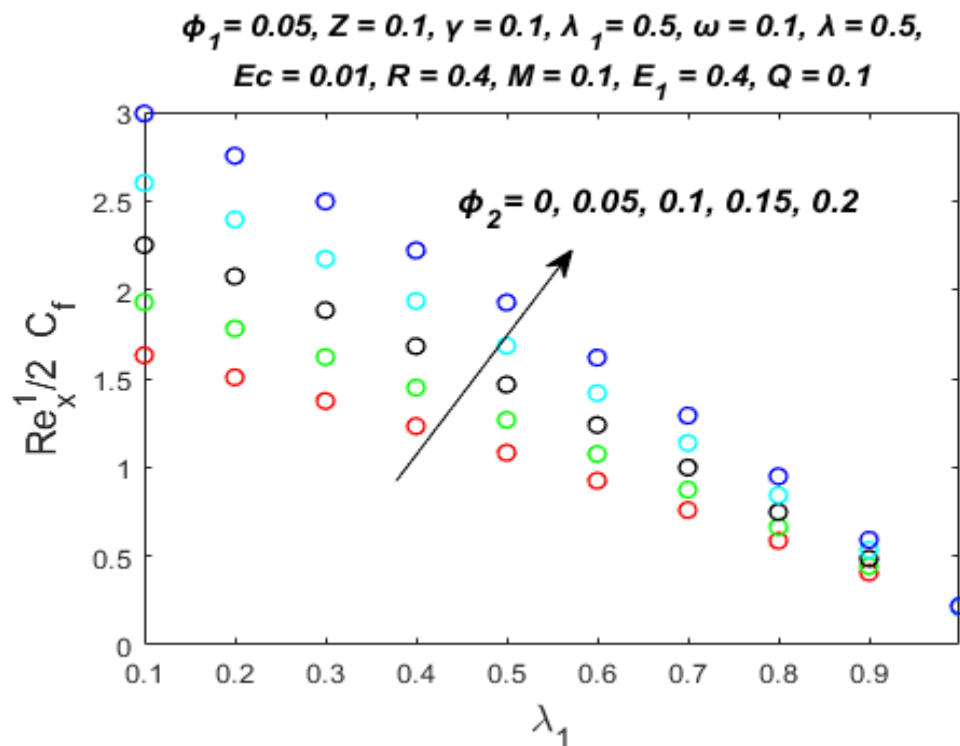


Figure 5.26: Skin friction towards λ_1 with various values of ϕ_2 .

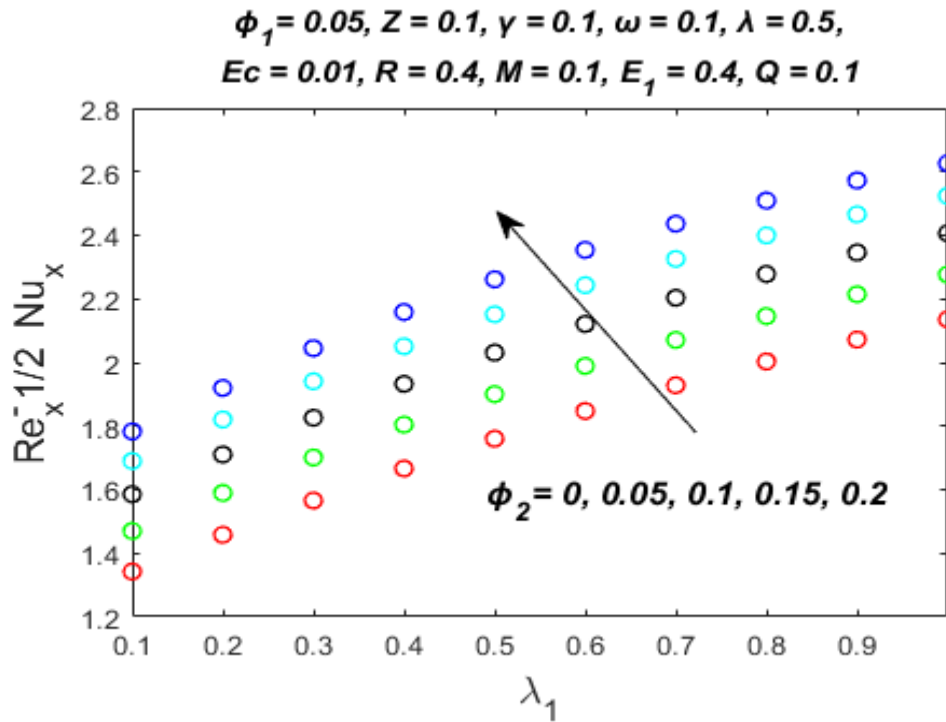


Figure 5.27: Nusselt number towards λ_1 with various values of ϕ_2 .

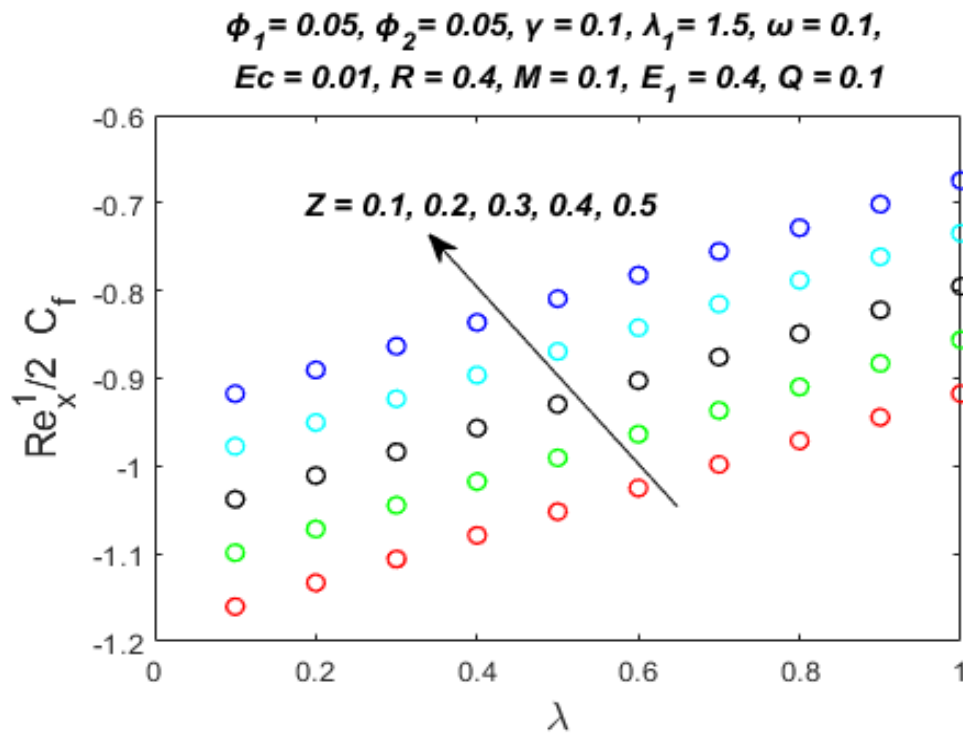


Figure 5.28: Skin friction towards λ with various values of Z .

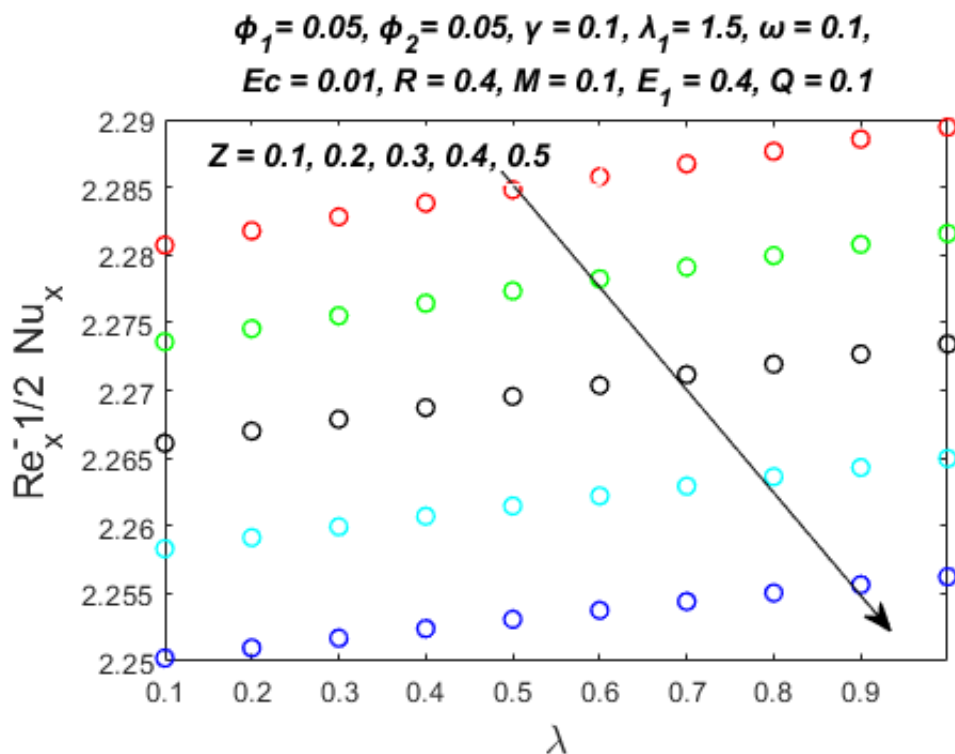


Figure 5.29: Nusselt number towards λ with various values of Z .

Table 5.5: Comparative values of stretching parameter λ_1 on $f''(0)$ and $-\theta'(0)$ if $\phi_1 = \phi_2 = Z = \lambda = R = Q = \gamma = M = Ec = \omega = E_1 = 0$.

λ_1	Wang [86]	Bachok <i>et al.</i> [87]	Waini <i>et al.</i> [89]		Present Evaluations	
	$f''(0)$	$f''(0)$	$f''(0)$	$-\theta'(0)$	$f''(0)$	$-\theta'(0)$
2.0	-1.88731	-1.887307	-1.887306490	2.627736190	-1.887306392	2.627741231
1.0	0	0	0	1.986760057	0	1.986797489
0.5	0.71330	0.713295	0.713293939	1.595480754	0.713293484	1.595497651
0.0	1.232588	1.232588	1.232586110	1.127977904	1.232586055	1.127974546

Table 5.6: Comparative values of skin friction coefficient $f''(0)$ and Nusselt number $-\theta'(0)$ for several values of ϕ_2 , ϕ_1 and λ_1 if $Z = \lambda = R = Q = \gamma = M = Ec = \omega = E_l = 0$.

ϕ_2	λ_1	Waini <i>et al.</i> [88] $\phi_1 = 0$ (Cu/water)		Waini <i>et al.</i> [89]				Present Results			
				$\phi_1 = 0$ (Cu/water)		$\phi_1 = 0.05$ (Cu-Al ₂ O ₃ /water)		$\phi_1 = 0$ (Cu/water)		$\phi_1 = 0.05$ (Cu-Al ₂ O ₃ /water)	
		$f''(0)$	$-\theta'(0)$	$f''(0)$	$-\theta'(0)$	$f''(0)$	$-\theta'(0)$	$f''(0)$	$-\theta'(0)$	$f''(0)$	$-\theta'(0)$
0	0	-	-	1.232588	1.127964	1.408763	1.229275	1.232587676	1.127964367	1.408763013	1.229274844
0.03	0	-	-	1.425110	1.213918	1.605715	1.317395	1.425109996	1.213918328	1.605715180	1.317394637
0.05	0	-	-	1.553850	1.269379	1.738637	1.374810	1.553849595	1.269379146	1.738636826	1.374809951
0.05	-0.5	1.885501	0.706314	1.885501	0.706314	2.109729	0.791231	1.885501498	0.706314063	2.109729515	0.791230825
0.05	0	1.553850	1.269379	1.553850	1.269379	1.738637	1.374810	1.553849595	1.269379146	1.738636826	1.374809951
0.05	0.5	0.899208	1.733859	0.899208	1.733859	1.006144	1.856885	0.899208322	1.733859221	1.006144165	1.856884600

Chapter 6

Conclusion and Future Work

6.1 Conclusion Remarks

Hybrid nanofluids are extremely adaptable and have applications in numerous domains because of their improved thermal characteristics, such as a wide absorption range, low extinction, high thermal conductivity, and minimal frictional losses. The hybrid nanofluid flow across a Riga plate has an ability to raise the effectiveness and productivity of heat exchange systems, including cooling systems and electrical devices used for system thermal management. Due to the numerous applications of hybrid nanofluid, this research is based on hybrid nanofluid flow over a Riga surface placed in a porous medium. The stagnation point flow of a hybrid nanofluid (composed of copper and aluminum oxide nanoparticles with water as base fluid) is inspected in relation to mixed convection, Joule heating heat generation or absorption and viscous dissipation. The system of equations for the fluid model is expressed as a set of partial differential equations, which are refined into a set of ordinary differential equations via appropriate similarity transformation. Several significant results have been discovered from the numerical investigation of problem utilizing Bvp4c function in MATLAB software. The thorough examination of the under consideration flow, the study reveals practical outcomes. The velocity distribution shows an increment with rising values of nanoparticle volume fractions aluminum oxide ϕ_1 and the reverse is seen for nanoparticle volume fraction for copper ϕ_2 . The stretching ratio parameter λ_1 , modified Hartmann number

Z and the mixed convection parameter λ results in an enhancement of velocity profile while a decline in velocity is observed for porosity parameter ω . The nanoparticle volume fractions for both the nanoparticles raises the temperature of the hybrid nanofluid. In addition, the higher values of thermal radiation parameter R , Eckert number Ec , magnetic field parameter M and heat generation/absorption parameter Q also corresponds to higher temperature distribution. The reverse trend of temperature profile is noticed for raised stretching ratio parameter λ_1 , Prandtl number Pr , modified Hartmann number Z and the number for magnets and electrodes width γ . The Nusselt number $(Re_x^{-\frac{1}{2}}Nu_x)$ upsurges for improved values of γ but lessens down for higher Z . The skin friction coefficient $(Re_x^{\frac{1}{2}}C_f)$ also exhibits conflicting conduct for raised γ and Z . The skin friction coefficient $(Re_x^{\frac{1}{2}}C_f)$ augments for the mounting values of ϕ_1 but shrinks for increased λ_1 . Increased ϕ_1 and λ_1 leads to higher Nusselt number $(Re_x^{-\frac{1}{2}}Nu_x)$. The skin-friction coefficient $(Re_x^{\frac{1}{2}}C_f)$ and Nusselt number $(Re_x^{-\frac{1}{2}}Nu_x)$ climbs up by increase in ϕ_2 and λ .

6.2 Future Work

In the current work, the impact of flow of stagnation point of Hybrid nanofluid flowing by a linearly stretching Riga surface in the presence of mixed convection have been examined with few other considered assumptions. However, this conducted study opens the way to further interesting projects. Here are some fascinating works that could prove to be interesting in the future.

- The mixed convection flow of ternary hybrid nanofluid on a curved surface with activation energy and chemical reactions.
- The heat transfers of modified hybrid nanofluid flow using the Cattaneo Christov heat flux model under the impact of inclined MHD.
- Investigation of the oblique stagnation point flow of hybrid nanofluids across a stretching cylinder under the influence of thermal radiation and MHD.
- Dual stratification for hybrid nanofluid flow between parallel plates involving homogeneous heterogeneous reactions.

References

- [1] Choi. S. U. & Eastman. J. A. (1995). Enhancing thermal conductivity of fluids with nanoparticles (No. ANL/MSD/CP-84938; CONF-951135-29). Argonne National Lab. (ANL), Argonne, IL (United States).
- [2] Turcu. R., Darabont. A. L., Nan. A., Aldea. N., Macovei. D., Bica. D. & Biro. L. P. (2006). New polypyrrole-multiwall carbon nanotubes hybrid materials. *Journal of optoelectronics and advanced materials*. 8(2), 643-647.
- [3] Jana. S., Salehi-Khojin. A., Zhong. & W. H. (2007). Enhancement of fluid thermal conductivity by the addition of single and hybrid nano-additives. *Thermochimica acta*. 462(1-2), 45-55.
- [4] Suresh, S., Venkataraj, K. P., Selvakumar, P., & Chandrasekar, M. (2011). Synthesis of Al_2O_3 – Cu/water hybrid nanofluids using two step method and its thermo physical properties. *Colloids and Surfaces A: Physicochemical and Engineering Aspects*, 388(1-3), 41-48.
- [5] Suresh, S., Venkataraj, K. P., Selvakumar, P., & Chandrasekar, M. (2012). Effect of Al_2O_3 – Cu/water hybrid nanofluid in heat transfer. *Experimental Thermal and Fluid Science*, 38, 54-60.
- [6] Labib, M. N., Nine, M. J., Afrianto, H., Chung, H., & Jeong, H. (2013). Numerical investigation on effect of base fluids and hybrid nanofluid in forced convective heat transfer. *International Journal of Thermal Sciences*, 71, 163-171.
- [7] Madhesh, D., Parameshwaran, R., & Kalaiselvam, S. (2014). Experimental investigation on convective heat transfer and rheological characteristics of Cu– TiO_2 hybrid nanofluids. *Experimental Thermal and Fluid Science*, 52, 104-115.
- [8] Takabi, B., & Shokouhmand, H. (2015). Effects of Al_2O_3 –Cu/water hybrid nanofluid on heat transfer and flow characteristics in turbulent regime. *International Journal of Modern Physics C*, 26(04), 1550047.
- [9] Farooq, U., Afridi, M. I., Qasim, M., & Lu, D. (2018). Transpiration and viscous dissipation effects on entropy generation in hybrid nanofluid flow over a nonlinear radially stretching disk. *Entropy*, 20(9), 668.

- [10] Parsian, A., & Akbari, M. (2018). New experimental correlation for the thermal conductivity of ethylene glycol containing Al_2O_3 - Cu hybrid nanoparticles. *Journal of Thermal Analysis and Calorimetry*, 131, 1605-1613.
- [11] Chamkha, A. J., Dogonchi, A. S., & Ganji, D. D. (2019). Magneto-hydrodynamic flow and heat transfer of a hybrid nanofluid in a rotating system among two surfaces in the presence of thermal radiation and Joule heating. *AIP Advances*, 9(2).
- [12] Khashi'ie, N. S., Arifin, N. M., Pop, I., & Wahid, N. S. (2020). Flow and heat transfer of hybrid nanofluid over a permeable shrinking cylinder with Joule heating: A comparative analysis. *Alexandria Engineering Journal*, 59(3), 1787-1798.
- [13] Megahed, A. M., Reddy, M. G., & Abbas, W. (2021). Modeling of MHD fluid flow over an unsteady stretching sheet with thermal radiation, variable fluid properties and heat flux. *Mathematics and Computers in Simulation*, 185, 583-593.
- [14] Gailitis, A. (1961). On a possibility to reduce the hydrodynamical resistance of a plate in an electrolyte. *Appl. Magnetohydrodyn.*, 12, 143-146.
- [15] Ahmed, N., Saba, F., Khan, U., Khan, I., Alkanhal, T. A., Faisal, I., & Mohyud-Din, S. T. (2018). Spherical shaped (A $g-Fe_2O_4/H_2O$) hybrid nanofluid flow squeezed between two Riga plates with nonlinear thermal radiation and chemical reaction effects. *Energies*, 12(1), 76.
- [16] Nayak, M. K., Shaw, S., Makinde, O. D., & Chamkha, A. J. (2019). Investigation of partial slip and viscous dissipation effects on the radiative tangent hyperbolic nanofluid flow past a vertical permeable Riga plate with internal heating: Bungiorno model. *Journal of Nanofluids*, 8(1), 51-62.
- [17] Shah, F., Khan, M. I., Hayat, T., Momani, S., & Khan, M. I. (2020). Cattaneo-Christov heat flux (CC model) in mixed convective stagnation point flow towards a Riga plate. *Computer Methods and Programs in Biomedicine*, 196, 105564.
- [18] Abbas, N., Malik, M. Y., & Nadeem, S. (2020). Transportation of magnetized micropolar hybrid nanomaterial fluid flow over a Riga surface. *Computer methods and programs in biomedicine*, 185(1), 105136.
- [19] Wakif, A., Chamkha, A., Animasaun, I. L., Zaydan, M., Waqas, H., & Sehaqui, R. (2020). Novel physical insights into the thermodynamic irreversibilities within dissipative EMHD fluid flows past over a moving horizontal riga plate in the coexistence of wall suction and joule heating effects: a comprehensive numerical investigation. *Arabian Journal for Science and Engineering*, 45, 9423-9438.
- [20] Khashi'ie, N. S., Arifin, N. M., Sheremet, M., & Pop, I. (2021). Shape factor effect of radiative $Cu-Al_2O_3/H_2O$ hybrid nanofluid flow towards an EMHD plate. *Case Studies in Thermal Engineering*, 26, 101199.
- [21] Nadeem, S., Ahmad, S., & Khan, M. N. (2021). Mixed convection flow of hybrid nanoparticle along a Riga surface with Thomson and Troian slip condition. *Journal of Thermal Analysis and Calorimetry*, 143(3), 2099-2109.
- [22] Merkin, J. H. (1986). On dual solutions occurring in mixed convection in a porous medium. *Journal of engineering Mathematics*, 20(2), 171-179.

- [23] Ahmad, S., & Pop, I. (2010). Mixed convection boundary layer flow from a vertical flat plate embedded in a porous medium filled with nanofluids. *International Communications in Heat and Mass Transfer*, 37(8), 987-991.
- [24] Momin, G. G. (2013). Experimental investigation of mixed convection with water- Al_2O_3 & hybrid nanofluid in inclined tube for laminar flow. *Int. J. Sci. Technol. Res*, 2(12), 195-202.
- [25] Mehryan, S. A. M., Izadpanahi, E., Ghalambaz, M., & Chamkha, A. J. (2019). Mixed convection flow caused by an oscillating cylinder in a square cavity filled with Cu- Al_2O_3 /water hybrid nanofluid. *Journal of Thermal Analysis and Calorimetry*, 137(3), 965-982.
- [26] Ahmad Khan, S., Khan, M. I., Hayat, T., Faisal Javed, M., & Alsaedi, A. (2019). Mixed convective non-linear radiative flow with TiO_2 -Cu-water hybrid nanomaterials and induced magnetic field. *International Journal of Numerical Methods for Heat & Fluid Flow*, 29(8), 2754-2774.
- [27] Elsaid, E. M., & Abdel-Wahed, M. S. (2021). Mixed convection hybrid-nanofluid in a vertical channel under the effect of thermal radiative flux. *Case Studies in Thermal Engineering*, 25(4), 100913.
- [28] Lok, Y. Y., Amin, N., Campean, D., & Pop, I. (2005). Steady mixed convection flow of a micropolar fluid near the stagnation point on a vertical surface. *International Journal of Numerical Methods for Heat & Fluid Flow*, 15(7), 654-670.
- [29] Rostami, M. N., Dinarvand, S., & Pop, I. (2018). Dual solutions for mixed convective stagnation-point flow of an aqueous silica-alumina hybrid nanofluid. *Chinese journal of physics*, 56(5), 2465-2478.
- [30] Ghalambaz, M., Roşca, N. C., Roşca, A. V., & Pop, I. (2020). Mixed convection and stability analysis of stagnation-point boundary layer flow and heat transfer of hybrid nanofluids over a vertical plate. *International Journal of Numerical Methods for Heat & Fluid Flow*, 30(7), 3737-3754.
- [31] Khashi'ie, N. S., Arifin, N. M., Hafidzuddin, E. H., Wahi, N., & Pop, I. (2019). Mixed convective stagnation point flow of a thermally stratified hybrid Cu- Al_2O_3 /water nanofluid over a permeable stretching/shrinking sheet. *ASM Sci. J*, 12(1), 17-25.
- [32] Anantha Kumar, K., Sugunamma, V., & Sandeep, N. (2020). Influence of viscous dissipation on MHD flow of micropolar fluid over a slendering stretching surface with modified heat flux model. *Journal of Thermal Analysis and Calorimetry*, 139(4), 3661-3674.
- [33] Jamaludin, A., Naganthran, K., Nazar, R., & Pop, I. (2020). MHD mixed convection stagnation-point flow of Cu- Al_2O_3 /water hybrid nanofluid over a permeable stretching/shrinking surface with heat source/sink. *European Journal of Mechanics-B/Fluids*, 84, 71-80.
- [34] Khashi'ie, N. S., Arifin, N. M., Pop, I., Nazar, R., Hafidzuddin, E. H., & Wahi, N. (2020). Non-axisymmetric Homann stagnation point flow and heat transfer past a stretching/shrinking sheet using hybrid nanofluid. *International Journal of Numerical Methods for Heat & Fluid Flow*, 30(10), 4583-4606.

- [35] Hayat, T., Saif, R. S., Ellahi, R., Muhammad, T., & Alsaedi, A. (2018). Simultaneous effects of melting heat and internal heat generation in stagnation point flow of Jeffrey fluid towards a nonlinear stretching surface with variable thickness. *International Journal of Thermal Sciences*, 132, 344-354.
- [36] Hayat, T., Nadeem, S., & Khan, A. U. (2019). Numerical analysis of Ag–CuO/water rotating hybrid nanofluid with heat generation and absorption. *Canadian Journal of Physics*, 97(6), 644-650.
- [37] Tayebi, T., Öztop, H. F., & Chamkha, A. J. (2020). Natural convection and entropy production in hybrid nanofluid filled-annular elliptical cavity with internal heat generation or absorption. *Thermal Science and Engineering Progress*, 19, 100605.
- [38] Shoaib, M., Raja, M. A. Z., Sabir, M. T., Nisar, K. S., Jamshed, W., Felemban, B. F., & Yahia, I. S. (2021). MHD hybrid nanofluid flow due to rotating disk with heat absorption and thermal slip effects: an application of intelligent computing. *Coatings*, 11(12), 1554.
- [39] Masood, S., Farooq, M., & Anjum, A. (2021). Influence of heat generation/absorption and stagnation point on polystyrene–TiO₂/H₂O hybrid nanofluid flow. *Scientific Reports*, 11(1), 22381.
- [40] Jalili, P., Azar, A. A., Jalili, B., Asadi, Z., & Ganji, D. D. (2022). Heat transfer analysis in cylindrical polar system with magnetic field: a novel hybrid analytical and numerical technique. *Case Studies in Thermal Engineering*, 40(2), 102524.
- [41] Tabassum, R., Al-Zubaidi, A., Rana, S., Mehmood, R., & Saleem, S. (2022). Slanting transport of hybrid (MWCNTs-SWCNTs/H₂O) nanofluid upon a Riga plate with temperature dependent viscosity and thermal jump condition. *International Communications in Heat and Mass Transfer*, 135(7), 106165.
- [42] Khan, M. R., Algarni, S., Alqahtani, T., Alsallami, S. A., Saeed, T., & Galal, A. M. (2022). Numerical analysis of a time-dependent aligned MHD boundary layer flow of a hybrid nanofluid over a porous radiated stretching/shrinking surface. *Waves in Random and Complex Media*, 1-17.
- [43] Xia, W. F., Ahmad, S., Khan, M. N., Ahmad, H., Rehman, A., Baili, J., & Gia, T. N. (2022). Heat and mass transfer analysis of nonlinear mixed convective hybrid nanofluid flow with multiple slip boundary conditions. *Case Studies in Thermal Engineering*, 32(3), 101893.
- [44] Dero, S., Smida, K., Lund, L. A., Ghachem, K., Khan, S. U., Maatki, C., & Kolsi, L. (2022). Thermal stability of hybrid nanofluid with viscous dissipation and suction/injection applications: Dual branch framework. *Journal of the Indian Chemical Society*, 99(6), 100506.
- [45] Aminuddin, N. A., Nasir, N. A. A. M., Jamshed, W., Ishak, A., Pop, I., & Eid, M. R. (2023). Impact of Thermal Radiation on MHD GO-Fe₂O₄ /EG Flow and Heat Transfer over a Moving Surface. *Symmetry*, 15(3), 584.
- [46] Yahaya, R. I., Mustafa, M. S., Arifin, N. M., Pop, I., Ali, F. M., & Isa, S. S. P. M. (2023). Hybrid nanofluid flow past a biaxial stretching/shrinking permeable surface with radiation effect: Stability analysis and heat transfer optimization. *Chinese Journal of Physics*.

- [47] Mahesh, R., Mahabaleshwar, U. S., Kumar, P. V., Öztop, H. F., & Abu-Hamdeh, N. (2023). Impact of radiation on the MHD couple stress hybrid nanofluid flow over a porous sheet with viscous dissipation. *Results in Engineering*, 17(3), 100905.
- [48] Rasool, G., Wang, X., Yashkun, U., Lund, L. A., & Shahzad, H. (2023). Numerical treatment of hybrid water based nanofluid flow with effect of dissipation and Joule heating over a shrinking surface: Stability analysis. *Journal of Magnetism and Magnetic Materials*, 571(12), 170587.
- [49] Zainal, N. A., Nazar, R., Naganthran, K., & Pop, I. (2022). Unsteady stagnation point flow past a permeable stretching/shrinking Riga plate in Al_2O_3 -Cu/ H_2O hybrid nanofluid with thermal radiation. *International Journal of Numerical Methods for Heat & Fluid Flow*, 32(8), 2640-2658.
- [50] Khan, U., Zaib, A., Ishak, A., Waini, I., Madhukesh, J. K., Raizah, Z., & Galal, A. M. (2022). Impact of buoyancy and stagnation-point flow of water conveying Ag-MgO Hybrid nanoparticles in a vertical contracting/expanding Riga wedge. *Symmetry*, 14(7), 1312.
- [51] Nidhi, & Kumar, L. (2022). Cu- Al_2O_3 /engine oil Williamson hybrid nanofluid flow over a stretching/shrinking Riga plate with viscous dissipation and radiation effect. *Heat Transfer*, 51(2), 2279-2305.
- [52] Ghazwani, H. A. (2023). Time-dependent mixed stagnation point hybrid nanofluid flow with radiative heat flux and viscous dissipation effects over a movable EMHD Riga plate. *International Journal of Modern Physics B*, 2450090.
- [53] Khan, U., Mahmood, Z., Eldin, S. M., Makhdoum, B. M., Fadhl, B. M., & Alshehri, A. (2023). Mathematical analysis of heat and mass transfer on unsteady stagnation point flow of Riga plate with binary chemical reaction and thermal radiation effects. *Heliyon*, 9(3), e14472.
- [54] Khashi'ie, N. S., Arifin, N. M., Wahid, N. S., & Pop, I. (2023). Insight into Unsteady Separated Stagnation Point Flow of Hybrid Nanofluids Subjected to an Electro-Magnetohydrodynamics Riga Plate. *Magnetochemistry*, 9(2), 46.
- [55] Yahaya, R. I., Arifin, N. M., Pop, I., Ali, F. M., & Isa, S. S. P. M. (2023). Dual Solutions of Unsteady Mixed Convection Hybrid Nanofluid Flow Past a Vertical Riga Plate with Radiation Effect. *Mathematics*, 11(1), 215.
- [56] Shoukat, Z., Zubair, M. H., Farman, M., Akgül, A., Sultan, M., Sharipov, S. S., ... & Algarni, H. (2023). Impacts of joule heating with Cattaneo-Christove heat flux model in a MHD flow of Eyring-Powell fluid on a Riga plate. *Alexandria Engineering Journal*, 64, 741-748.
- [57] Elsaid, E. M., & Abdel-wahed, M. S. (2022). MHD mixed convection Ferro Fe_2O_4 /Cu-hybrid-nanofluid runs in a vertical channel. *Chinese Journal of Physics*, 76(3), 269-282.
- [58] Abdelaziz, A. H., El-Maghlany, W. M., El-Din, A. A., & Alnakeeb, M. A. (2022). Mixed convection heat transfer utilizing Nanofluids, ionic Nanofluids, and hybrid nanofluids in a horizontal tube. *Alexandria Engineering Journal*, 61(12), 9495-9508.

- [59] Khan, S. U., Usman, Raza, A., Kanwal, A., & Javid, K. (2022). Mixed convection radiated flow of Jeffery-type hybrid nanofluid due to inclined oscillating surface with slip effects: a comparative fractional model. *Waves in Random and Complex Media*, 1-22.
- [60] Asghar, A., Ying, T. Y., & Zaimi, K. (2022). Two-dimensional magnetized mixed convection hybrid nanofluid over a vertical exponentially shrinking sheet by thermal radiation, joule heating, velocity and thermal slip conditions. *Journal of Advanced Research in Fluid Mechanics and Thermal Sciences*, 95(2), 159-179.
- [61] Wahid, N. S., Arifin, N. M., Khashi'ie, N. S., Pop, I., Bachok, N., & Hafidzuddin, M. E. H. (2022). MHD mixed convection flow of a hybrid nanofluid past a permeable vertical flat plate with thermal radiation effect. *Alexandria Engineering Journal*, 61(4), 3323-3333.
- [62] Khan, U., Adnan, & Haleema, B. (2022). Thermal performance in nanofluid and hybrid nanofluid under the influence of mixed convection and viscous dissipation: numerical investigation. *Waves in Random and Complex Media*, 1-19.
- [63] Jiang, X., Hatami, M., Abderrahmane, A., Younis, O., Makhdoum, B. M., & Guedri, K. (2023). Mixed convection heat transfer and entropy generation of MHD hybrid nanofluid in a cubic porous cavity with wavy wall and rotating cylinders. *Applied Thermal Engineering*, 226, 120302.
- [64] Hussain, S. M., Mahat, R., Katbar, N. M., Ullah, I., Kumar, R. V., Prasannakumara, B. C., ... & El Din, S. M. (2023). Artificial neural network modeling of mixed convection viscoelastic hybrid nanofluid across a circular cylinder with radiation effect: Case study. *Case Studies in Thermal Engineering*, 50(4), 103487.
- [65] Wahid, N. S., Arifin, N. M., Khashi'ie, N. S., Pop, I., Bachok, N., & Hafidzuddin, M. E. H. (2022). Hybrid nanofluid stagnation point flow past a slip shrinking Riga plate. *Chinese Journal of Physics*, 78, 180-193.
- [66] Zainal, N. A., Nazar, R., Naganthran, K., & Pop, I. (2022). Slip effects on unsteady mixed convection of hybrid nanofluid flow near the stagnation point. *Applied Mathematics and Mechanics*, 43(4), 547-556.
- [67] Khashi'ie, N. S., Wahid, N. S., Md Arifin, N., & Pop, I. (2022). MHD stagnation-point flow of hybrid nanofluid with convective heated shrinking disk, viscous dissipation and Joule heating effects. *Neural Computing and Applications*, 34(20), 17601-17613.
- [68] Yahaya, R. I., Arifin, N. M., Pop, I., Ali, F. M., & Isa, S. S. P. M. (2023). Dual solutions for the oblique stagnation-point flow of hybrid nanofluid towards a shrinking surface: Effects of suction. *Chinese Journal of Physics*, 81, 193-205.
- [69] Khashi'ie, N. S., Waini, I., Wahid, N. S., Arifin, N. M., & Pop, I. (2023). Unsteady separated stagnation point flow due to an EMHD Riga plate with heat generation in hybrid nanofluid. *Chinese Journal of Physics*, 81, 181-192.
- [70] Yahaya, R. I., Md Arifin, N., Pop, I., Md Ali, F., & Mohamed Isa, S. S. P. (2023). Dual solutions for MHD hybrid nanofluid stagnation point flow due to a radially shrinking disk with convective boundary condition. *International Journal of Numerical Methods for Heat & Fluid Flow*, 33(2), 456-476.

- [71] Zainodin, S., Jamaludin, A., Nazar, R., & Pop, I. (2023). MHD Mixed Convection Flow of Hybrid Ferrofluid through Stagnation-Point over the Nonlinearly Moving Surface with Convective Boundary C–ondition, Viscous Dissipation, and Joule Heating Effects. *Symmetry*, 15(4), 878.
- [72] Al Nuwairan, M., Hafeez, A., Khalid, A., & Aldhafeeri, A. (2022). Multiple solutions of melting heat transfer of MHD hybrid based nanofluid flow influenced by heat generation/absorption. *Case Studies in Thermal Engineering*, 35, 101988.
- [73] Yaseen, M., Rawat, S. K., Shafiq, A., Kumar, M., & Nonlaopon, K. (2022). Analysis of heat transfer of mono and hybrid nanofluid flow between two parallel plates in a Darcy porous medium with thermal radiation and heat generation/absorption. *Symmetry*, 14(9), 1943.
- [74] Asghar, A., Chandio, A. F., Shah, Z., Vrinceanu, N., Deebani, W., Shutaywi, M., & Lund, L. A. (2023). Magnetized mixed convection hybrid nanofluid with effect of heat generation/absorption and velocity slip condition. *Heliyon*, 9(2), e13189.
- [75] Kumar, A., Dash, A. P., Ray, A. K., Sethy, P., & Kasireddy, I. (2023). Unsteady mixed convective flow of hybrid nanofluid past a rotating sphere with heat generation/absorption: an impact of shape factor. *International Journal of Numerical Methods for Heat & Fluid Flow*, 33(11), 3691-3715.
- [76] Mahmood, Z., Eldin, S. M., Rafique, K., & Khan, U. (2023). Numerical analysis of MHD tri-hybrid nanofluid over a nonlinear stretching/shrinking sheet with heat generation/absorption and slip conditions. *Alexandria Engineering Journal*, 76, 799-819.
- [77] Dowling. D. R., Kundu. P. K., and Cohen, I. M. (2012). *Fluid Mechanics*. (6th ed.) Germany: Elsevier Science.
- [78] Pritchard, P. J., Fox, R. W., & McDonald, A. T. (2010). *Introduction to fluid mechanics*. John Wiley & Sons.
- [79] Durst, F., & Arnold, I. (2008). *Fluid mechanics: an introduction to the theory of fluid flows* (Vol. 675). Berlin: Springer.
- [80] Whitaker, S. (1977). *Fundamental Principles of Heat Transfer*. (1st ed.) United Kingdom.: *Elsevier Science and Technology Books*.
- [81] Hosseinzadeh, K., Asadi, A., Mogharrebi, A. R., Ermia Azari, M., & Ganji, D. D. (2021). Investigation of mixture fluid suspended by hybrid nanoparticles over vertical cylinder by considering shape factor effect. *Journal of Thermal Analysis and Calorimetry*, 143(2), 1081-1095.
- [82] Zari, I., Shafiq, A., & Khan, T. S. (2021). Simulation study of Marangoni convective flow of kerosene oil based nanofluid driven by a porous surface with suction and injection. *International Communications in Heat and Mass Transfer*, 127(4), 105493.
- [83] White, F. M., & Majdalani, J. (2006). *Viscous fluid flow* (Vol. 3, pp. 433-434). New York: McGraw-Hill.
- [84] Kierzenka, J., & Shampine, L. F. (2008). A BVP solver that controls residual and error. *Journal of Numerical Analysis, Industrial and Applied Mathematics*, 3(1-2), 27-41.

- [85] Dinarvand, S. (2019). Nodal/saddle stagnation-point boundary layer flow of CuO–Ag/water hybrid nanofluid: a novel hybridity model. *Microsystem Technologies*, 25(7), 2609-2623.
- [86] Wang, C. Y. (2008). Stagnation flow towards a shrinking sheet. *International Journal of Non-Linear Mechanics*, 43(5), 377-382.
- [87] Bachok, N., Ishak, A., & Pop, I. (2011). Stagnation-point flow over a stretching/shrinking sheet in a nanofluid. *Nanoscale research letters*, 6, 1-10.
- [88] Waini, I., Ishak, A., & Pop, I. (2020). MHD flow and heat transfer of a hybrid nanofluid past a permeable stretching/shrinking wedge. *Applied Mathematics and Mechanics*, 41(3), 507-520.
- [89] Waini, I., Ishak, A., & Pop, I. (2020). Hiemenz flow over a shrinking sheet in a hybrid nanofluid. *Results in Physics*, 19, 103351.
- [90] Eldabe, N. T., Gabr, M. E., Zaher, A. Z., & Zaher, S. A. (2021). The effect of Joule heating and viscous dissipation on the boundary layer flow of a magnetohydrodynamics micropolar-nanofluid over a stretching vertical Riga plate. *Heat Transfer*, 50(5), 4788-4805.
- [91] Khatun, S., Islam, M. M., Mollah, M. T., Poddar, S., & Alam, M. M. (2021). EMHD radiating fluid flow along a vertical Riga plate with suction in a rotating system. *SN Applied Sciences*, 3, 1-14.
- [92] Khashi'ie, N. S., Md Arifin, N., & Pop, I. (2020). Mixed convective stagnation point flow towards a vertical Riga plate in hybrid Cu- Al_2O_3 /water nanofluid. *Mathematics*, 8(6), 912.
- [93] Zari, I., Ali, F., Khan, T. S., & Shafiq, A. (2022). Radiative Hiemenz flow towards a stretching Riga plate in hybrid nanofluid. *International Communications in Heat and Mass Transfer*, 139, 106492.
- [94] Hale, N. P. (2006). A sixth-order extension to the matlab bvp4c software of j. kierzenka and l. shampine. *Department of Mathematics, Imperial College London*.